2013

Opto-VLSI-based adaptive optical power splitter/combiner for next generation dynamic optical telecommunication networks

Haithem A. Mustafa
Edith Cowan University

Opto-VLSI-based adaptive optical power splitter/combiner for next generation dynamic optical telecommunication networks

Haithem A. Mustafa
Edith Cowan University, hmustafa@our.ecu.edu.au

Edith Cowan University

Copyright Warning

OPTO-VLSI-BASED ADAPTIVE OPTICAL POWER SPLITTER/COMBINER FOR NEXT GENERATION DYNAMIC OPTICAL TELECOMMUNICATION NETWORKS

By

Haithem Ali Babiker Mustafa

Master degree (MEMS/NEMS, University of Trento, Italy

M-Tech and B-Tech (Electrical Engineering), Cape Peninsula University of Technology, South Africa

B.Sc (Physics and Mathematics), University of Khartoum, Sudan

A thesis submitted in fulfilment of the requirements for the degree of

Doctor of Philosophy

at

Electron Science Research Institute

Faculty of Health, Engineering and Science

EDITH COWAN UNIVERSITY

Principal Supervisor: **Prof. Kamal Alameh**

Director of Electron Science Research Institute, Edith Cowan University

2013

USE OF THESIS

The Use of Thesis statement is not included in this version of the thesis.

DECLARATION

Hereby I, Haithem A. B. Mustafa, declare that Opto-VLSI-based adaptive optical power splitter/combiner for next generation dynamic optical telecommunication networks is my own original work and that all sources have been accurately reported and acknowledged, and that this document has not previously in its entirety or in part been submitted at any university in order to obtain an academic qualification.

I also grant permission for the Library at Edith Cowan University to make duplicate copies of my thesis as required.

Haithem A. B. Mustafa 5th November 2013

To my parents (May Allah bless them),

To my wife,

To all of my brothers, sisters, and best friends,

T all of my teachers,....

ACKNOWLEDGEMENTS

First of all, I would like to thank God for reaching the goal I dreamed of, and then my Supervisor, Professor Kamal Alameh for his support, patience and trust in me. He has given me a unique opportunity and I have taken advantage of it, to experimentally improve my knowledge in the field of Photonics for Fibre optics and optical communication. I really appreciate all his contributions of time, ideas, and funding to build my Ph.D. experience productive and remarkable. Throughout my study period I have learned that Ph.D is not only a degree, it is also about the skills that I have developed.

Especially, I would like to thank Dr. Feng Xiao who has been a very good Co-supervisor and so supportive. He has shared with me his knowledge and experience in different ways including research discussions. Throughout my journey with him, I have gained and built hand on experience on various electronics and optical instrumentations. I really appreciate all his contributions of time and ideas on making highly significance experimental results for my PhD thesis. Other thanks are to be extended to Dr. Mikhail Vasiliev, Dr. Sreten Askrapa, and Dr. Hoang Nguyen for their useful discussion and encouragement.

I would especially like to thank Linda Arthur, who is the office administrator on the time I have joined the Electron Science Research Institute (ESRI). Her support has not limited to documents and papers work but has also been extended to help us in many ways including sharing backed cakes and fruits from her garden, reading and editing of our thesis. I really found myself very thankful for her great help and support. Other thanks are to be extended to Paul Roach and Tiella Turkovic for their great help.

My special thanks to my colleague, Valentina Tiporlini, for her company and walking together all the way to the destination, and I'm looking forward to walk together to the Vice chancellor for offering us the title 'Dr'. A very special thank you to Dr. Ayman Karar who has been walking with us 'me and Vale' and sharing our discussion which included fun, plans, research topics, engagement, and happiness. I knew Ayman since my undergraduate study back home; we were classmates in the department of physics, University of Khartoum. It happened accidentally that we met again here in Perth after each of us being overseas while studying the master degree. So, I got so much to share with him, he is more than just a colleague, May God bless him, his great wife, and his little son.

Many thanks to all my colleagues who I joined at ESRI (Dr. Ahmed Abdelrahman, Arie Paap, David Michel, Dr. Kavitha Venkataraayan, Dr. Mohammad Nur E Alam, Steven Silva) and those who have joined us later (Yamna Elmouedden, Ramzy Alghamedi, Ali Sardarinejad, Praveen Akkihebbal Satyaprakash, Samarth Trivedi, Vi Nguyen Le, Devendra Maurya, and Dr. Baofu Ding) for their valuable discussions in different topics which have had a positive reflection in many things including my thesis.

Other thanks are to be extended to my friends in Perth city (Dr. Elsamual Elhepir, Dr. M Elkhatim, Mr. Elsadig Edris) and also those back home (Ashraf Salah, M Abdelmajeed, Bakry Abdullah, and M Salih Abdeljaleel) who have fully supported and encouraged me to reach my goal.

Many thanks, to my parents, uncles, brothers, and sisters for their support and who have stood by my side to reach this stage. A very especial thank you to my lovely wife, who has had the greatest contribution on my PhD thesis by being so supportive, positive, patient and so many other things that she has sacrificed to be by my side.

Finally, thank you to the Faculty of Health, Engineering and Science for their financial assistance and to Edith Cowan University for the award of doctor of philosophy.

Haithem A. B. Mustafa

5th November 2013

PUBLICATIONS

Journal Articles:

1. **H. A. B. Mustafa**, F. Xiao, and K. Alameh, “Transversal Optical RF Filter Employing Reconfigurable Optical Combiner,” submitted.

2. F. Xiao, **H. A. B. Mustafa,** and K. Alameh, “1×N wavelength selective adaptive optical power splitter,” submitted.

3. **H. A. B. Mustafa,** F. Xiao, and K. Alameh, “Multiport Broadband Opto-VLSI-based Adaptive RF Power Splitter/Combiner,” submitted.

4. **H. A. B. Mustafa,** F. Xiao, and K. Alameh, “A 1×N lossless adaptive optical power splitter employing an Opto-VLSI processor,” *IEEE, Photonic Journal*, vol. 5, No. 6, pp.7902410- 7902419, Dec 2013.

5. **H. Mustafa**, F. Xiao, and K. Alameh, "Reconfigurable optical power splitter/combiner based on Opto-VLSI processing," *Optics Express,* vol. 19, pp. 21890-21897, 2011/10/24 2011.

6. **H. A. B. Mustafa**, F. Xiao, and K. Alameh, "Adaptive Optical Splitter Employing an Opto-VLSI Processor and a 4-f Imaging System," *Journal of Lightwave Technology,* vol. 28, pp. 2761-2765, Oct 1 2010.

Conferences Proceeding:

7. **H. A. B. Mustafa**, X. Feng, and K. Alameh, " A 1×4 Opto-VLSI-Based Broadband Adaptive RF splitter," in *the 8th Asia-Pacific Microwave Photonics Conference (**APMP2013**), GIST Gwangju, Korea, April 22-24,* 2013.

8. **H. A. B. Mustafa**, X. Feng, and K. Alameh, "Opto-VLSI-based variable RF power splitter," in *High Capacity Optical Networks and Enabling Technologies (HONET), 2012 9th International Conference on*, 2012, pp. 171-174.

9. **H. A. B. Mustafa**, X. Feng, and K. Alameh, "A 1×4 adaptive optical splitter based on Opto-VLSI processor," in *High Capacity Optical Networks and Enabling Technologies (HONET), 2011*, 2011, pp. 346-349.

10. **H. A. B. Mustafa**, X. Feng, and K. Alameh, "Photonic microwave filter employing an opto-VLSI-based adaptive optical combiner," in *High Capacity Optical Networks and Enabling Technologies (HONET), 2011*, 2011, pp. 205-209.

11. **H. A. B. Mustafa,** F. Xiao, and K. Alameh, "Broadband Adaptive RF Splitter Based on Opto-VLSI Processing," in**,** *Hong Kong Optical Engineering International Conference (HKOEIC2011)2011, HongKong 25-26 Nov.*

12. **H. A. B. Mustafa**, X. Feng, and K. Alameh, "A 1×2 adaptive optical splitter based on Opto-VLSI processor," in *High-Capacity Optical Networks and Enabling Technologies (HONET), 2010*, 2010, pp. 200-203.

ABSTRACT

The demand for optical power splitters is growing globally, due to the rapid deployment of fibre-to-the-premises, optical metropolitan area network (MAN), and active optical cables for TV/Video signal transport. Optical splitters play an important role in passive optical network (PON) technology by enabling several hundred users to share one optical line terminal. However, current PONs, which use fixed optical power splitters, have limited reconfigurability particularly in adding/dropping users to/from an optical network unit.

An adaptive optical power splitter (OPS) can dynamically reallocate the optical power in the entire network according to the real-time distribution of users and services, thus providing numerous advantages such as improve an optical network efficiency, scalability, and reliability. An adaptive OPS is also important for realizing self-healing ring-to-ring optical MAN, thus offering automatic communication recovery when line break occurs. In addition, future optical line protection systems will require adaptive optical splitters to switch optical signals from faulty lines to active power lines, avoid the use of optical attenuators and/or amplifiers, and achieve real time line monitoring. An adaptive OPS can also be incorporated in tunable optical dispersion compensators, optical attenuator and optical gain equalizer, and reconfigurable optical switches.

This thesis proposes and demonstrates the principle of a novel Opto-VLSI-based adaptive optical splitter/combiner for next generation dynamic optical telecommunication networks. The proposed splitter structure enables an input optical power to be split adaptively into a larger number of output fibre ports, through optimized phase holograms driving the Opto-VLSI processor. The new adaptive optical splitter has additional advantages including lossless operation, adequate inter-port crosstalk, compressed hardware and simple user interface.

This thesis demonstrates, in particular, the concept of an adaptive optical power splitter employing an Opto-VLSI processor and a 4-f imaging system experimentally in three stages as follow: (i) a 1×2 adaptive optical power splitter based on an Opto-VLSI processor, a fibre collimator array and 4-f imaging systems (single lens), (ii) a 1×4 adaptive optical power splitter based on an Opto-VLSI processor, a fibre array and 4-f imaging systems (single lens), and (iii) a 1×N lossless adaptive optical power splitter structure integrating an Opto-VLSI processor, optical amplifiers, a fibre array, and an array of 4-f imaging systems (lens array). The thesis also demonstrates the concept of an

adaptive optical signal combiner which enables multiple signals to be combined with user-defined weight profiles into a single fibre port.

Experimental results demonstrate that an input optical signal can arbitrarily be split into *N* signals and coupled into optical fibre ports by uploading optimized multicasting phase holograms onto the Opto-VLSI processor. They also demonstrate that *N* input optical signals can be dynamically combined with arbitrary weights into a single optical fibre port. Excellent agreement between theoretical and experimental results is demonstrated. The total insertion loss of the optical power splitter is only 5 dB. Results also show that the optical amplifiers can compensate for the insertion and splitting losses, thus enabling lossless splitter operation. A crosstalk level around -25 dB and a wavelength spectral range exceeding 40 nm is experimentally realized.

In addition, a novel broadband adaptive RF power splitter/combiner based on Opto-VLSI processor is proposed and experimentally demonstrated. By uploading optimized multicasting phase holograms onto the software-driven Opto-VLSI processor, the input RF signal is dynamically split and directed to different output ports, with user-defined splitting ratios. Also, multiple input RF signals can be dynamically combined with arbitrary user-defined weights. As a proof-of-concept demonstration, two input RF signals are dynamically combined with different user-defined weight profiles.

We also propose and demonstrate a photonic microwave filter based on the use of an Opto-VLSI-based adaptive optical combiner. The experimental results demonstrate that the developed Opto-VLSI-based adaptive optical combiner can dynamically route multiple input optical signals to a single output, with user-defined weight profiles, thus realising a tunable microwave filter.

Overall this Opto-VLSI-based adaptive optical power splitter should allow as many as 32 output ports to be supported while achieving high splitting resolution and dynamic range. This will greatly enhance the efficiency of optical communication networks.

LIST OF TABLES

LIST OF FIGURES

CONTENTS

GLOSSARY

AWG	Arrayed Waveguide Gratings
CMOS	Complementary Metal–Oxide–Semiconductor
CW	Continuous Wave
EOM	Electro-Optic Modulator
EDFA	Erbium-Doped Fibre Amplifiers
FBG	Fibre Bragg Grating
FTTB	Fibre to the Building
FTTC	Fibre to the Curb
FTTH	Fibre to the Home
FTTP	Fibre to the Premises
FT	Fourier Transform
FBT	Fused Bi-Conical Taper
HDF	High Dispersion Fibre
ITO	Indium-Tin Oxide
LC	Liquid Crystal
LCOS	Liquid Crystal On Silicon
MESFET	Metal–Oxide–Semiconductor Field-Effect Transistor
MAN	Metropolitan Area Network
MEMS	Micro-Electro-Mechanical Systems
MMI	Multimode Interference
OLT	Optical Line Terminal
ODC	Optical Dispersion Compensator
OLP	Optical Line Protection
ONU	Optical Network Unit
OPS	Optical Power Splitter
OSA	Optical Spectrum Analysers
PON	Passive Optical Network
PD	Photodetector
PSP	Photonic RF Signal Processing

PC	Photonics Crystals
PLC	Planar Lightwave Circuit
PCB	Printed Circuit Board
QWP	Quarter-Wave-Plate
RF	Radio Frequency
ROADM	Reconfigurable Optical Add-Drop Multiplexer
SOA	Semiconductor Optical Amplifier
SLM	Spatial Light Modulator
SLPM	Spatial Light Phase Modulator
TEC	Thermal Electric Cooler
VLSI	Very-Large-Scale-Integrated
WDM	Wavelength Division Multiplexer

CHAPTER 1

NATURE AND SCOPE OF THE STUDY

1.1 BACKGROUND

The demand for optical power splitters is growing globally, due to the rapid deployment of fibre-to-the-premises (FTTP), optical metropolitan area network (MAN), and active optical cables for TV/Video signal transport [1-3]. Optical splitters play an important role in passive optical network (PON) technology by enabling several hundred users to share one optical line terminal (OLT) at the central office distributing optical power to a large number of optical network units (ONUs), each of which in turn is shared by many users [2, 4, 5], at the customer end of the network, as illustrated by Fig. 1.1.

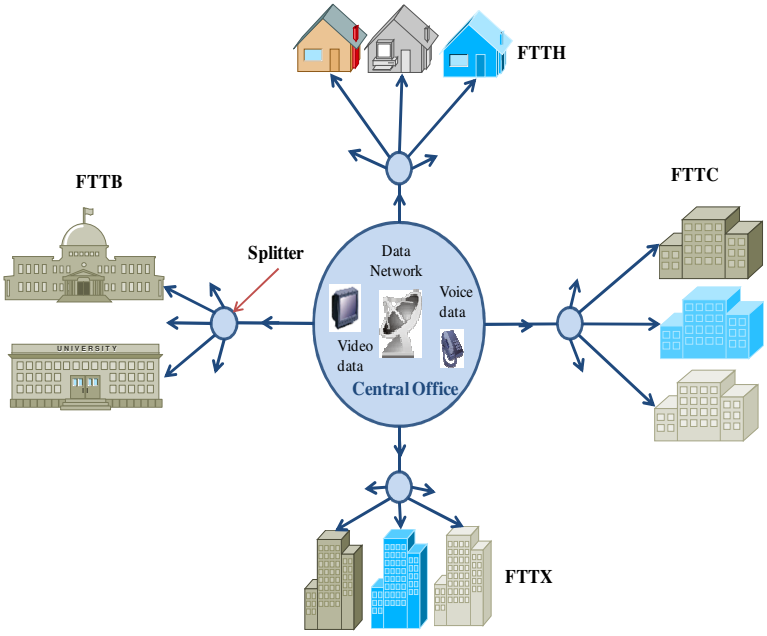

Fig. 1.1. Passive Optical networks schematic diagram. FTTH: Fibre-to-the (Home, Business, Curb, ...)

However, current PONs, which use fixed optical power splitters, have limited reconfigurability particularly in adding/dropping users to/from an ONU. For instance, both the number of subscribers in each ONU and the path distances of each ONU can be dif-

ferent [6], thus the optical power of each ONU can vary from moment to moment. The major problem when deploying optical networks is attaining the minimum optical loss that is caused mainly by the passive optical splitter [7]. An adaptive optical power splitter (OPS) can dynamically reallocate the optical power in the entire network according to the real-time distribution of users and services, thus providing numerous advantages such as improvement of optical network efficiency and network scalability, and greater network reliability [5, 6].

Fig. 1.2 shows the linear architecture of a passive optical network formed by a series of 1×2 optical power splitters [6]. The linear architecture comprises a number of apartments (A_1, A_2, A_3,...., A_m) connected serially via number of 1×2 optical power splitters (S_1, S_2, S_3,...., S_m). The first OPS receives the main input optical power P_{in} and then splits it into two output optical signals, P_{in1}, to supply the first apartment and P_1, which is split by the second OPS. The following power splitters split the input optical power they receive into two outputs in the same way as the first OPS. Each of the outputs (P_1, P_2, P_3...., P_m) offer an input to the next OPS in the serial connection, while each of the other outputs (P_{in1}, P_{in2} P_{in3},...., P_{inm}) offer input power to a subsequent apartment.

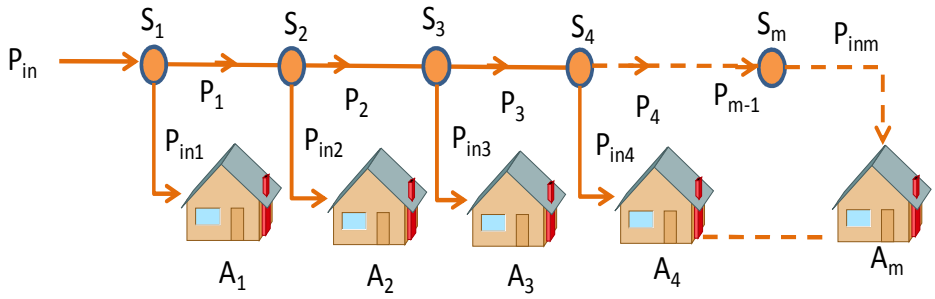

Fig. 1.2. Linear architecture of passive optical network formed by series of 1×2 optical power splitters. Adaptive optical power splitters can equalize the power distributed to each unit.

If the OPS has a fixed splitting ratio (50%:50%), the last apartment has the highest power attenuation with respect to the other apartments. The power differences among all the apartments will cause fluctuation in service quality. However, if the power splitting ratio of each OPS is adaptive, then the input power received by all apartments can be equalized. In addition, by using adaptive OPSs, the cost of equipment and network

expansion can be reduced through distribution on demand [1]. This will allow many new users to subscribe to the network in the future without service interruption.

An adaptive optical power splitter is also necessary for implementing a self-healing ring in a MAN [8, 9], offering a popular protection mode that automatically recovers communication from failure. The dual fibre ring PON design shown in Fig. 1.3, is an ideal application for the adaptive OPS [6, 10]. The network architecture comprises two fibre rings, each of which is a set of serially connected 1×2 optical power splitters. Each optical power splitter in the outer ring has a corresponding power splitter pair in the inner ring. Each pair of power splitters has its own output connected to a common subnetwork, while only one splitter of each pair receives the power signal. One of the two-ends of each ring is connected to the OLT via an optical power splitter which splits the main input optical power signal into two paths, Path 1 via the outer ring, and Path 2 via the inner ring.

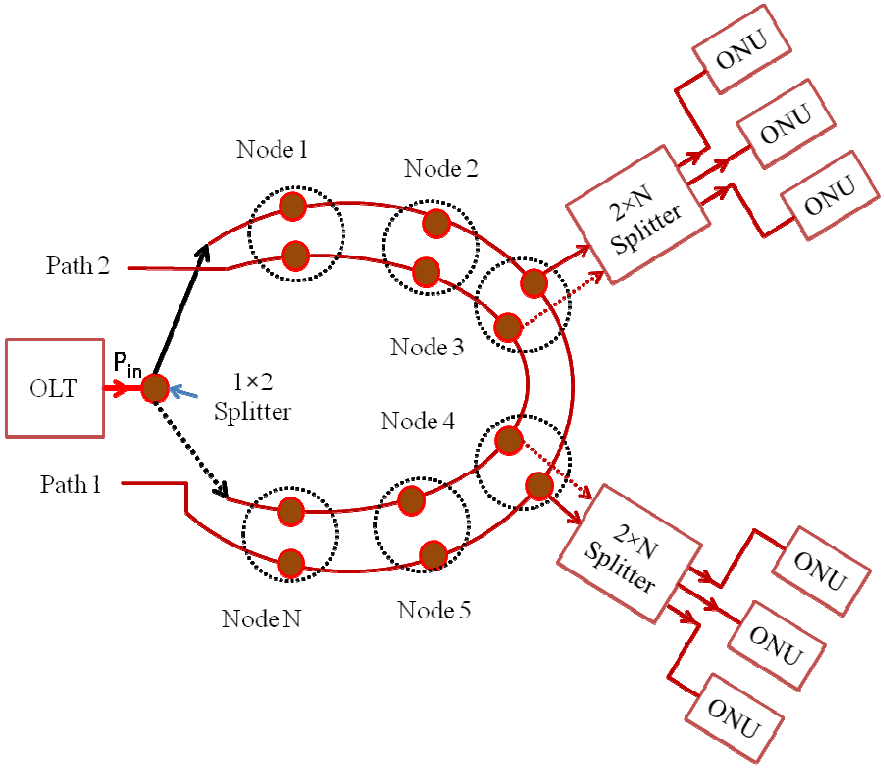

Fig. 1.3. Dual fibre ring structural design in PON. The network architecture comprises two fibre 'outer and inner' rings; each of which is a set of serially connected 1×2 optical power splitters. Each 1×2 optical power splitter on outer ring has a pair on the inner ring, each two pairs form one network node.

In normal operation, the optical signals from the OLT to the OUNs flow via the outer fibre ring. If a cable break happens, part of the signal power from the OLT will be directed to the second ring-to-ring via the second set of power splitters. An adaptive optical power splitter at the OLT can switch the main input power from a ring to another ring without losses. An adaptive optical power splitter at each node point can maintain constant output power at all nodes, thus providing each sub-network with a constant input power signal.

Adaptive OPSs can incorporate in long-haul node-to-node networks where optical line protection (OLP) is required [11]. There are three OLP schemes presently deployed [12, 13],1:1,1+1, and 1-1, where a 1×2 optical switch is required to (i) transfer the optical power from the primary fibre line to the secondary fibre line dynamically, (ii) avoid the use of optical power attenuators and optical amplifiers, and (iii) monitor both lines instantaneously [14]. Fig. 1.4 illustrates how using adaptive OPSs to replace the 1×2 optical switches in the 1+1 approach can provide advantages for all protection schemes.

Wen Liuand Keyu Wu have reported a new intelligent bi-directional EDFA design for metropolitan optical networks (MAN) amplifying both receiving and transmitting channels instantaneously [15]. It integrates a post-amplifier and a pre-amplifier function within one module. It also employs an adaptive splitter not only to adjust the gain between the forward and backward directions but also to use all pump power efficiently.

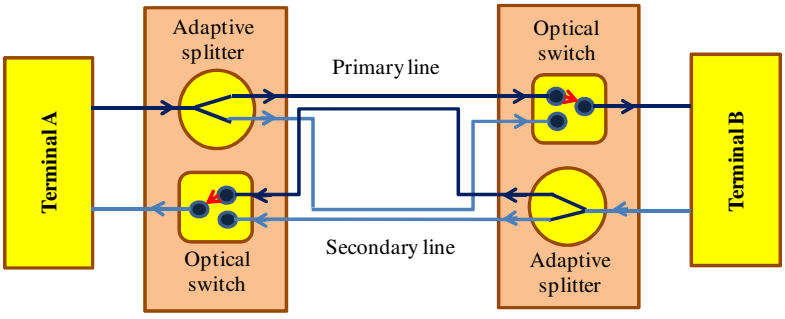

Fig. 1.4. Optical line protection (OLP) schemes '1+1 and 1:1' employing an adaptive optical power splitter.

RF power splitters are key elements for applications based on RF signal processing, such as beamforming networks and smart antenna systems [16, 17]. A multi-port reconfigurable broadband RF power splitter with variable splitting ratios allows such systems

to operate with a high degree of flexibility, thus achieving multiple functions that are not possible with conventional fixed-ratio splitters [18]. Adaptive OPS can also be used to dynamically split an RF-modulated optical signal into many output ports, thus realizing, in conjunction with broadband photodetectors, a broadband adaptive RF power splitter.

Another potential application for the adaptive optical splitter is in photonic signal processing [19], particularly, photonic RF transversal filters, where both lightweight and broadband are of prime concerns. Photonics-based RF filters have several advantages, namely, (i) they can provide optical delay lines with very low loss independent of the RF signal, (ii) they have very high time bandwidth products, (iii) they are immune to electromagnetic interference and (iv) they can attain high speed sampling frequencies [20].

A tunable optical dispersion compensator (ODC), based on the use of an adaptive optical power splitter, has been experimentally demonstrated [21]. Dispersion compensation is achieved by splitting the input signal between two dispersive media and then adding the resulting signals. Tunable compensation is attained by controlling the power splitting ratio of the input signal between two dispersive media [21].

Finally, an adaptive optical power splitter can be used as variable optical attenuator and dynamic optical gain equalizer for WDM or any other application. It is also suitable for use as an optical switch.

In summary, adaptive optical power splitters can be used in many applications including:

- Passive optical network
- Implementing a self-healing ring in a MAN
- Optical line protection (OLP)
- A bidirectional EDFA
- Integrated with broadband photodetectors for realizing a broadband adaptive RF power splitter
- Photonic signal processing
- Tunable optical dispersion compensator (ODC)
- Tunable optical attenuator.
- Tunable optical gain equalizer.
- Optical switching.

1.2 MOTIVATION

Currently, the majority of optical power splitters are passive, meaning they provide constant splitting ratios. Several technologies have been used for realizing an optical power splitter. For instance, fused bi-conical taper (FBT) is a successful technique that has been used to realize an optical fibre coupler/splitter and other fibre optic components [22]. Simple fused structure of fibre coupler or splitter has been achieved by simply heating, stretching, and tapering two optical fibres [23].

Single or multi mode fibre couplers are made using fused bi-conical taper (FBT) technique with very low access loss. The coupling ratio is determined by the related parameters of the taper's length and the diameter of the coupler structure in the region of the taper's waist [23, 24]. However, this technique is impractical not only in changing the splitting ratio adaptively but also in increasing the splitter output port count.

Waveguide planar lightwave circuit (PLC) technology is very useful for fabricating compact and high performance optical devices, including, optical power splitters wavelength division multiplexers (WDM), and optical switches [25]. PLC-optical power splitters offer high reliability and stability, low insertion loss, and low cost [26]. In addition, no external power is required for either FBT or PLC-based optical power splitters. However, both techniques, FBT and PLC can provide different splitting ratios during their fabrication process, but once the device is fabricated the splitting ratio in no longer changeable.

Micro-electro-mechanical systems (MEMS) is a technological approach that offers many advantages such as integration of multiple functional units in a tiny area, which is the key importance when developing smart and complicated devices such as MEMS micro-mirrors arrays also known as MEMS-based spatial light phase modulator (SLPM) [27, 28]. MEMS-based SLPM is a diffractive element based on an array of micro-mirrors enabling optical phase control of a light beam in free space [29-31]. It has potential applications in areas such as femto second pulse shaping [32], wavelength division multiplexing [33], variable optical attenuator [34, 35], and tunable fibre laser [36]. MEMS-based SLPM offers high-speed operation 'hundreds of microseconds' and polarization insensitivity compared with a liquid-crystal-based SLPM (LC-SLPM) 'several milliseconds.' MEMS-SLPMs are useful for realizing passive optical power splitters or variable optical attenuators but are not yet mature enough for realizing adaptive optical power splitters which have a large number of output ports [37].

The Opto-VLSI processor well known as a spatial light modulator (SLM) is a diffraction element based on Liquid Crystal on Silicon (LCOS) technology for light beam phase modulation [38, 39]. The Opto-VLSI processor is well designed to accomplish polarization-insensitive operation by incorporates a quarter-wave-plate (QWP) and aluminum mirror layers. In addition, the Opto-VLSI processor offers precise and linear phase modulation characteristics, high diffraction efficiency, and easy private computer control. The Opto-VLSI processor has been used in many applications, including:

- Photonic microwave and RF signal processing [40]
- Adaptive wavelength division multi/demultiplexer [41]
- Reconfigurable optical add-drop multiplexer (ROADM) [42, 43]
- Tunable dual/multi-wavelength fibre laser [44, 45]
- Optical interconnect [46]
- High speed optical correlators [47]

The development and deployment of fibre optics and optical communication networks has created a new research field for dynamic optical networks [48, 49]. Dynamic optical networks require dynamic optical devices such as adaptive optical power splitters. Recently, only a few adaptive optical power splitter structures have been reported and more details will be discussed in Chapter Two. However, these techniques have many limitations including, tolerance to environmental perturbations, high polarization dependence, and a limited numbers of output ports.

An Opto-VLSI processor integrated with optical components and a fibre optics port, could realize an adaptive optical power splitter. This adaptive optical splitter can be reconfigured via software to provide arbitrary optical power splitting ratios for multiple output channels. In addition, the adaptive splitter will have attractive features, such as a simple architecture, ability to synthesize arbitrary and accurate splitting ratios, low power loss, and easy user interface.

1.3 RESEARCH OBJECTIVES

The primary objective of this PhD project is to develop and demonstrate the concept of an adaptive optical power splitter based on Opto-VLSI technology and a 4-f imaging system, and to design an algorithm that can optimize the distribution of optical power in optical communications networks. In particular, the project will investigate the capability of the Opto-VLSI processor to adaptively split an optical beam into different output ports and then control the power of each port through multicasting computer-generated phase holograms.

During the process of realising the primary objective, several secondary objectives will be identified and achieved. These are:

- Develop an efficient algorithm for generating multicasting phase holograms for adaptive optical power splitting.
- Demonstrate a 1×2 adaptive optical splitter structure based on the use of an Opto-VLSI processor in conjunction with fibre collimator array and 4-f imaging system.
- Extend the number of the output ports of the splitter by demonstrate a 1×4 adaptive optical splitter based on an Opto-VLSI processor in conjunction with fibre array and 4-f imaging system.
- Develop a 1×N lossless adaptive optical splitter by incorporating Erbium-Doped Fibre Amplifiers (EDFAs) at different locations within the splitter structure.
- Demonstrate the concept of an adaptive optical combiner, with an array of fibre ports each having a different optical signal, which can combine the input signals into a single fibre port with a user-defined combination-weight.
- Implement the developed adaptive optical power splitter for realizing a broadband variable RF splitter/combiner.
- Apply the developed adaptive optical splitter in Photonic RF Signal Processing (PSP).

1.4 THE SIGNIFICANCE OF THE THESIS

Fibre-to-the-Home (FTTH) optical access networks are deployed on a large scale in many countries and Australia is currently in the process of deploying FTTH. Optical splitters are one of the main components required to establish efficient optical access networks. The need for these splitters is mainly to split the optical power to different subscribers.

This PhD thesis provides a novel architecture for optical splitters with the unique advantage of splitting the power adaptively in order to optimize the distribution of optical power in optical communication networks.

This PhD research project explores an adaptive splitter architecture that provides *N* numbers of splitting output ports with low insertion loss. This architecture is based on the use of an Opto-VLSI processor, which enables non-mechanical beam shaping, in combination with a fibre array, a 4f imaging system, and Erbium-Doped Fibre Amplifiers (EDFAs) for splitting loss compensation. The original contributions of this study include:

- Novel structures of an adaptive optical power splitter using an Opto-VLSI processor in combination with:
    1) A fibre collimator array and a single lens imaging system.
    2) A fibre array and a 4-f imaging system 'single lens'.
    3) A fibre array and an array of 4-f imaging system 'lens array'.
- Experimental Demonstration of an adaptive optical power combiner.
- Experimental Demonstration of a broadband variable RF splitter/combiner.
- Implementation of the adaptive optical combiner in photonic signal processing by experimentally realizing a reconfigurable photonic microwave filter.

1.5 OUTLINE OF THE LITERATURE STUDY

The literature study follows a logical approach in which the starting point is a general discussion about the need for adaptive optical splitters, including their applications.
The strategy review begins with Chapter Two which introduces and discusses various techniques used for realizing an adaptive optical splitter.

The study continues in Chapter Three where an introduction to Opto-VLSI technology is presented. It explores characteristics of the Opto-VLSI processor and its applications. The literature study concludes with a review of computer algorithm for generating multicasting phase hologram.

Chapter Four and Five presents the novel Opto-VLSI-based adaptive optical power splitter/combiner structures and show experimental results that demonstrate their concepts.

Chapter Six discusses the application of the developed splitter/combiner structures in photonic RF signal processing and experimentally demonstrate transversal RF filters hat can be tuned via the reconfiguration of the Opto-VLSI processor.

1.6 LAYOUT OF THE THESIS

In order to achieve the objectives of the study discussed above the following chapters and content of this dissertation are structured as follows:

Chapter 2: reviews the reported structures for splitting an optical signal adaptively.

Chapter 3: introduces Opto-VLSI technology by presenting the Opto-VLSI structure, the beam steering analysis, and the computer generated hologram. The Opto-VLSI and beam multicasting capability is also presented in this chapter.

Chapter 4: details the experimental demonstration of the proposed adaptive optical power splitter based on the use of Opto-VLSI processor and 4-f imaging system. The proof-of-concept of an adaptive optical combiner is also presented in this chapter.

Chapter 5: reports on the experimental demonstration of the proof-of-concept of a broadband adaptive RF power splitter/combiner based on the use of Opto-VLSI processor.

Chapter 6: presents the experimental demonstration of Photonic Microwave Filter employing an Opto-VLSI-Based adaptive optical combiner.

Chapter 7: concludes the dissertation. It reviews the study in terms of the research problems, construct development and empirical findings and ends with recommendations for further study.

1.7 SUMMARY

This chapter has introduced the background and context of the study, covering the research objectives and the significance of the thesis. The primary research objective, which is to develop an adaptive optical splitter based on an Opto-VLSI processor and 4-f imaging system, has been discussed. Several secondary objectives, which are crucial for realizing the primary research objective, have also been discussed.

The chapter concluded with the layout of the dissertation in order to achieve the objectives of the study.

The next chapter introduces several techniques that have already been reported for realizing an adaptive optical power splitter.

CHAPTER 2

ADAPTIVE OPTICAL POWER SPLITTERS OVERVIEW

2.1 INTRODUCTION

Optical power splitter devices can be divided into two types, namely, passive and dynamic splitters. Passive optical splitters split the optical beam up to *N* beams output ports with fixed splitting ratios, while the splitting ratios of a dynamic optical splitter can be arbitrary. Passive optical splitters with different ratios such as 1×2, 1×4, 1×8, and 1×16 are readily available products in the market.

Several different technologies for realising passive optical beam splitters have already been reported. Most of these structures use photonics crystals (PC), and are based on the waveguide branching (Y-branches) [50, 51], directional coupling [52, 53], multimode interference (MMI) [54, 55], and ring resonator theories [56, 57]. However, some splitters can be designed so that during their fabrication they will generate different fixed power ratios at the output ports [58]. For example, MMI-based devices with tapered MMI regions have demonstrated variable power splitting ratio capabilities. However, continuous tuning of the splitting ratio within a single device structure cannot be achieved with this approach [59]. Bent MMI structures, with arbitrary power splitting ratios, have been reported [60]. Arbitrary splitting is achieved by inducing a specific wavefront phase change via an angular bend within the MMI region. Since the splitting ratio is a function of the width of the MMI region [61], it is impractical to achieve dynamic splitting ratio for a small number of output ports. Recently, new approaches, based on plasmonic nanoslits for realizing passive optical power splitters, have been reported [62, 63]. However, while surface Plasmon technology is a new promising research field, it is not yet to be proven viable for many future applications including optical splitters.

Adaptive optical power splitters based on several techniques have already been reported. In this Chapter, different techniques for realizing adaptive optical power splitting will be reviewed.

2.2 PASSIVE OPTICAL POWER SPLITTER INCORPORATING SOAs

Fig. 2.1 illustrates a simple dynamic optical splitter structure realized by incorporating a semiconductor optical amplifier (SOA) into each output port of a PLC-based passive splitter [64]. However, such a structure is relatively expensive and has fundamental limitations, namely, high output noise levels generated by the individual optical amplifiers, and the difficulty in controlling the output power level, since the optical amplifier gain depends on the power level of the split optical signal.

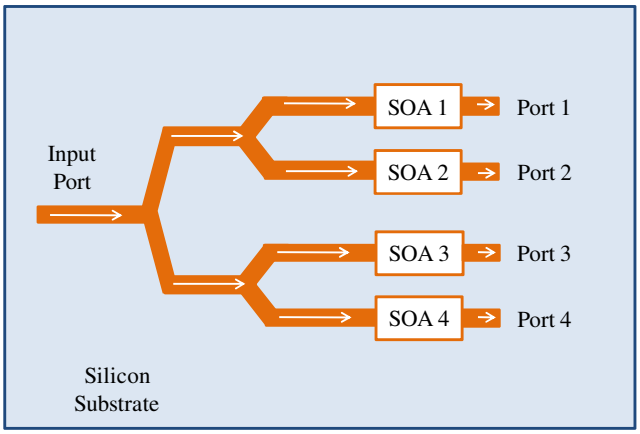

Fig. 2.1. Dynamic splitter by incorporating an optical amplifier into each output port of a passive splitter based on planar lightwave circuits.

2.3 MACH-ZEHNDER INTERFERENCE TECHNIQUE

An adaptive optical power splitter can be realized by using Mach-Zehnder interference techniques. Fig. 2.2 shows a reported optical splitter structure where two single mode fibre couplers are used to realise a Mach-Zehnder interferometer [65]. The common fibres of the couplers form the two interference arms (Arm_1 and Arm_2) of the interferometer.

An input optical power launched into the input port P_{in} is split into two output ports, P_1, and P_2. The power level of each output is a function of the optical phase difference of the two interference arms. Therefore, variable splitting ratio of, P_1/P_2 is achieved by controlling the optical phase difference of the two interference arms. Different methods, such as electric field [66], magnetic field or heat can be applied to vary the arms' length, thus controlling the optical phase difference between the two arms.

The main disadvantage of this technique is impractically for achieving multiport output power.

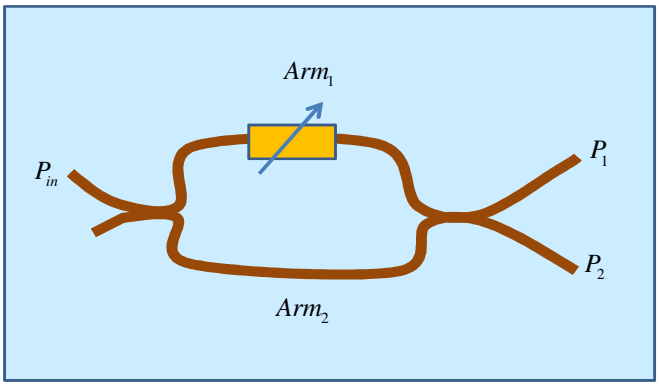

Fig. 2.2. Configuration of Mach-Zehnder interference using two fibre couplers, thus realizing a variable optical power splitter.

2.4 VARIABLE TRANSMISSION-REFLECTION FILM BASED SPLITTERS

An adaptive optical power splitter can also be achieved by using variable transmission-reflection thin film, where an incident optical signal is split into two signals i.e. transmitted and reflected signals, as is illustrated in Fig. 2.3 [65]. The thin film is designed to have linear variable transmission-reflection along the film plane. The transmitted and reflected signals are varied by rotating the film around its axis. Liming Zheng and Meili Zhu have reported a dynamic splitter using the same principle on channel waveguide [67]. This technique not only has a limited number of output ports but also has limited reliability due to the need to mechanically move the film.

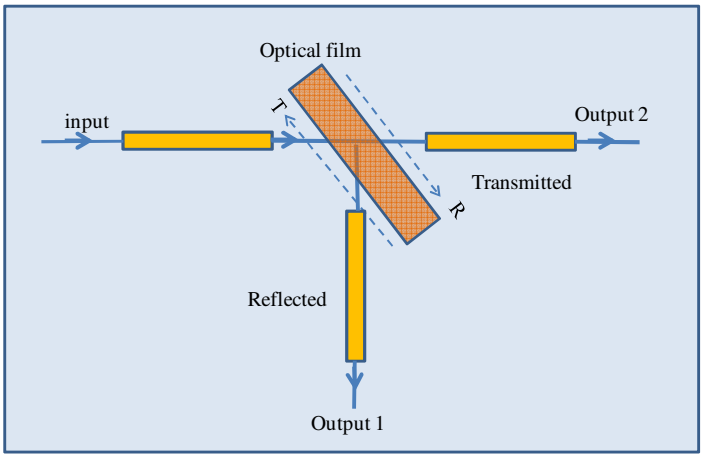

Fig. 2.3. Adaptive optical power splitter based on the use of optical film with linear variable transmission-reflection.

2.5 ACOUSTO-OPTIC BASED OPTICA POWER SPLITTERS

An RF signal applied to an acoustic crystal will generate an acoustic wave inside the crystal [68]. The frequency of the acoustic wave is equal to the RF signal frequency and its intensity is proportional to input electrical signal intensity [65]. Fig. 2.4 shows an example of an optical beam splitter based on acousto-optic effects using a material such as $LiNbO_3$. An incident optical beam of specific incident angle, 'Bragg angle', passing through the crystal interacts with a traveling-wave index perturbation generated by the acoustic wave. As a result, part of the optical beam is deflected by 2 Θ_B and frequency shifted by an amount equals to the acoustic frequency. The power ratio of the deflected and incident optical beams is called the diffraction efficiency and is expressed by:

$$\eta = sin^2\left[\frac{\pi.\Delta n.L}{\lambda cos\theta_B}\right] \tag{2.1}$$

where Δn is the crystal index perturbation resulted from acoustic wave, L is the distance the optical beam travels through the acoustic wave, λ is the vacuum wavelength of the optical beam, and θ_B is Bragg angle determined by

$$sin\theta_B = \frac{\lambda}{2£} \tag{2.2}$$

where £ is the acoustic wavelength.

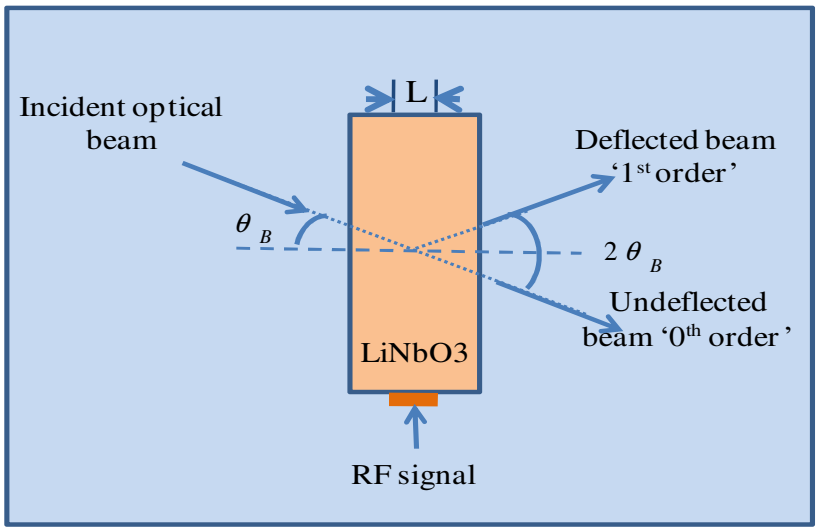

Fig. 2.4. Adaptive optical power splitter based on acousto-optic deflection effect.

This technique allows controlling only the power of the deflected '1storder' at an incidence angle equals to the Bragg angle, which is precisely determined. Note that any deviation from Bragg angle results in the appearance of more uncontrollable deflected beams (more orders cause power loss of 1storder). Therefore, this technique is impractical not only for 1×2 splitters but also for higher output port counts.

2.6 MOVABLE HALF WAVE PLATE BASED 1×2 ADAPTIVE OPTICAL SPLITTERS

A 1×2 adaptive optical power splitter structure based on the use of a half wave plate and optical polarization components has experimentally been demonstrated [69], where an arbitrary optical splitting ratio is realized by mechanically rotating a half wave plate, as illustrated in Fig. 2.5. The splitter consists of a standard collimator, birefringent displacers, a rotatable half wave plate, half wave plates, a roof prism, and a dual fibre collimator.

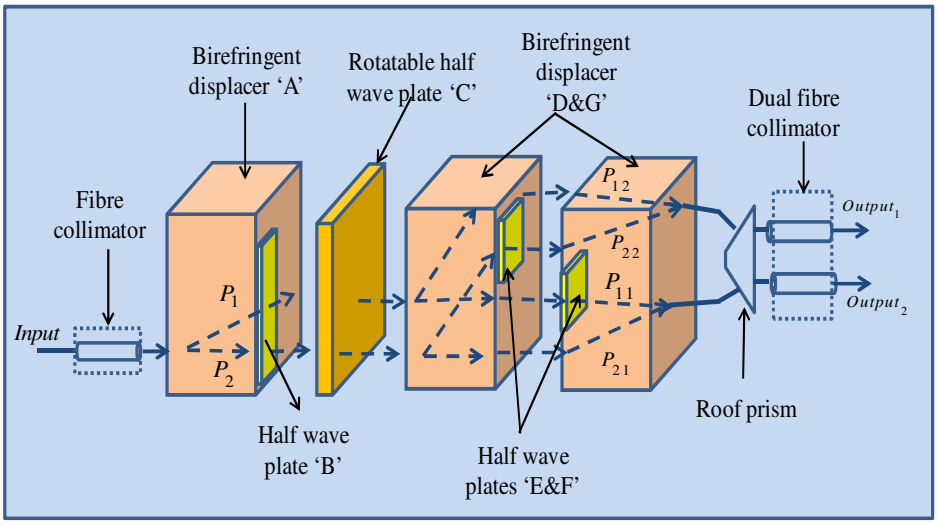

Fig. 2.5. Adaptive optical power splitter structure based on the use of a rotatable half wave plate and optical polarization components.

The operation of the splitter is briefly explained as follows: The input fibre collimator is used to launch the input optical beam. The birefringent displacer 'A' is used as a first displacer to split the input optical beam into two perpendicular polarized lights P_1 and P_2. The half wave plate 'B' is used to transfer Beam P_2 into same polarization state of Beam P_1. The rotatable half wave plate 'C' is used to change the state polarization of both Beams P_1 and P_2. The birefringent displacer 'D' is used as a second displacer to separate Beams P_1 and P_2 into two pairs of light; each one will have perpendicular component, P_{11}, P_{12} and P_{21}, P_{22}, respectively. The half wave plate 'F' is used to transfer Beam P_{22} into the same polarization state of as- Beam P_{12}. The half wave plate 'E' is used to transfer Beam P_{11} into same polarization state of Beam P_{21}. The birefringent displacer 'G' is used to combine 'P_{12} and P_{22}' and 'P11 and P_{21}' into two output beams, $Output_1$and $Output_2$, respectively. The roof prism couples the output light into the dual fibre collimator.

The main disadvantages of this splitter structure are (i) limited reliability due to the wear and tear of the mechanically rotated wave plate, and (ii) the inability to independently control the output power levels of the split signals.

2.7 FIBRE BRAGG GRATINGS (FBGS) BASED ADAPTIVE OPTICAL SPLITTERS

An adaptive optical splitter employing thermally-tuned fibre Bragg grating (FBGs) has also been reported [70]. The device structure comprises a circulator and a dynamic FBG which can achieve different reflection ratios corresponding to the size of the current applied across the dynamic FBG as in Fig. 2.6. The circulator has three Ports P_0, P_2 and P_3, and the dynamic FBG has two Ports, P_1 and P_4. The input light to Port P_0 output from Port P_3 reaches the FBG through Port P_4. The dynamic FBG comprises an optical fibre whose refractive index varies with the temperature. A thermal electric cooler (TEC), is attached to one flat side section of the optical fibre and acts as a heat sink and temperature controller to maintain that section of the optical fibre at a predetermined temperature. A thin layer of thermal epoxy is attached to ensure good thermal conductivity between the optical fibre and the TEC. Micro heating elements 'thermal resistance' are electrically connected together in series by bonding wires, as in Fig. 2.6(b).

When an electrical current is applied across the two terminals of the series of heating elements, each element will generate a constant temperature profile as long as the current remains constant. The cross sections of the optical fibre between each two elements has approximately the same temperature as that of the TEC, due to the large contact area of the fibre cross sections with the TEC than the heating elements, and the TEC has larger heat transfer capacity. Hence, a series of hot spots distributed along the optical fibre section, that generates a periodic pattern of refractive indices. By varying the current, the temperatures of the hot spots changes, leading to change in the periodic refractive indices. The reflected wavelength is determined by the pitch of the dynamic FBG, and the distance between two hot spots.

As shown in Fig. 2.6, all light passes through Port P_1 when no electrical current is applied across the heating elements i.e. no Bragg grating effect is experienced; this state is called 'all pass' state. All light passes through the Port P_2 when a maximum electrical current is applied across the heating elements. In this case, the Bragg condition is met with nearly 100% reflection; this state is called 'all reflect' state.

While the principle of this structure is easy to understand, it is impractical, however, due to its high packaging cost and limited tolerance to environmental perturbations (temperature, vibrations, etc).

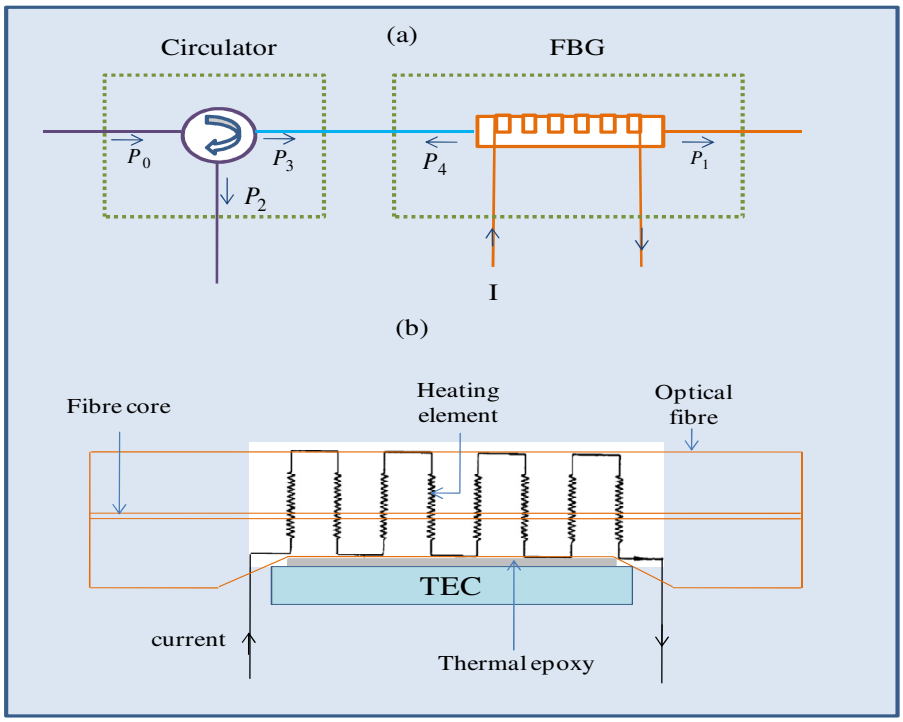

Fig. 2.6. (a) Adaptive optical splitter employing thermally-tuned fibre Bragg grating (FBGs) device structure comprising a circulator and a dynamic FBG, (b) FBG layout.

2.8 DYNAMIC SPLITTER BASED ON OPTO-VLSI PROCESSORS

The first attempt for realizing an optical power splitter based on the use of an Opto-VLSI processor was reported by Matic [71]. He demonstrated a passive splitter with reconfigurable output port count. For realizing dynamic splitting ratio, a 1×3 dynamic optical splitter using an Opto-VLSI processor, in conjunction with custom-made piecewise linear optics has been reported [72], as illustrated in Fig. 2.7. However, this splitter architecture requires custom-made piecewise linear optics integrated with a fibre collimator array, making its mass production very difficult, especially when the number of output ports is large.

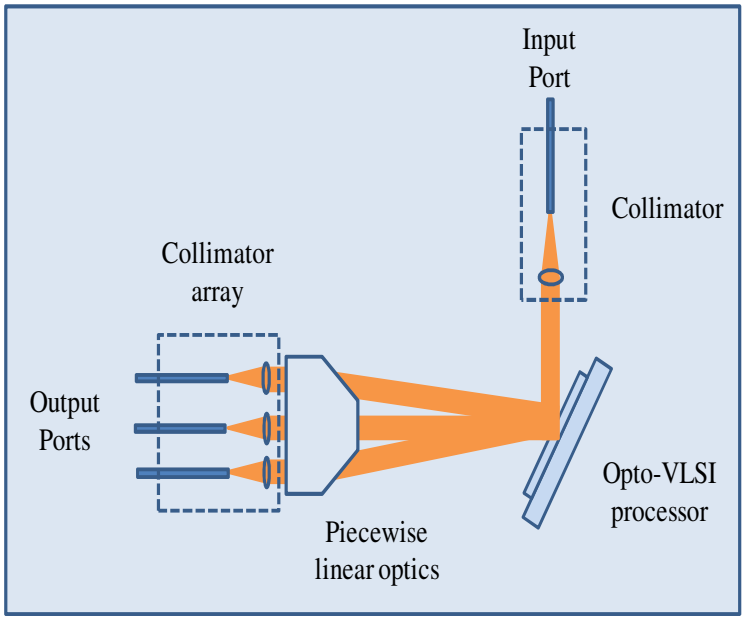

Fig. 2.7. Dynamic splitter based on Opto-VLSI employing custom-made piecewise linear optics.

2.9 SUMMARY

In this chapter, we have discussed and reviewed the techniques that have recently been reported for realizing adaptive optical power splitting ratios. These included, a passive splitter incorporating semiconductors optical amplifiers, Mach-Zehnder interference technique, variable transmission-reflection film, acousto-optic principles, movable half wave plate, fibre Bragg gratings (FBGs), and Opto-VLSI processors.

CHAPTER 3

OPTO-VLSI FOR SPATIAL MODULATION OF LIGHT

3.1 INTRODUCTION

Optical devices for beam steering have many applications particularly in optical communication and photonic microwave signal processing. Several technologies including lenslet array, micro-mirrors array, and liquid crystal on silicon (LCOS) have been developed to demonstrate mainly beam steering without any moving part [73]. During the last Four decades, potential research efforts have focused on enhancing the physical dimensions, resolution, fill factor, and response time, leading to highly efficient LCOS technology.

An Opto-VLSI processor is a motionless reconfigurable optical device based on LCOS and has been widely used in a variety of applications due to its capability to shape/steer polarized incident laser beams by applying an electric field across the liquid crystal layout.

This chapter presents a brief discussion on the Opto-VLSI processor architecture and its principle of operation. In Section 3.2, we describe a generic Opto-VLSI processor structure, and then discuss its beam steering capability in Section 3.3. The theory of Opto-VLSI processing is presented in Section 3.4. The chapter continues by introducing computer generated steering hologram in Section 3.5 and particularly simulated annealing algorithm in Section 3.6. Finally, the generation of multicasting phase hologram in discussed in Section 3.7.

3.2 OPTO-VLSI PROCESSOR STRUCTURES

The Opto-VLSI processor, also known as spatial light modulator (SLM), is an electronically-driven, motionless diffractive element that can steer/reshape an incident laser beam. Illustrated in Fig. 3.1, an Opto-VLSI processor in corporate an array of liquid crystal (LC) cells addressed by a Very-Large-Scale-Integrated (VLSI) circuit [74] that generates phase holograms capable of arbitrary steering and /or multicasting input laser beams. By depositing a quarter-wave-plate (QWP) layer between the LC layer and the aluminum mirror polarization-insensitive operation can be accomplished [75]. Also the use of a transparent Indium-Tin Oxide (ITO) layer as a ground electrode minimizes the optical insertion loss of the Opto-VLSI processor. The voltage of each pixel can individually be adjusted using memory elements that can select a voltage level between zero and saturation voltage, then apply it, through both electrodes, across each LC cell.

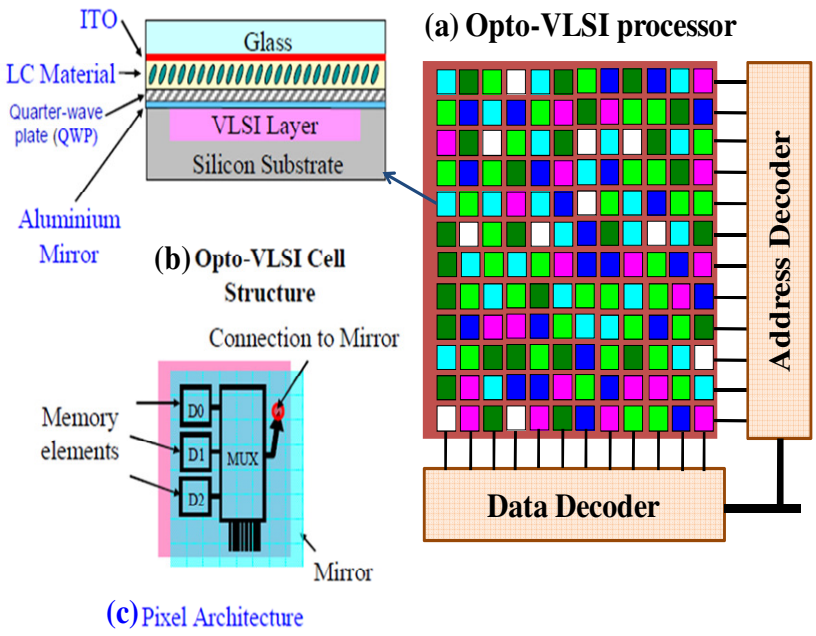

Fig. 3.1. (a) 2D Opto-VLSI processor layout, (b) Opto-VLSI cell structure and (c) pixel architecture.

3.3 NONMECHANICAL OPTICAL BEAM STEERING

The principle of nonmechanical beam steering can be understood by considering the effect of a prism on an incident collimated beam normal to a surface, as illustrated in Fig.3.2(a). The light beam changes its speed as it moves from air to the glass of the prism, thus the light is refracted in the glass and bent after exiting the prism by and angle that depends on the refractive indices of the two media (Snell's law) and the apex angle of the prism [76].

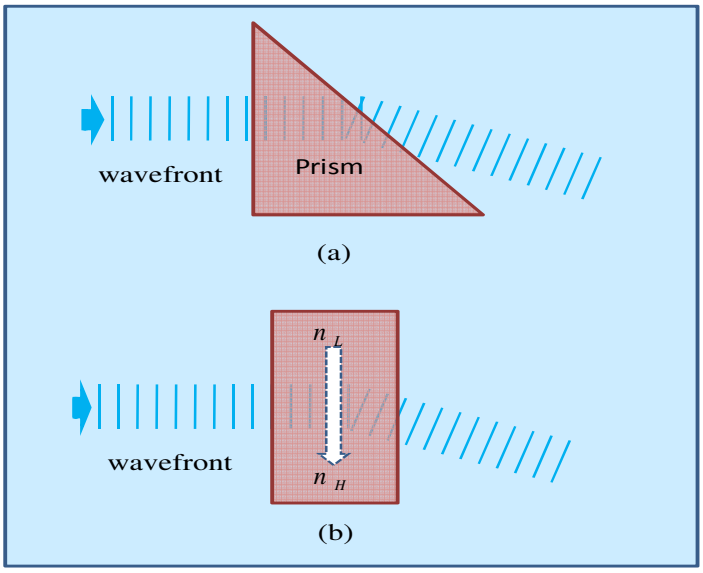

Fig.3.2. (a) Beam steering prism principle and (b) graded refractive index thin film.

A prism can also be constructed with a thin film that has a gradual change in the refractive index from a lower value to a higher value across the horizontal direction of the optical path, as illustrated in Fig.3.2(b), and this results in a gradual change in the average propagation velocity within the material [73]. Therefore, due to the difference in the propagation velocity, the beam is steered towards the region of higher refractive index. Light steering by a prism is the basis of the beam steering mechanism of the Opto-VLSI processor.

3.4 OPTO-VLSI PROCESSOR FOR BEAM STEERING

In an Opto-VLSI processor, the VLSI circuit allows changing the refractive index of the LC layer by independently driving each pixel by a voltage, thus applying an electric field across the LC layer. Typically, the individual electrodes are addressed independently using a 8-bit controller (i.e. with a digital voltage level of 0 to 255). Typical behaviour of a prism can be emulated by electronically addressing the individual pixels of LC, as shown in Fig. 3.3. Since the LC switching speed is inversely proportional to the square of the thickness of the LC layer [77], keeping the liquid crystal layer thin leads to a fast response.

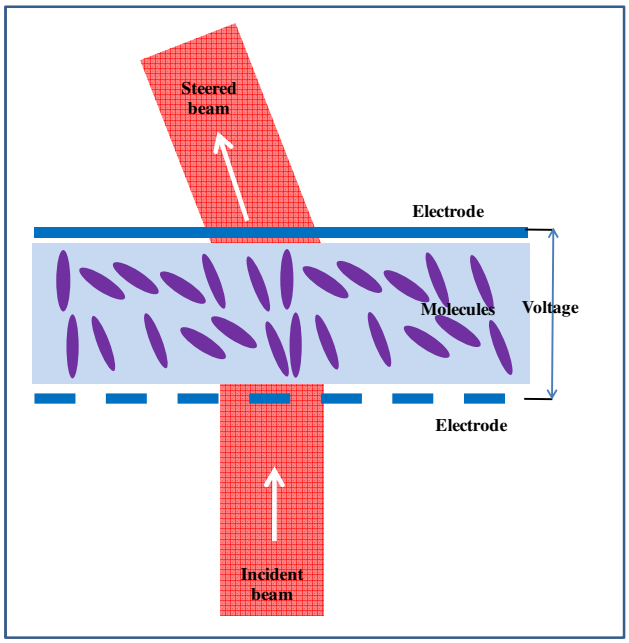

Fig. 3.3 An optical beam experiencing deflection after passing through liquid crystal molecules.

A prism can be realised by driving the liquid crystal based-optical processor with a modulo 2π sawtooth ramp, as shown in Fig. 3.4. By changing the period and maximum phase of the saw-tooth waveform, an adaptive grating can be realised that can steer incident beam along arbitrary directions [73, 78].

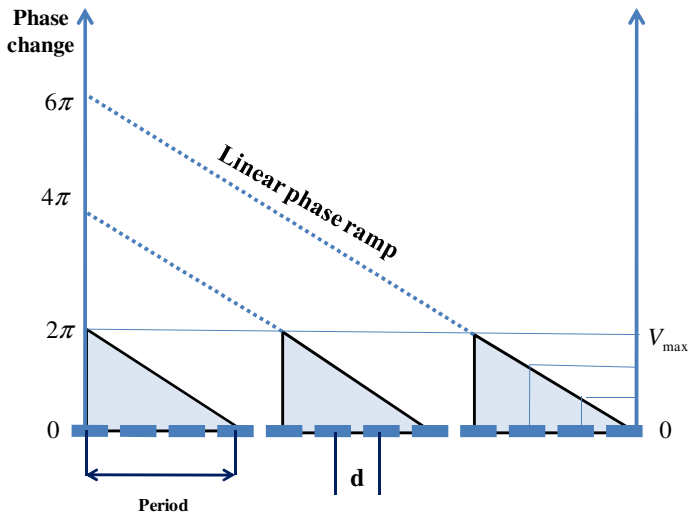

Fig. 3.4 A prism formed by addressing electronically a pixel block with a saw-tooth-like phase profile with a maximum phase shift of 2π.

The quantised voltage applied across the liquid crystal pixels electrodes of grating period results in a step-wise phase ramp and the incident beam will be steered to a certain angle given by:

$$\theta = arcsin\left(\frac{\lambda}{q \times d}\right) \tag{3.1}$$

where λ is the wavelength of the incident beam, q is the number of pixels within the grating's period, d is the pixel pitch.

A large grating period $(q \times d)$ leads to a smaller steering angle. Fig. 3.5 and Fig. 3.6 shows different phase gratings formed by uploading phase hologram corresponding to a grating period of 256 and 128 steps, respectively, onto a 1-D Opto-VLSI processor. Higher diffraction orders are generated due to the quantisation of the grating period, leading to poor diffraction efficiency. The first order diffraction efficiency η_1 is given by [79]:

$$\eta_1 = \left(\frac{\sin(\pi/q)}{\pi/q}\right)^2 \tag{3.2}$$

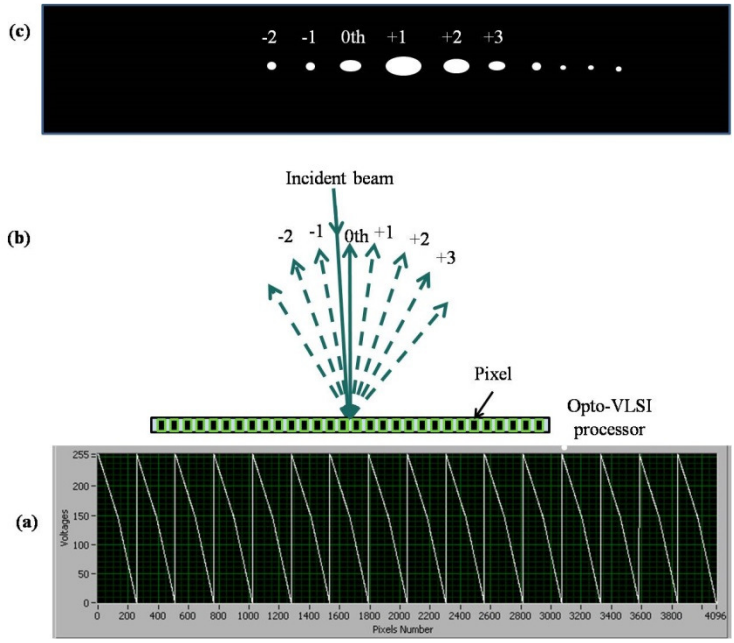

Fig. 3.5. (a) A 1×4096 Opto-VLSI processor addressed electronically to form a phase grating with a grating period of 256 pixels. (b) Incident beam steered to angle θ =0.19 degree and (c) high diffraction orders are generated due to the quantisation of the grating period.

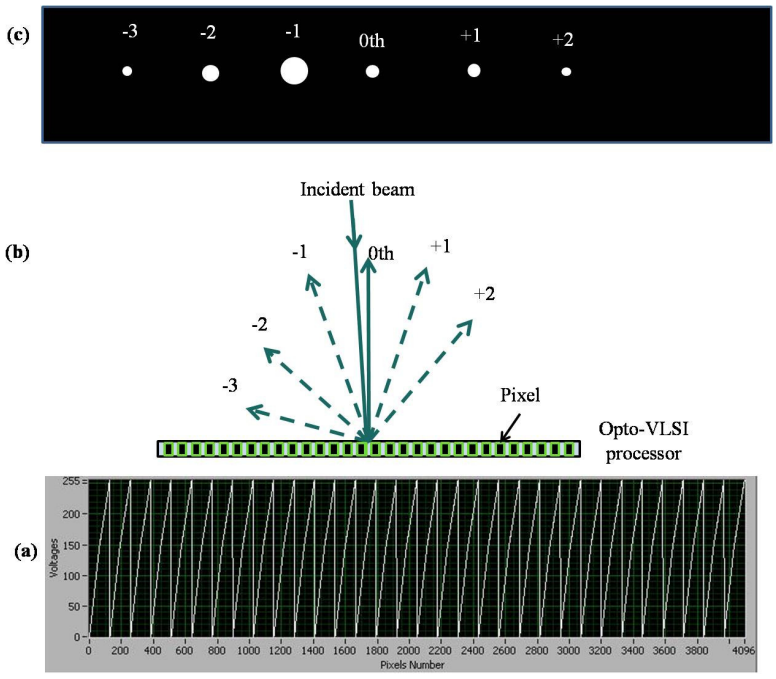

Fig. 3.6. (a) A 1×4096 Opto-VLSI processor addressed electronically to form a grating with a grating period of 128 pixels. (b) Incident beam steered to angle θ =0.38 degree and (c) high diffraction orders are generated due to the quantisation of the grating period.

Switching from high to low phase levels called flyback as illustrated in Fig. 3.7, has significant effect on the diffraction efficiency i.e. the flyback region steers a portion of the incident beam along an undesired direction. The diffraction efficiency can be expressed theoretically by rewriting Equation 3.2 as follows [80]:

$$\eta_{total} = \left(\frac{\sin(\pi/q)}{\pi/q}\right)^2 \left(1 - \frac{\Lambda_F}{q.d}\right)^2 \tag{3.3}$$

where Λ_F is the width of the flyback region. Investigation of the pixilation as well as the flyback effects on the diffraction efficiency of an Opto-VLSI processor has been reported in [81]. Experimental results have shown that the flyback significantly reduces the steering efficiency when the number of pixels per phase hologram period is low [81].

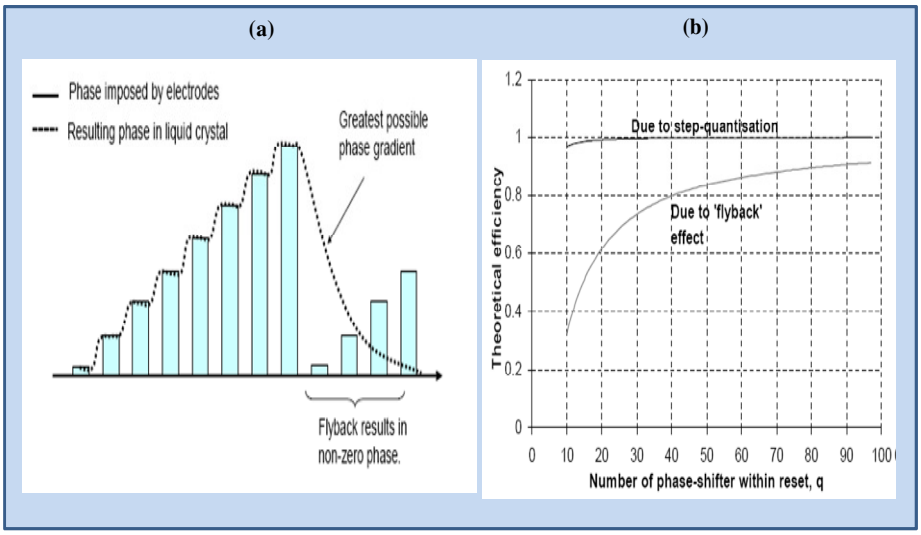

Fig. 3.7. Flyback region due to switching from high to low phase levels. (b) impact of flyback on diffraction efficiency [81].

3.5 COMPUTER-GENERAED PHASE HOLOGRAM

The essential problem of generating phase holograms is to calculate the phase distribution, $h(x,y)$ in the hologram plane for a target diffracted intensity pattern, $T(v,u)$, which is given by:

$$T(v,u) = \iint h(x,y)e^{2\pi j(ux+vy)}dxdy \tag{3.4}$$

The ideal hologram profile for beam steering/multicasting applications can be found by analysing the simple wave propagation equation:

$$U = e^{j(\vec{k}.\vec{r}-wt)} \tag{3.5}$$

where,

$\vec{k}$ is the propagation constant determine the beam direction

$\vec{r}$ is the position vector.

When the wavefront encounters a linear phase retardation across a plane $e^{j(\vec{a}.\vec{r})}$, the new wavefront will be in the form of, $e^{j(\vec{k}'.\vec{r}-wt)}$ travelling in a direction, $\vec{k}' = \vec{k} + \vec{a}$. If a hologram provides a linear varying phase profile, the beam direction can be changed without distorting the beam itself. Since the phase levels of 0 and 2π are equivalent, a sawtooth grating profile can be generated by varying the phase linearly from 0 to 2π. Therefore, an approximation to the sawtooth grating proposed by Dammann [82] can be realised by an Opto-VLSI processor. Fig. 3.8 illustrates the difference between a sawtooth grating and a Dammann grating. The theoretical calculation of the diffraction efficiency of Dammann grating is simply based on Fourier transform (FT) and is given by [83]:

$$\eta = \frac{|\int F(u)du|^2}{\int |F(u)|^2 du} \tag{3.6}$$

where

$F(u)$ is Fourier transform of the desired signal shape, and $f(x)$ represents the target diffracted pattern.

For example if, $f(x) = \delta(x - x_o)$, then $F(u) = \exp(j2\pi u x_o)$, and $\eta = 100\%$. This theoretical value is impossible to achieve by practical phase holograms.

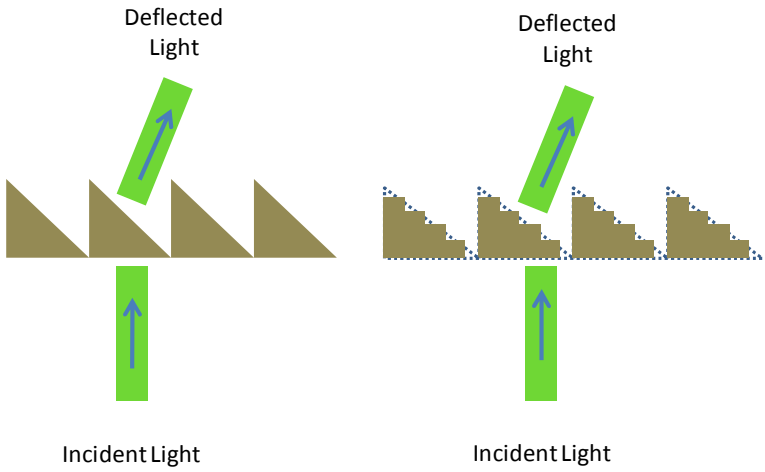

Fig. 3.8. Sawtooth grating (on the left) and Dammann grating (on the right).

Several computer algorithms, such as the genetic, simulated annealing, conjugate-gradient, Gerchberg-Saxton and projection-onto-constraint-sets algorithms [84-88], have been used for generating optimized steering/multicasting phase holograms that produce a target far-field distribution, defined by the replay beam positions and the corresponding target diffracted intensity pattern.

3.6 SIMULATED ANNEALING ALGORITHM

Simulated annealing is a random search technique proposed and developed to deal with highly nonlinear problems by finding the global minimum of a cost function that may possess several local minima. The technique is based on emulating the physical process i.e. a metal cools and freezes into a minimum energy crystalline structure. Dames et al. [89] converted the simulated annealing principle into a computer algorithm that generate phase hologram distribution for a target diffracted intensity profile. A flow chart that describes the simulated annealing is illustrated in Fig. 3.9. Typically, the algorithm starts from an initial random hologram pattern, $h(x, y)$ and computes the resulting diffraction field. Fourier transform is used to compute the diffracted beam $H(k, l)$ and can be expressed as [84]

$$H(k,l) = DFT\big(h(m,n)\big) \tag{3.7}$$

where (k,l) represents the coordinates in the output plane. The cost function can be computed by [84]

$$C = \sum(H(k,l) - |H_T(k,l)|^2)^2 \tag{3.8}$$

where $T(k,l)$ is the target intensity at defined point in the diffraction field. By randomly changing h and recalculating the cost function, the target requirement is achieved.
The termination of the algorithm occurs after a certain number of iterations. If the cost meets the target requirement, the program will terminate before completing the number of iterations. The probability of finding the appropriate pixel/s is exponential function of temperature while the temperature is exponential function of the total number of desired iterations [84].

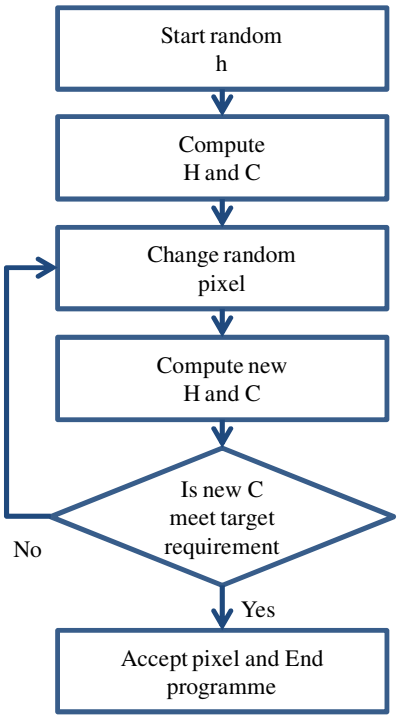

Fig. 3.9. A flow chart describes simulated annealing algorithm [84] .

3.7 OPTO-VLSI AND MULTICASTING PHASED HOLOGRAM

For multicasting applications by means of splitting an optical beam to *N* numbers of beams in different direction or positions, computer generated hologram (CGH) algorithms can be used to compute the desired far-field distribution that define the split-beam profile 'peak amplitude' at specified position, as illustrated in Fig. 3.10.

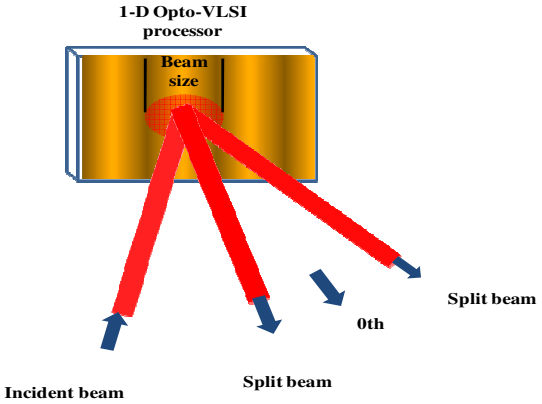

Fig. 3.10. Opto-VLSI processor can be used for beam multicasting by means of splitting an optical beam to N numbers of beams to different direction with controllable intensity of each split beam.

To accurately split an incident optical beam onto an Opto-VLSI processor, a high splitting-angle resolution is required and is given by:

$$\alpha = \arcsin\left(\frac{\lambda}{N \times d}\right) \tag{3.11}$$

where λ is the wavelength of the incident beam, N is the number of pixels illuminate by the incident beam, d is the pixel pitch. Table 3.1 shows high angle resolution can be achieved by illuminating more pixels. High resolution leads to accurately splitting the optical beam to the right direction, thus avoiding optical loss caused by the quantization of the splitting angle.

Table 3.1. Splitting angle resolution for a given number of pixels 'N'. Small angle leads to high splitting angle resolution.

N pixels	Resolution (rad)
500	0.001722
1000	0.000861
1500	0.000574
2000	0.000431
2500	0.000344

In this PhD project, a special algorithm has particularly been developed to compute the targeted phased distribution of the replay-field. According to the Opto-VLSI characteristics, the computed phased distribution is used to compute the discrete voltage distribution needed to derive the pixels of the Opto-VLSI processor.

A LabVIEW computer program was especially developed to drive the Opto-VLSI processor and generate the desired phase holograms that split an input signal arbitrarily and accurately to multiple output optical fibre ports, and also combine multiple input signals with arbitrary weights into a single output optical fibre port. For a target diffracted intensity profile, an optimised phase hologram can always be generated, which minimizes the zeroth order diffraction and maximizes the signal-to-crosstalk ratio at every output port. Experimental results will be presented in the next chapter.

3.8 SUMMARY

In this chapter, we have briefly discussed and reviewed the fundamental of the Opto-VLSI technology, covering the analysis of nonmechanical optical beam steering, computer-generated phase holograms, simulated annealing algorithm, and multicasting phase holograms.

CHAPTER 4

OPTO-VLSI-BASED ADAPTIVE OPTICAL POWER SPLITTERS

4.1 INTRODUCTION

The key parameters that are considered when assessing an optical power splitter includes insertion loss, output port count, compact size and cost.The use of a reconfigurable Opto-VLSI processor, in conjunction with optical components, could lead to a adaptive optical power splitter that has additional advantages including:

(i) Both optical signal splitting and combining are achieved through software using the same structure.

(ii) High diffraction efficiency (i.e. lower optical loss) as more pixels are covered by the input optical beams.

(iii) Low inter-port crosstalk.

(iv) Simple user interface.

(v) Compressed hardware and compact packaging.

This chapter presents the experimental results of the proposed Opto-VLSI-based adaptive optical power splitter. The first part (Section 4.2) begins with the description and advantages of a 4-*f* imaging system configuration, followed with the integration of the Opto-VLSI processor with the 4-f imaging system for the realisation of an adaptive optical splitter. The second part (Sections 4.3- 4.5) demonstrates the principles of several adaptive optical power splitter structures, implemented through:

(i) Integration of the Opto-VLSI processor with, a fibre collimator array and 4-f imaging systems (single lens).

(ii) Integration of the Opto-VLSI processor with, a fibre array, and a 4-f imaging system (single lens).

(iii) Integration of the Opto-VLSI processor with, a fibre array, optical amplifiers, and an array of 4-f imaging system (lens array).

In Section 4.6, we also demonstrate the use of the proposed splitter as an adaptive optical combiner that combines optical signals launched into multiple input ports into a sin-

gle output port with variable combination ratios. The chapter concludes with a discussion on the total insertion loss (Section 4.7) of the splitter and how it can be minimised.

4.2 PROPOSED ADAPTIVE OPTICAL POWER SPLITTER

4.2.1 4-*f* imaging system

Typically, the 4-*f* imaging system configuration is used in many optical devices [90-92]. The configuration of a 4-*f* imaging system can be approached in different ways [91]. A simple schematic diagram of a 4-*f* imaging system set-up built of two identical cascade lenses of focal lens '*f*' as illustrated in Fig. 4.1. A fibre input port located at the input plane'S_1'emits a diverging spherical wave which is then collimated via Fourier lens 'L_1'. The collimated beam is transformed by Fourier plane 'S_2'to Fourier lens 'L_2', which is then focused back into the output fibre port. This set-up allows the input optical beam to travel a distance of 4-*f* till the beam is focused back into the output fibre port where the output plane 'S_3' is located.

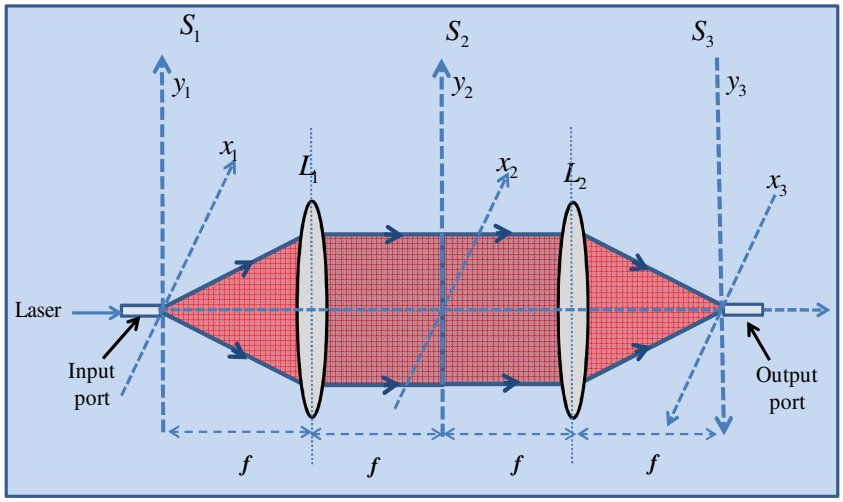

Fig. 4.1. Schematic diagram of 4-f imaging system configuration.

The size of the collimated beam can be determined using the beam magnification formula given by [93]

$$M = \frac{w''}{w_0} = \frac{1}{\sqrt{\left(\frac{f-s}{f}\right)^2 + \left(\frac{z_R}{f}\right)^2}} \tag{4.1}$$

where s is the distance between the lens and the input port, $w_0$is the size of the input optical beam, w'' is the size of the collimated optical beam, and z_R is called Rayleigh range and is given by [93]

$$z_R = \frac{\pi w_0^2}{\lambda} \tag{4.2}$$

In the case of a 4-f imaging system where the input port is placed accurately at a distance $s = f$, the size of the expanded beam is given by

$$w'' = \frac{\lambda f}{\pi w_0} \tag{4.3}$$

where λ is the wavelength of the input optical beam.

The horizontal offset of the input fibre port causes an error on the output Gaussian beam size. To investigate the input fibre position offset effect on the beam output size, Eq.(4.1) can be rewritten as

$$w'' = \frac{w_0}{\sqrt{\left(\frac{\pm\Delta z}{f}\right)^2 + \left(\frac{z_R}{f}\right)^2}} \tag{4.4}$$

where $\pm\Delta z = f - s$, is the horizontal offset of the input fibre port. The positive/negative offset value refers to the fibre distance from the lens, whether it is bigger/smaller than the actual focal length *'f'*.

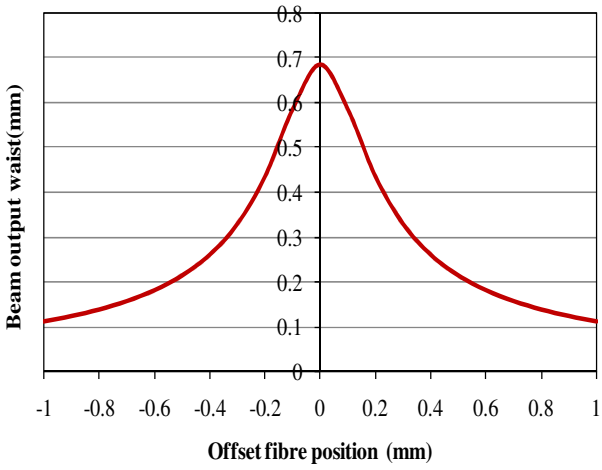

Fig. 4.2. The effect of the horizontal offset of the input fibre port on the output beam size.

For example, an input beam of w_0 = 9μm, λ =1550nm, and a lens of focal length f=12.5mm, the output beam waist is 0.68mm. Fig. 4.2 shows the output beam waist versus the horizontal offset of the input fibre port. It is clear that the maximum value (0.68mm) of the beam's waist is at zero offset, which is the typical value calculated using Eq. (4.5).

4.2.2 Opto-VLSI processor integrated with a 4-f imaging system

The transmission-mode 4-*f* imaging system configuration shown in Fig. 4.1 can be modified to a reflection-mode configuration by using an Opto-VLSI processor, a single Fourier lens, and a fibre array port as illustrated in Fig. 4.3. Forming a 4-f imaging system using an Opto-VLSI processor in combination with a Fourier lens and a fibre array port offers advantages such as:

- Simple configuration.
- Allows an input optical beam to be expanded and focused back into the output ports.
- Easy packaging through compressed hardware.

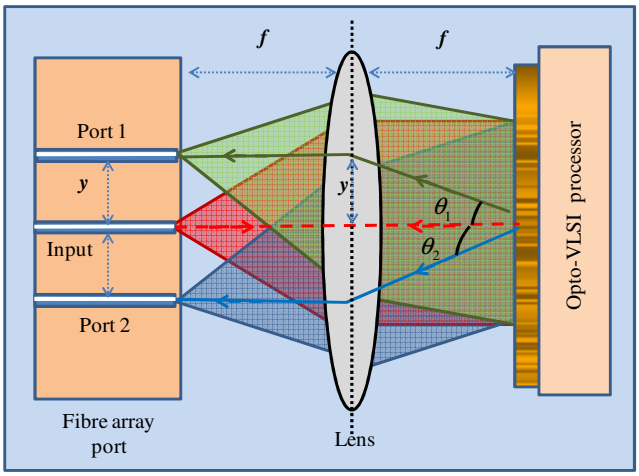

Fig. 4.3. An opto-VLSI processor integrated with Fourier lens and Fibre array port to form a 4-f imaging system configuration.

The corresponding splitting angle of each output port with respect to the 0^{th} order is expressed by

$$tan\theta_1 = \frac{y}{f}, \quad tan\theta_2 = \frac{-y}{f} \tag{4.5}$$

where y is the fibre-to-fibre space of the fibre array port and f is the focal length. Eq. (4.5) shows that the splitting angle depends on two parameters, the focal length and the fibre-to-fibre spacing. Therefore, in addition, the lens diameter (relevant to the optical beam size), and the Opto-VLSI active window size, must be collectively considered in order to design the proposed device structure.

An adaptive optical power splitter can be realised through two designs:

(i) Opto-VLSI processor employing single lens to form a 4-f imaging system.

(ii) Opto-VLSI processor employing lens array to form an array of a 4-f imaging system.

A fibre array or a fibre collimator array can be used in the first approach, illustrated in Fig. 4.4, in order to investigate the limitation of splitting an input optical signal and couple it into a large number of output ports. The second design, illustrated in Fig. 4.5, is capable of solving most of the limitations of the first design.

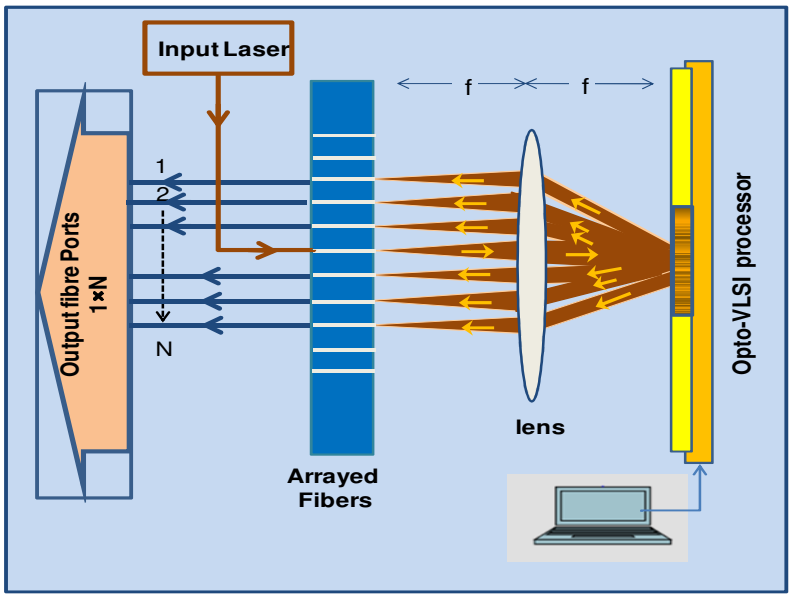

Fig. 4.4. Opto-VLSI-based adaptive optical power splitter employing a single 4-f imaging system.

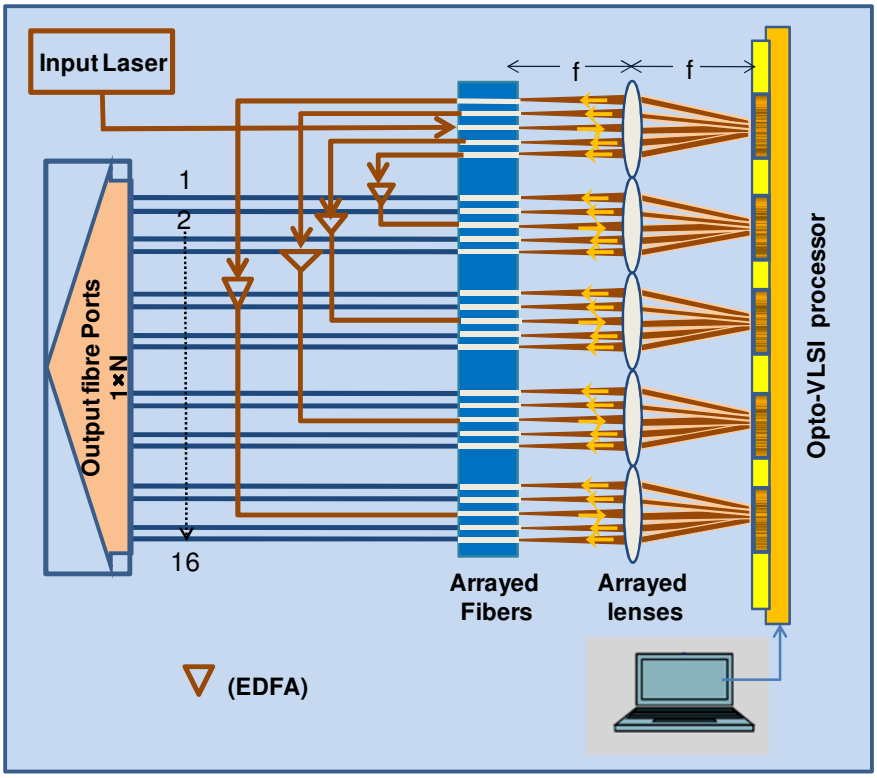

Fig. 4.5. Opto-VLSI-based adaptive optical power splitter employing an array of 4-f imaging systems.

4.3 DEMONSTRATION OF 1×2 ADAPTIVE OPS

4.3.1 System description

The structure of the proposed adaptive optical power splitter is shown in Fig. 4.6. It consists of an Opto-VLSI processor, a lens, and an optical fibre collimator array, aligned to form a 4-f imaging system. The Opto-VLSI processor has 1×4096 pixels with pixel size of 1.0 μm wide and 6.0 mm length, and 1.8μm pixel pitch (i.e. 0.8 μm of dead space between pixels).

To prove the concept of adaptive optical splitting, only three ports of the fibre collimator were used, thus demonstrating a 1×2 adaptive optical power splitter. The experimental setup is shown in Fig. 4.7. A 1550 nm laser source of +5 dBm optical power was used as an input signal, and launched through Port 3 of the fibre collimator array. Port 1 and Port 2 were used as the output ports. The spacing between the fibre collimator elements was 3 mm. A lens of focal length f = 100 mm was placed between and at an equal distance, f, from both the fibre collimator array and the Opto-VLSI processor.

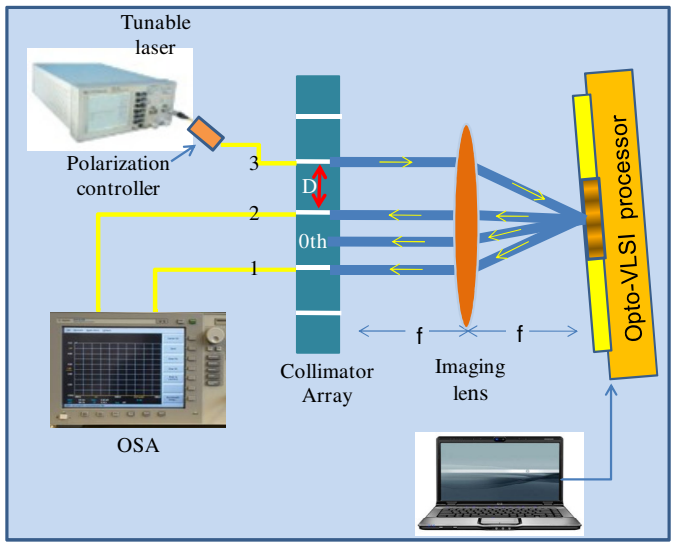

Fig. 4.6. Schematic diagram of the proposed adaptive optical power splitter, employing an Opto-VLSI processor, a 4-f imaging system, and a fibre collimator array of 3mm fibre-to-fibre spacing.

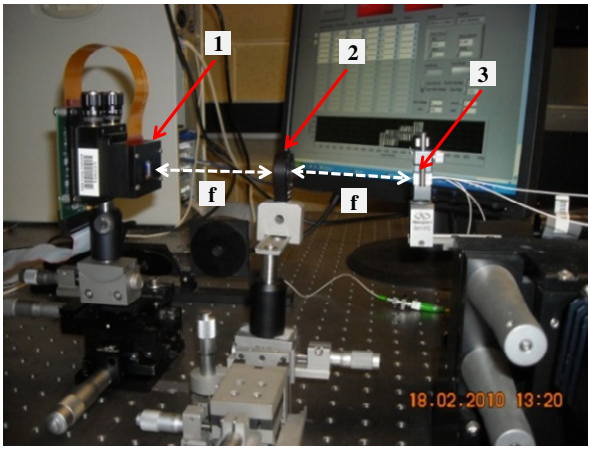

Fig. 4.7. Experimental set-up of the proposed adaptive optical power splitter based the use of (1) Opto-VLSI processor in conjunction with (2) lens imaging, and (3) fibre collimator array.

With no phase hologram uploaded onto the Opto-VLSI processor, only the 0^{th} order diffraction beam was reflected back and focused through the imaging system onto a spot in between the fibre collimator ports, resulting in minimum crosstalk coupled into ports 1 and 2. Fig. 4.8 shows the beam waist profile as it is propagated through the 4-f imaging system. The beam diameter at the fibre collimator was 0.5 mm, and then expanded to 0.72 mm at the lens, which focused it to 0.4 mm at the Opto-VLSI processor. Upon reflection off the Opto-VLSI processor, the beam diameter expanded to 0.72 mm at the

lens and reduced to around 0.5 mm at the fibre collimator, then coupled, through the lens of the fibre collimator, into the output fibre ports.

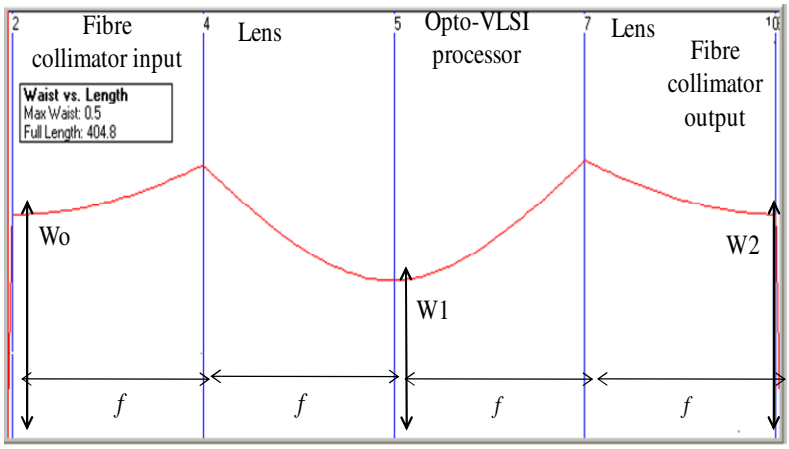

Fig. 4.8. Simulation results showing the optical beam waist along the 4-f imaging system. W0 is the input beam waist at the input fibre collimator, W1 is the beam waist at the Opto-VLSI processor, and W2 is the waist of the reflected beam as it reaches the output fibre collimator.

By driving the Opto-VLSI processor with an optimized multicasting phase hologram, the optical beam illuminating the Opto-VLSI processor was split into two different optical beams (in addition to the 0^{th} order beam) which propagated along the optimized directions so that they were respectively coupled back into Port 1 and 2 of the fibre collimator through the 4-f imaging system. The split optical beams coupled into the two output ports propagated along angles equal to $\theta = \pm \arctan(D/2f) \approx \pm 0.86^{\circ}$ with respect to the 0^{th} order beam. Two optical spectrum analyzers (OSA) were used to monitor the split signals coupled into the two output ports.

Note that a fibre collimator array, rather than a fibre array, was used in this experiment to avoid stringent alignment conditions, such as the use of highly accurate optical stages, in order to maximize the optical power coupled into the output ports. Note also that the diameter of the focused optical beam at the Opto-VLSI processor was relatively large, in order to illuminate a large number of pixels, leading to a high diffraction efficiency and high splitting resolution. This 4-f imaging system enabled adaptive optical splitting with large tolerance to misalignment to be achieved.

4.3.2 Experimental Results and Discussion

Several splitting ratios were employed to demonstrate the adaptive power splitting capability of the proposed optical splitter. Fig. 4.9 shows the measured output powers, P_1 and P_2, at Port 1 and Port 2, respectively, corresponding to different splitting ratios.

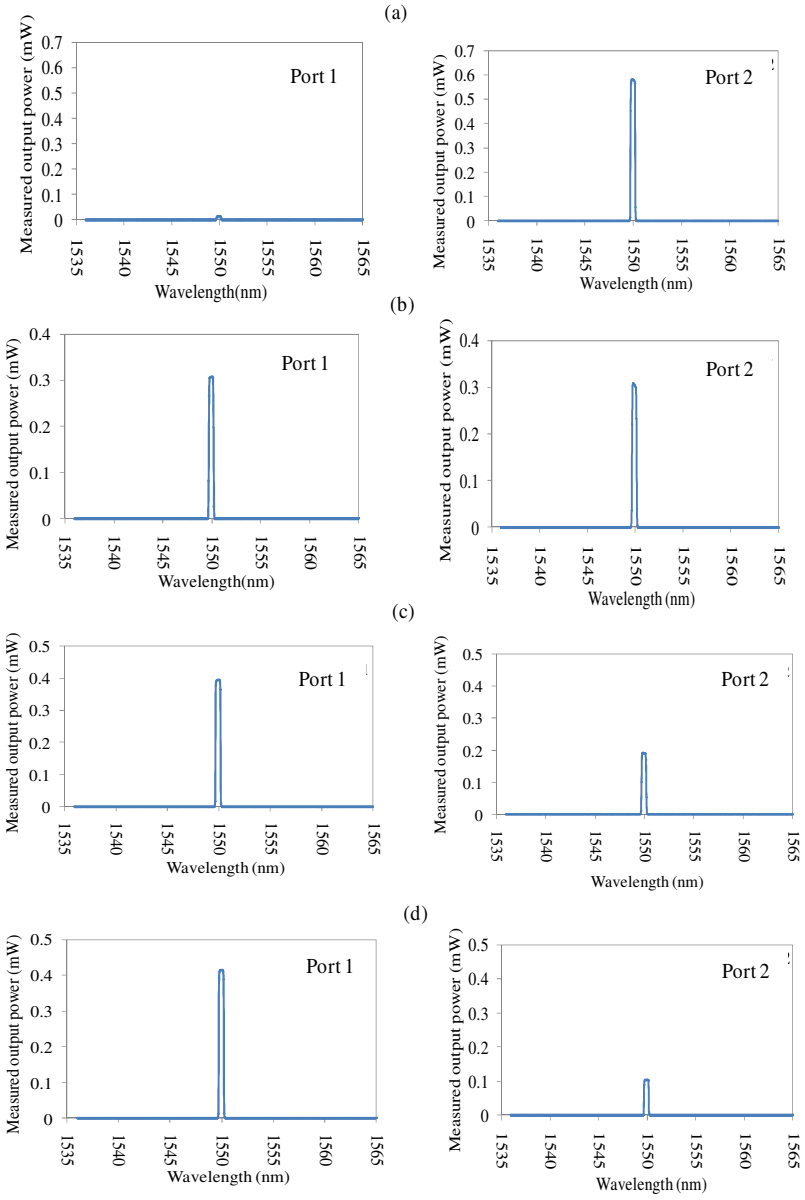

Fig. 4.9. Measured output power at Port 1 and Port 2 (i.e., P_1 and P_2) for different splitting ratios. (a) Splitting ratio P_1/P_2=0, (b) P_1/P_2 =1, (c) P_1/P_2 =2, and (d) P_1/P_2 =4.

For a splitting ratio equal to zero (i.e. P_1=0), as shown in Fig. 4.9(a), the input signal was steered to Port 2, through a steering phase hologram, resulting in a very small signal power being measured at Port 1. The splitting ratio can continuously be changed

from 0.021 (-16.6 dB) to around 50 (17 dB). When the splitting ratio was changed to 1.0 (i.e. splitting the input power equally to the two output ports), the measured output power at Port 1 and Port 2 were 307 μW and 305 μW, respectively, as illustrated in Fig. 4.9(b). Fig. 4.9(c) and (d) show the output power at Port 1 and Port 2 when the splitting ratios were set to 2 and 4, respectively. Excellent agreements between the measured power values at the two output ports and the splitting ratios are displayed in Fig. 4.9.

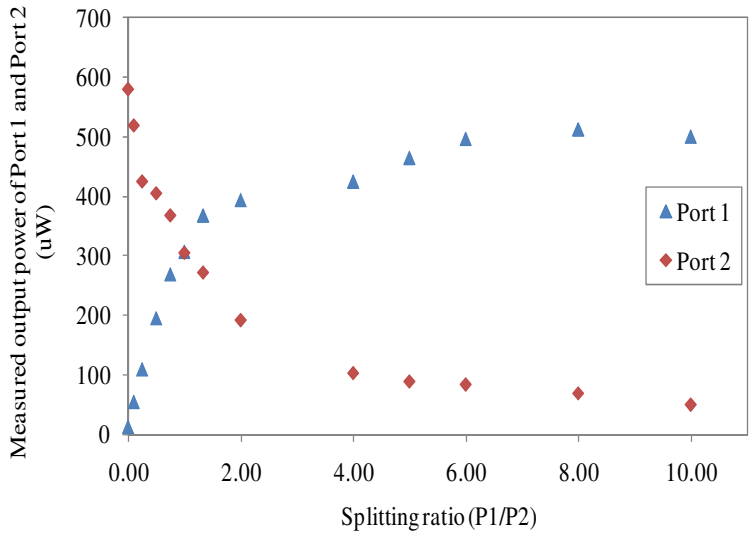

Fig. 4.10. Measured output powers at Port1 (▲) and Port 2 (♦) versus the splitting ratio (P_1/P_2).

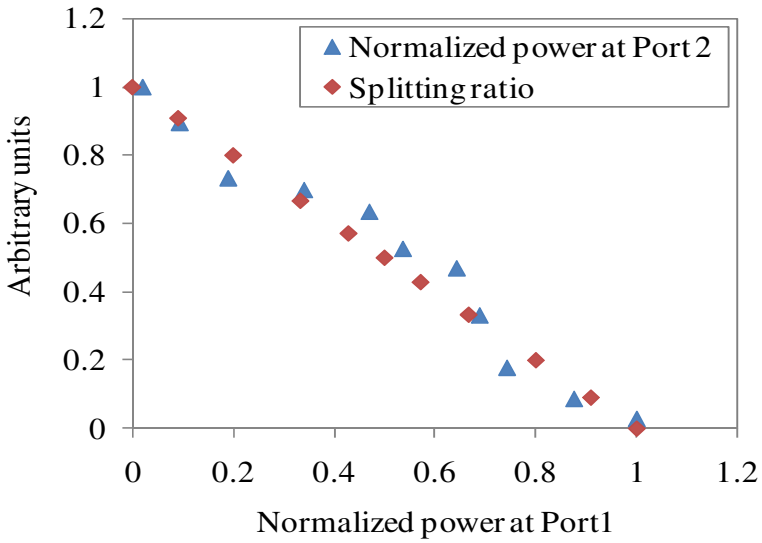

Fig. 4.11. Normalized output power at Port 2 (▲) and the corresponding splitting ratio (arbitrary units) (♦) versus the normalized power at Port 1.

Fig. 4.10 shows the measured optical power levels at the two output fibre ports versus the splitting ratio, and demonstrates the ability of the adaptive splitter structure to realize arbitrary splitting ratios.

Fig. 4.11shows the measured normalized power at Port 2 (P_2/P_{tot}, where P_{tot} $=P_1+P_2$) as well as the simulated splitting ratio versus the normalized power at Port 1 (P_1/P_{tot}). It is noted that the sum of the power levels at the two output ports is constant, demonstrating that the total output power split into Port 1 and Port 2 remains invariable every time a new optimized multicasting phase hologram is uploaded for realizing a target splitting ratio. Fig. 4.11demonstrates that the output power can be arbitrarily split between the two output ports.

To investigate the bandwidth of the proposed adaptive optical splitter, a tunable laser source of wavelength range from 1525nm to 1575nm was used at the input fibre port. The measured output power at ports 1 and 2 versus wavelength are shown in Fig. 4.12, for a splitting ratio equal to 1.0. The measured maximum output power fluctuations at the two output ports was less than 0.1 dB over a wavelength span from 1525 to 1575 nm, demonstrating a splitter bandwidth in excess of 50 nm.

The total insertion loss of the optical power splitter was about 5 dB, to which the Opto-VLSI processor contributed around 3dB due to its low fill factor. The beam steering loss was 0.5 dB and the fibre collimator array in conjunction with the lens contributed the remaining 1.5 dB of insertion loss.

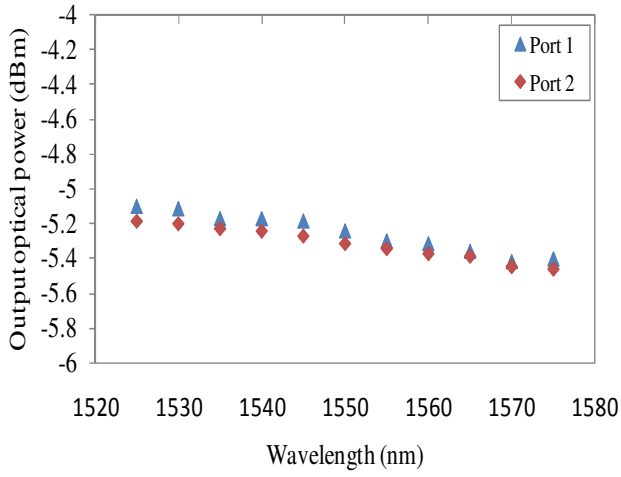

Fig. 4.12. Measured output power at ports 1 and 2 versus wavelength for a splitting ratio = 1.0.

4.4 DEMONSTRATION OF 1×4 ADAPTIVE OPS

In the previous Section 4.3, the concept of an adaptive optical splitter employing an Opto-VLSI processor, a 4-f imaging system (single lens), and fibre collimator array has been demonstrated. Experimental results have demonstrated that an input optical signal can arbitrarily be split into two signals and coupled into optical fibre ports by uploading optimized multicasting phase holograms onto the Opto-VLSI processor. The number of output ports for this structure was limited to two ports because the spacing of the fibre collimator array was large (3mm) thus requiring a large beam steering angle which increases the insertion loss. In this section, the fibre collimator array will be replaced with a fibre array of 250um fibre-to-fibre spacing to eliminate the need for large steering angles.

4.4.1 System description

The structure of the proposed adaptive optical power splitter is shown, through an experimental setup, in Fig. 4.13. It consists of an Opto-VLSI processor, a lens, and an optical fibre array, aligned to form a 4-f imaging system. The Opto-VLSI processor has 1×4096 pixels with pixel size of 1.0 μm wide and 6.0 mm length, and 1.8μm pixel pitch (i.e. 0.8 μm of dead space between pixels). To demonstrate the 1×4 adaptive optical splitter, a custom-made fibre array with spacing 250 μm was used, thus the split beam angles were θ= ±0.58, ±1.16 with respect to 0^{th} order beam direction, as illustrated in Fig. 4.13. The power of the 0^{th} order beam was coupled to a fibre port for monitoring the diffraction efficiency of the Opto-VLSI processor.

A 1550 nm laser source with an output optical power of+1.5dBm was used as the input signal, and launched through the input port of the splitter. A lens of focal length f = 25 mm was placed between and at an equal distance, f, from both the fibre array and the Opto-VLSI processor. With no phase hologram uploaded onto the Opto-VLSI processor, only the 0^{th} order diffraction beam was reflected back and focused through the imaging system into same fibre input port 5 centred the four output fibre ports, resulting in minimum crosstalk into ports 2, and 3, as illustrated in Fig. 4.13. The 0^{th} order signal was directed to optical spectrum analysers (OSA), via a circulator, in order to monitor the diffraction efficiency. The input signal from the input port at the fibre array was collimated through a lens, to an optical beam diameter of 5.48 mm, which illuminated around 3046 pixels of the Opto-VLSI processor, leading to both high diffraction efficiency and high optical splitting.

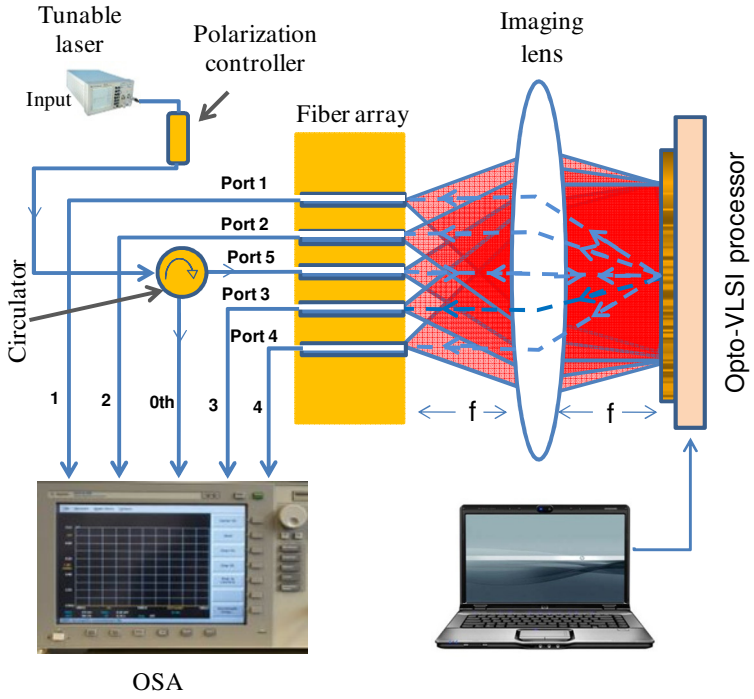

Fig. 4.13. Schematic diagram of the adaptive optical splitter employing an Opto-VLSI processor, a 4-f imaging systems, and a fibre array of 250 µm fibre-to-fibre spacing.

By driving the Opto-VLSI processor with an optimized multicasting phase hologram, the optical beam illuminating the Opto-VLSI processor was split into four different optical beams (in addition to the 0^{th} order beam) which propagated along the optimized directions so that they were coupled back into the fibre output ports through the 4-f imaging system. The split optical beams coupled into the output ports propagated along angles equal to $\theta_{2,3} = \pm 0.58^{\circ}$, and $\theta_{1,4} = \pm 1.16^{\circ}$ with respect to the 0^{th} order beam direction. Optical Spectrum Analyzers (OSAs) were used to monitor the power levels of the split optical signals coupled into the output ports 1, 2, 3 and 4.

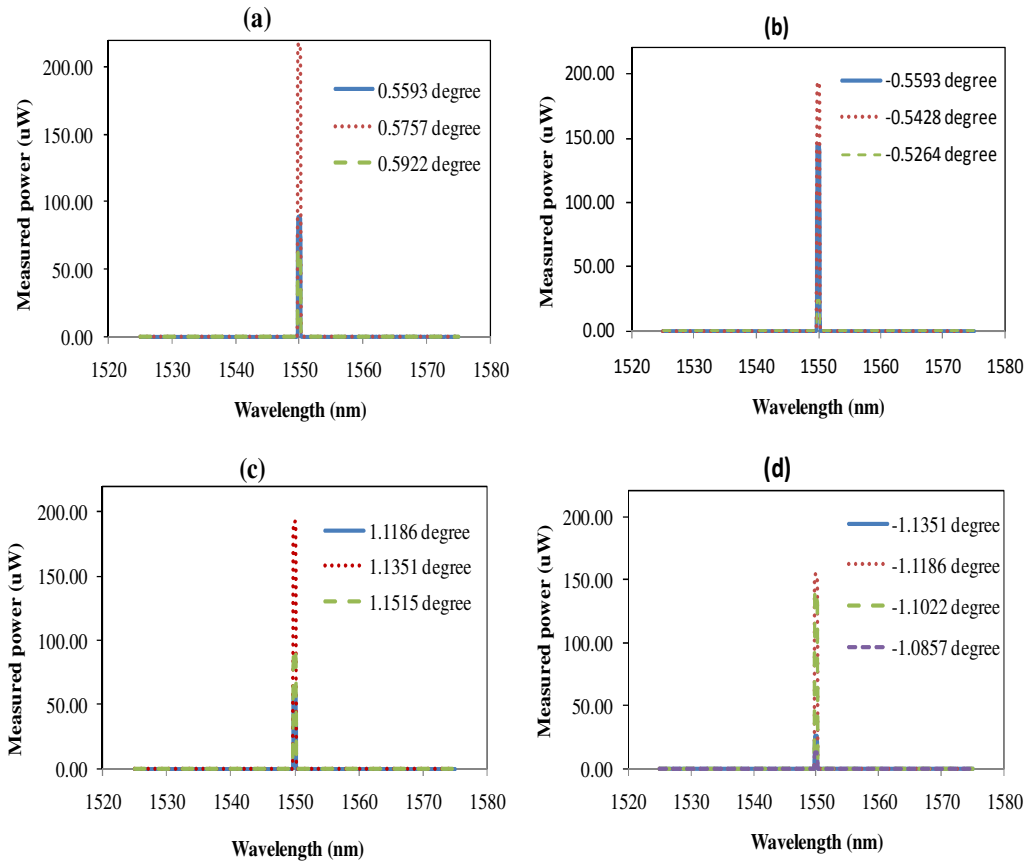

Fig. 4.14. The measured optical power coupled into each output '(a) port 2, (b) port 3, (c) port 1, (d) port 4' for different splitting angles. The angle coupled high power into the output port is selected to be the corresponding splitting angle for the particular output fibre port.

4.4.2 Experimental Results and Discussion

To determine the corresponding splitting angle of each output fibre port, the output power coupled into each output port for different splitting angles was measured. Fig. 4.14 shows the measured output optical power coupled into each output port for different splitting angles. The experimental results show that the splitting angles 1.1351°, 0.5757°, -0.5428°, and -1.1186°, correspond to Port 1, Port 2, Port 3, and Port 4, respectively.

Several scenarios with different splitting ratios were attempted in the experiments to demonstrate the adaptive optical power splitting capability of the proposed adaptive optical power splitter. Table 4.1 shows the measured output power levels, P_1, P_2, P_3 and P_4 of the splitter, coupled into Port 1, Port 2, Port 3 and Port 4, respectively, corresponding to different splitting ratios (H_n).

As shown in Table.4.1, in Scenario 1 a multicasting hologram corresponds to a splitting profile H_1=1.0:1.0:1.0:1.0 was used, demonstrating that the input optical power is split equally into the four output ports, resulting in uniform optical power distribution at all the four output ports. In Scenarios 2, a splitting profile H_2=1.0:1.0:0.01:1.0 was used, which corresponds to the case when the output signal in Port 3 was attenuated by 20 dB. In Scenario 3, the signals coupled to Port 2 and Port 3 were switched off by uploading a phase hologram corresponding to a splitting ratio of H_3=1.0:0.0:0.0:1.0, respectively. The measured crosstalk level was around -30 dB. In Scenario 4 the output optical signals coupled to Port 2 and Port 3 were attenuated by 3 dB corresponding to a splitting profile of H_4=1.0:0.5:0.5:1.0.

Table 4.1. Different splitting profiles corresponding to optimised multicasting holograms uploaded onto the Opto-VLSI processor, and the corresponding measured output optical power levels at Ports 1-4.

Splitting ratio	P 1 (dBm)	P 2 (dBm)	P 3 (dBm)	P 4 (dBm)
H_1=1.0:1.0:1.0:1.0	-13.18	-13.47	-13.37	-13.76
H_2=1.0:1.0:0.01:1.0	-13.16	-13.47	-33.01	-12.59
H_3=1.0:0.0:0.0:1.0	-11.87	-42.50	-43.93	-11.54
H_4=1.0:0.5:0.5:1.0	-12.30	-16.60	-16.83	-12.10

Fig. 4.15(a) shows the measured optical power coupled into the four output ports when the output power coupled into Port 1 was varied while keeping the power levels at Port 2, Port 3, and Port 4 constant. It is obvious from Fig. 4.15(a) that arbitrary output power splitting ratio can be attained for an output port while keeping the optical power at the other ports unchanged. The measured maximum output power uniformity for the fixed-weight output ports (2, 3 and 4) was less than 2 dB. Fig. 4.15(b) shows the measured optical power levels coupled into the output fibre ports while the splitting ratios for both Port 1 and Port 4 were varied while the splitting ratios for Port 2 and Port 3 were fixed. The measured maximum output power fluctuation for the fixed-weight output ports was also around 2 dB.

Fig. 4.15 demonstrates the ability of the adaptive optical splitter structure to realize arbitrary optical splitting ratios through the use of optimized multicasting phase holograms. The measured output power splitting ratios are in excellent agreement with the user defined ratios. Note that the crosstalk for dynamic splitting is around -30 dB.

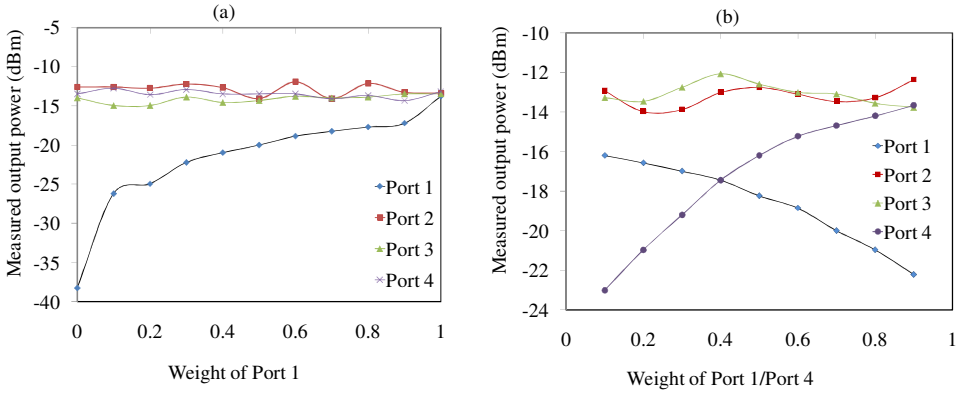

Fig. 4.15. (a) Measured optical power coupled into the output fibre ports when varying the weight of Port 1 while keeping the splitting ratios for others output fibre ports constant. (b) Measured optical power coupled into the output fibre ports when varying the weights of Port 1and Port 4 while keeping the splitting ratios for Port 2 and Port 3 weights unchanged.

To investigate the spectral bandwidth of the proposed adaptive optical splitter, a broadband light source with spectra range from 1525nm to 1575nm was used at the input fibre port (Port 5). The measured optical spectra at Ports 1-4 are shown in Fig. 4.16, for a splitting ratio equal to 1.0:1.0:1.0:1.0. The measured maximum output power fluctuation for the four output ports was around 2.0 dB over a wavelength span from 1525 to 1570 nm, demonstrating a splitter bandwidth in excess of 40 nm. The total insertion loss of the adaptive optical power splitter was 5 dB.

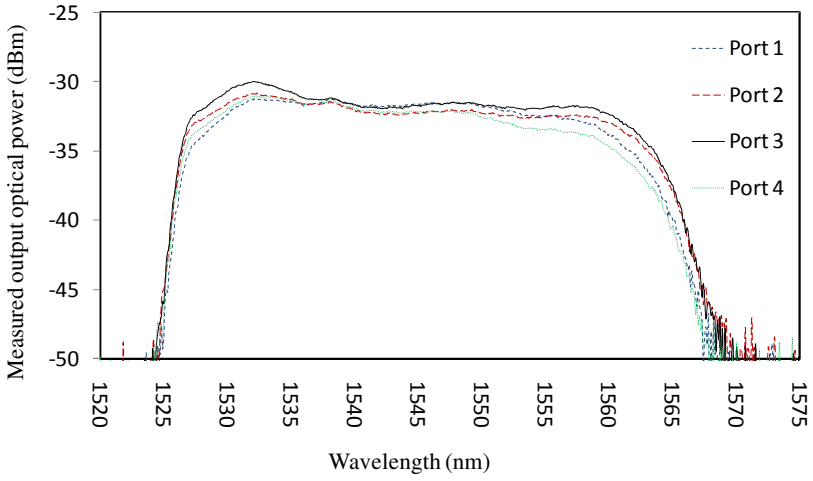

Fig. 4.16. Measured optical spectra at Ports 1-4 of the adaptive optical splitter for a uniform splitting profile of 1.0:1.0:1.0:1.0. Input signal launched at Port 5 is the Amplified Spontaneous Emission (ASE) of an Erbium-Doped Fibre Amplifier (EDFA).

4.5 DEMONSTRATION OF 1×N ADAPTIVE OPS

In the previous Section 4.4, a 1×4adaptive optical splitter employing an Opto-VLSI processor, a 4-f imaging system (single lens), and fibre array has been demonstrated. Experimental results have demonstrated that an input optical signal can arbitrarily be split into two signals and coupled into optical fibre ports by uploading optimized multicasting phase holograms onto the Opto-VLSI processor. This approach doubled the output port count detailed in Section 4.3, however, with the use of a single-lens 4-f imaging system, a further increase in the output port count was impractical, due to the high insertion loss experienced by the split optical beams routed to the outer fibre ports, which require large beam steering angles for optimum beam coupling. In this section, a 4-*f* imaging system array based on lens array is incorporated into the structure of the proposed adaptive optical power splitter.

4.5.1 Lossless Adaptive Optical Power Splitter Architecture

Fig. 4.17 illustrates the concept of the proposed 1×N lossless adaptive optical power splitter, which comprises an Opto-VLSI processor, a fibre array, a lens array, and Erbium-Doped Fibre Amplifiers (EDFAs). The active area of the Opto-VLSI processor is divided into M pixel-blocks driven by multicasting phase holograms and aligned with an M-element lens array and a fibre array, thus forming an array of 4-f imaging systems. Each 4-f imaging system collimates and adaptively splits an input optical beam launched into the input optical fibre port, and then couples the split beams into different output fibre ports, thus realizing an adaptive optical power splitter. A laser signal is typically launched into the input fibre port (Master block), split into *P* output optical signals via the uploaded multicasting phase hologram, and then coupled into *P* output fibre ports. Each output optical signal emerging from each output port is amplified by an Erbium-Doped Fibre Amplifier (EDFA) to compensate for the various insertion and splitting losses. Each amplified optical signal is then launched into another input fibre port and adaptively split via another multicasting phase hologram uploaded onto another pixel block dedicated to adaptively splitting that amplified optical signal.

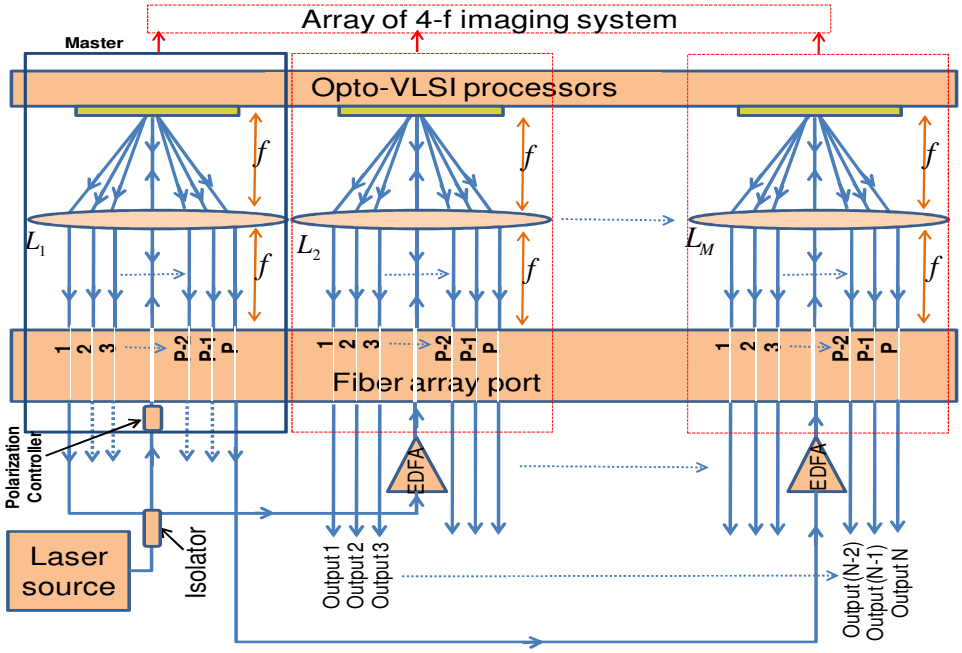

Fig. 4.17. Schematic diagram of the proposed 1×N lossless adaptive optical power splitter employing an Opto-VLSI processor, optical amplifiers and an array of 4-f imaging systems.

The role of the software-driven Opto-VLSI processor is to adaptively split an incident light beam into many different angles, with user-defined splitting ratios, by uploading optimized multicasting phase holograms onto the various pixel blocks. By driving a pixel-block with an optimized multicasting phase hologram, each incident 'input' optical beam illuminating that pixel block can be split into *P* different optical beams. These split beams propagate along appropriate directions and couple back into the output fibre ports through the corresponding 4-f imaging system. For M pixel-blocks, each splits its input optical beam into P beams, the total number of the output fibre ports that can be attained is $N = (M-1)\times P$.

4.5.2 Experimental Results and Discussion

To demonstrate the concept of the proposed 1×N lossless adaptive optical power splitter, several experiments were carried out. Fig. 4.18(a) shows the first experiment, which was set up to align the various optical components of the splitter. The splitter demonstrator consisted of an Opto-VLSI processor, a 2-element lens array with adjustable lens spacing, and a 1×64 optical fibre array. All components were aligned to form two 4-f imaging systems as shown in Fig. 4.18(a). The Opto-VLSI processor used in the experiments has 1×4096 pixels, a pixel size of 1.0 μm×6.0 mm, a pixel pitch of 1.8 μm (i.e.,

0.8 μm of dead space between pixels), and an active area of 7.4 mm×6.0 mm. A fibre array of spacing 127 μm was used as the input/output fibre ports. The lens array had two elements, each of focal length (f) 9 mm and diameter 3mm, and was placed right at the middle of distance, f, between the Opto-VLSI processor and the fibre array. Two input fibre ports separated by a span of 29 fibre elements (i.e., 29×0.127mm=3.68mm) were used to launch two input optical signals of similar intensities. The measured laser power spectral density launched into one of the input fibre ports is shown in Fig. 4.18(b). The gap between the two lenses was 0.68mm (properly adjusted to match the spacing between the two input fibre ports). Both input optical signals were collimated through the corresponding lenses, at a diameter of 1.962 mm.

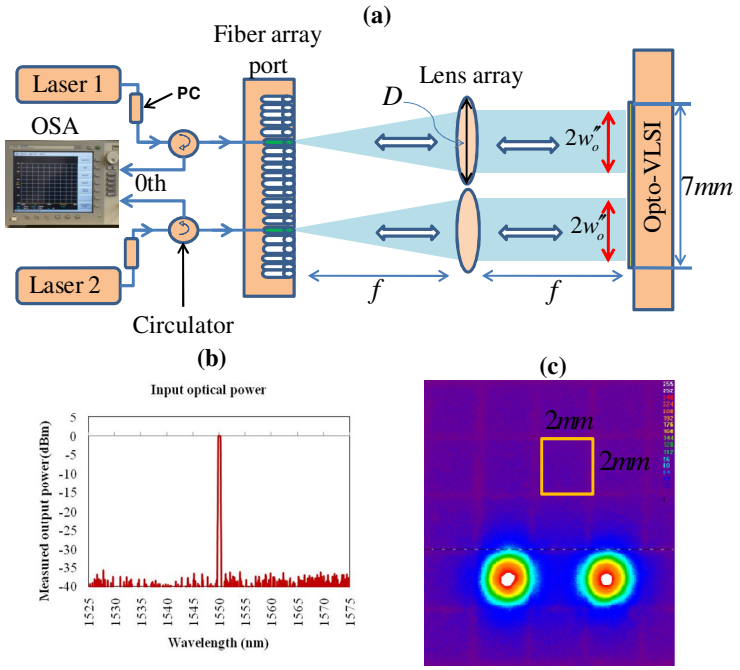

Fig. 4.18. (a) Experimental setup to demonstrate the concept of the proposed 1×N lossless adaptive optical power splitter. (b) Measured laser power launched into one of the input fibre ports. (c) Measured power densities of the input optical beams after collimation by the lens array.

The measured power densities of the input optical beams after collimation by the lens array are shown in Fig. 4.18(c). Each collimated beam illuminated around 1,090 pixels of the Opto-VLSI processor, thus attaining a high diffraction efficiency and high optical splitting angle resolution**.** The active area of the Opto-VLSI processor was divided into two pixel-blocks, separated by 934 un-addressed pixels.

A Labview program was especially implemented to generate optimized multicasting phase holograms that split the two input optical beams along different directions and the split beam were coupled into the various output fibre ports. The diffraction efficiency of the Opto-VLSI processor was measured by monitoring the 0^{th} order diffracted beams for the input signals coupled to their corresponding fibre ports and routed via optical circulators to an optical spectrum analyzer (OSA), as illustrated in Fig. 4.18(a).

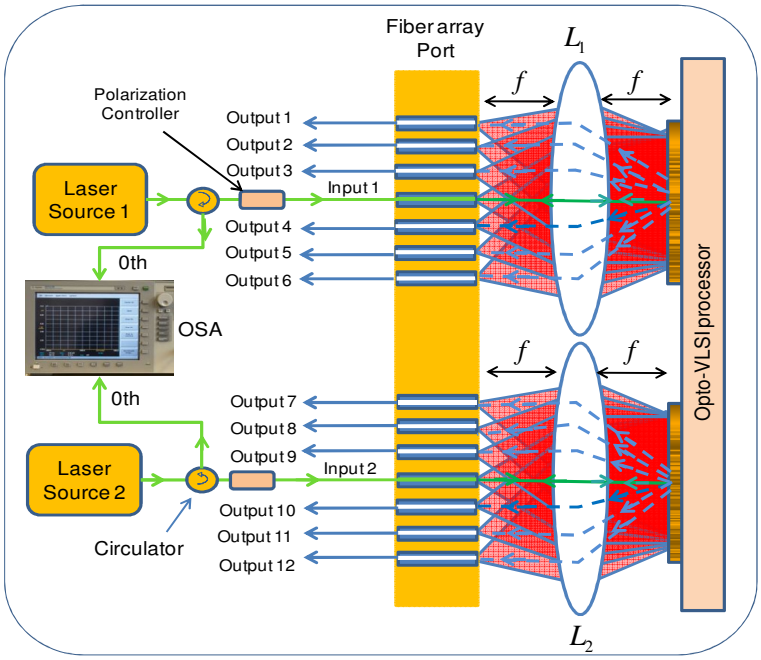

Fig. 4.19. Experimental setup used to demonstrate the capability of the proposed 1×N lossless adaptive optical power splitter to adaptively split an input optical signal into several output signals and couple them into different fibre ports. Two identical laser signals were launched into the input fibre ports and two multicasting phase holograms were uploaded onto the Opto-VLSI processor to adaptively split the input optical beams and route the split optical beams, through the 4-f imaging system, to the appropriate output fibre ports.

Another experiment was set up, as illustrated in Fig. 4.19, to demonstrate the capability of the proposed 1×N lossless adaptive optical power splitter to adaptively split an input optical signal into several output signals and couple them into different fibre ports. Two identical laser signals were launched into the input fibre ports 1 and 2 and two multicasting phase holograms were uploaded onto the Opto-VLSI processor to adaptively split the input optical beams and route the split optical beams, through the 4-f imaging system, to the appropriate output fibre ports. Without a phase hologram uploaded onto each pixel-blocks of the Opto-VLSI processor, only the zero's order diffraction beams

were reflected back and focused through the 4-f imaging systems into the same input optical fibre ports. The steering angle for each split optical beam should be within the maximum steering angle of the Opto-VLSI processor.

As shown in Fig. 4.19, two identical (1550 nm) laser sources with an output optical power of +3.6 dBm were used to launch input signals via optical circulators into the two input fibre ports of the adaptive optical power splitter. The measured power levels of the 0^{th} order coupled back into the input fibre ports were similar (~ -1.2 dBm). For both input optical beams, the split optical beams propagated along ±0.81°, ±1.62°, ±2.43° and ±3.24° with respect to the direction of the 0^{th} order beam. Split beams at ±3.24° displayed high insertion loss since they are close to the maximum steering angles (±3.4°) of the Opto-VLSI processor.

Several splitting scenarios were experimentally investigated to demonstrate capability of the proposed optical power splitter to adaptively split an input optical signal. Fig. 4.20 shows the measured output power levels at the output ports for different splitting ratio profiles. For each desired splitting ratio profile, optimized multicasting phase holograms were synthesized (using simulated annealing algorithms) and uploaded onto the Opto-VLSI processor. As shown in Fig. 4.20, while the generated multicasting hologram can accurately split the input optical signal routed to the output ports, the crosstalk level was, for some splitting scenarios, relatively high (~-20 dB). In order to reduce the crosstalk to below -25 dB, tone can intentionally introduce additional very small split signals and route them to other unused output ports, thus reshaping the crosstalk power distribution and avoiding the crosstalk beams to be routed along the intended split beam directions.

Fig. 4.20(a) shows the split signals for Scenario 1, where a multicasting hologram that corresponds to a splitting profile H_1= 1.0:1.0:1.0:1.0:1.0:1.0 was used. Fig. 4.20(a) demonstrates that the input optical power can be split equally into the output ports, resulting in uniform optical power distribution at all the output ports. Fig. 4.20(b) shows the split signals for Scenario 2, using multicasting hologram corresponds to a splitting profile H_2=1.0:1.0:1.0:1.0:1.0:0.2, this corresponds to the scenario where the output signals in Ports 6 and 12 were attenuated by 8 dB.

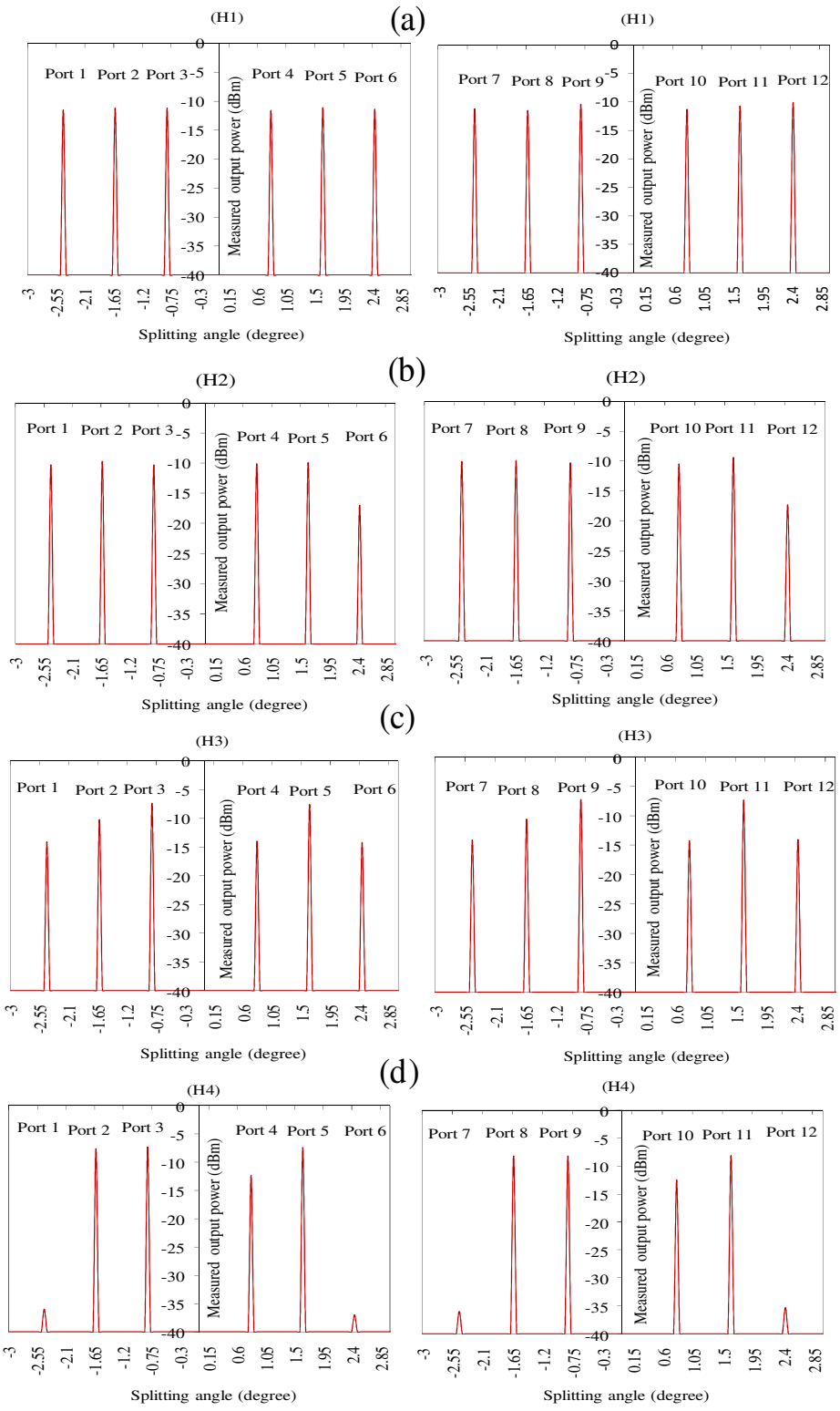

Fig. 4.20. Shows the measured output power levels at the output ports (1-6 and 7-12) when the two input signals (input 1 and input 2), respectively, were split by uploading a multicasting phase hologram corresponding to different splitting profile (a) H_1= 1.0:1.0:1.0:1.0:1.0:1.0 (b), H_2=1.0:1.0:1.0:1.0:1.0:0.2 and (c) H_3=0.2:1.0:0.5:.2:1.0:0.2, and (d) H_4=0.0:1.0:1.0:0.3:1.0:0.0 onto the Opto-VLSI pixel blocks.

Fig. 4.20(c) shows the split signals for Scenario 3, where a multicasting hologram corresponds to a splitting profile H_3=0.2:1.0:0.5:.2:1.0:0.2was used. For this scenario, the input optical power was arbitrarily split into the output ports, and the theoretical and experimental results are in excellent agreement for all the output fibre ports. Fig. 4.20(d) shows the split signals for Scenario 4. The signals coupled into Ports 1, 6, 7, and 12 were switched off (highly attenuated) while the signals coupled to Ports 4 and 10 were attenuated by only 4.5 dB using a phase hologram corresponding to a splitting profile H_4=0.0:1.0:1.0:0.3:1.0:0.0. For this scenario, the measured crosstalk level was around -25 dB.

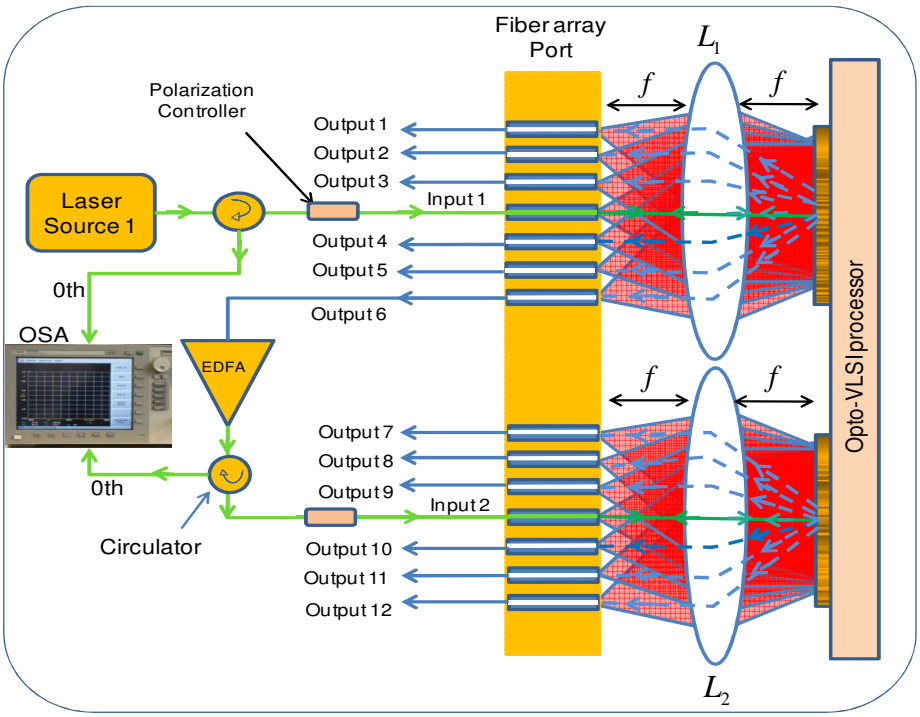

Fig. 4.21. Experimental setup used to demonstrate the concept of the proposed lossless 1×N lossless adaptive optical power splitter. A laser signal was launched into the input fibre Port 1 and split using a multicasting phase hologram into 6 optical signals, and then coupled into 6 output fibre ports. The output signal emerging from port 6 was amplified via EDFA to compensate for the various insertion and splitting losses. The amplified signal was launched into the fibre input Port 2 to undergo subsequent adaptive splitting via another multicasting phase hologram uploaded onto another pixel block dedicated to adaptively split that input signal.

Fig. 4.20 demonstrates the ability of the 1×N lossless adaptive optical power splitter structure to realize arbitrary optical splitting ratios through the use of optimized multi-casting phase holograms. It is important to notice that it is always possible to tailor the splitting profile in order to compensate for the slight misalignment of the optical components as well as the non-uniform fibre spacing of the fibre array.

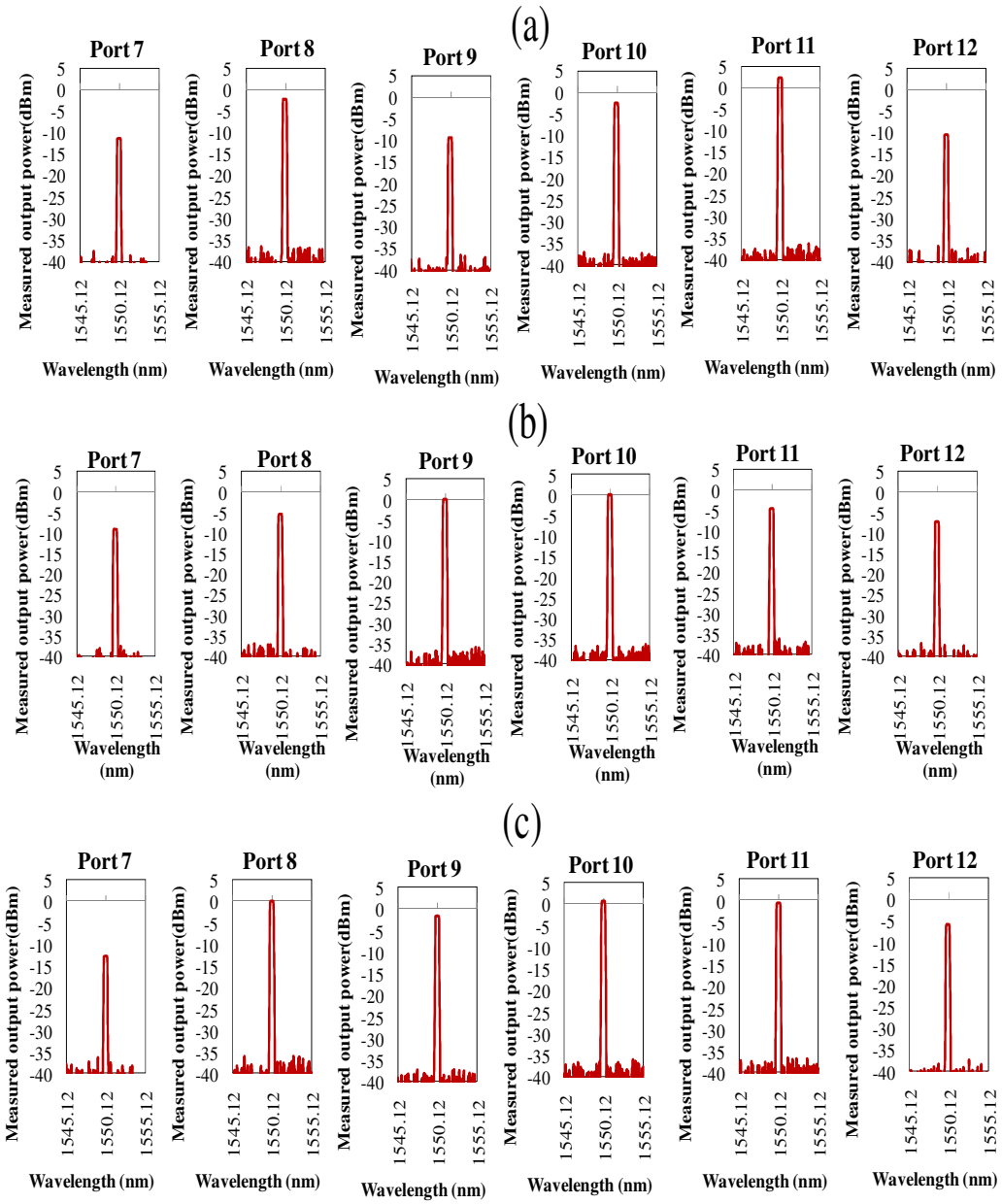

Fig. 4.22. Measured optical power coupled into the output fibre Ports 7-12 for different multicasting phase holograms corresponding to the following splitting profiles: (a) H_5= 0.05:0.3:0.05:0.3:1.0:0.05, (b) H_6=0.1:0.3:1.0:1.0:0.3:0.2 and (c) H_7=0.05:1.0:0.6:1.0:1.0:0.3 .

To demonstrate the lossless operation of the 1×N lossless adaptive optical power splitter, another experimental setup was used, which is shown in Fig. 4.21. A laser signal was launched into the input fibre Port 1, and split into 6 optical signals using a multicasting phase hologram uploaded onto the corresponding input pixel block. The 6^{th} split beam was then amplified via an Erbium-Doped Fibre Amplifier (EDFA), to compensate for the various insertion and splitting losses of the first splitting stage, then launched into another input fibre port and adaptively split via another multicasting phase hologram uploaded onto another pixel block dedicated to adaptively split that amplified optical signal.

Fig. 4.22 (a-c) show the measured optical power levels coupled into the output fibre ports 7-12 for different multicasting phase holograms uploaded into the Opto-VLSI processor, corresponding to splitting ratio profiles H_5= 0.05:0.3:0.05:0.3:1.0:0.05, H_6=0.1:0.3:1.0:1.0:0.3:0.2 and H_7=0.05:1.0:0.6:1.0:1.0:0.3, respectively. In Fig. 4.22(a) it is shown that an output optical signal power (Port 11) can be even higher than the input laser power.

Fig. 4.22(b and c) shows that some output optical signals have power levels higher or equal to power of the input laser, demonstrating the capability of the adaptive OPS to compensate for the various optical losses. It is important to mention that the higher the saturated output optical power of the EDFA the higher the splitter port count that can be used.

Fig. 4.20 and Fig. 4.22 demonstrate the ability of the proposed 1×N lossless adaptive optical power splitter structure to realize arbitrary optical splitting ratios through the use of optimized multicasting phase holograms and attain lossless operation.

To measure the spectral bandwidth of the proposed optical splitter, the output of a broadband light source, whose spectra range extends from 1525nm to 1575nm, was launched into the input fibre port (Port 5). The measured optical spectra at Ports 1-6 are shown in Fig. 4.23, for a splitting ratio H_8=0.4:0.8:0.8:0.8:1.0:0.0. The measured maximum output power fluctuation for the output ports was around 1.0 dB over a wavelength span from 1525 to 1570 nm, demonstrating a splitter bandwidth in excess of 40 nm.

The total insertion loss of a single 4-f imaging system, without EDFA compensation, was around 4.8 dB, mainly due to the Opto-VLSI processor, optical circulator, optical misalignment and imperfect optical components used in the experiments.

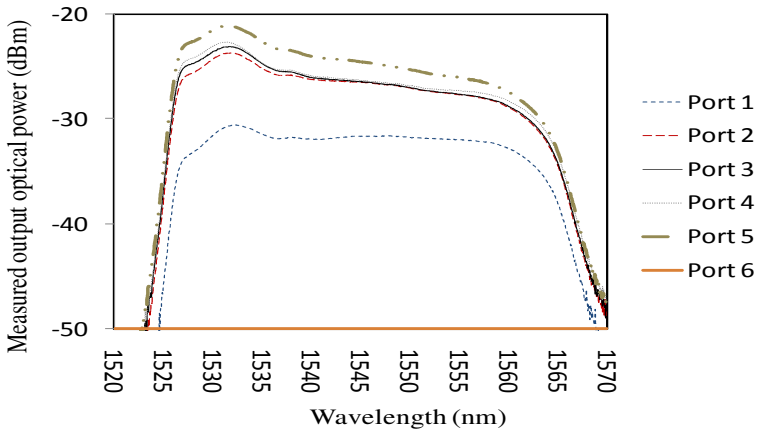

Fig. 4.23. Measured optical spectra at Ports 1-6 of the adaptive optical power splitter for a splitting profile corresponding to H_8=0.4:0.8:0.8:0.8:1.0:0.0. A broadband optical signal replaced the input laser source 1 of Fig. 5.21.

4.6 DEMONSTRATION OF AN ADAPTIVE OPTICAL COMBINER

4.6.1 System description

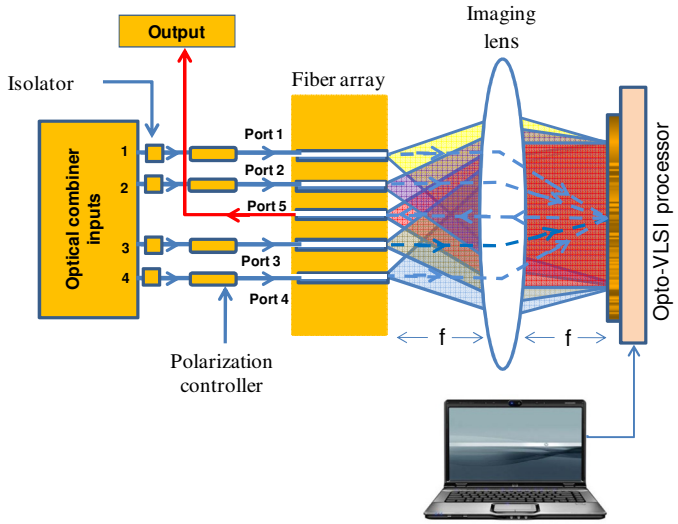

Fig. 4.24. Schematic diagram of the proposed adaptive optical combiner, employing an Opto-VLSI processor, a 4-f imaging systems, and a fibre array of 250 µm fibre-to-fibre spacing.

To demonstrate the principle of the adaptive optical combiner, four optical signals of equal power levels (-5.7dBm) were launched into Ports 1, 2, 3 and 4 as in Fig. 4.24, and, through a multicasting phase hologram, combined into Port 5, which was monitored using an optical spectrum analyser. A multicasting phase hologram uploaded onto the Opto-VLSI processor enabled the four optical signals launched into Ports 1-4 to be combined at Port 5 with a weight profile that matches the splitting profile of the corresponding multicasting phase hologram.

4.6.2 Experimental Results and Discussion

The principle of the adaptive optical combiner was demonstrated by launching four input signals into Ports 1, 2, 3 and 4 and measuring the output signal from Port 5. Fig. 4.25(a-d) show the output combined optical signal at Port 5 for the same phase holograms used in Table 4.1, which correspond to combining profiles of 1.0:1.0:1.0:1.0, 1.0:1.0:0.01:1.0, 1.0:0.0:0.0:1.0 and 1.0:0.5:0.5:1.0, respectively. Note that in Fig. 4.25(d) the power levels of the two centre channels are actually around 4 dB below those of the outside channels, as evident from Table 4.1, row 4. The discrepancy be-

tween theory and experimental measurements is attributed to measurement errors. Fig. 4.25(a-d) demonstrates the ability of the Opto-VLSI processor to combine the input optical signals with an arbitrarily weight profile and couple them into the output fibre Port 5.

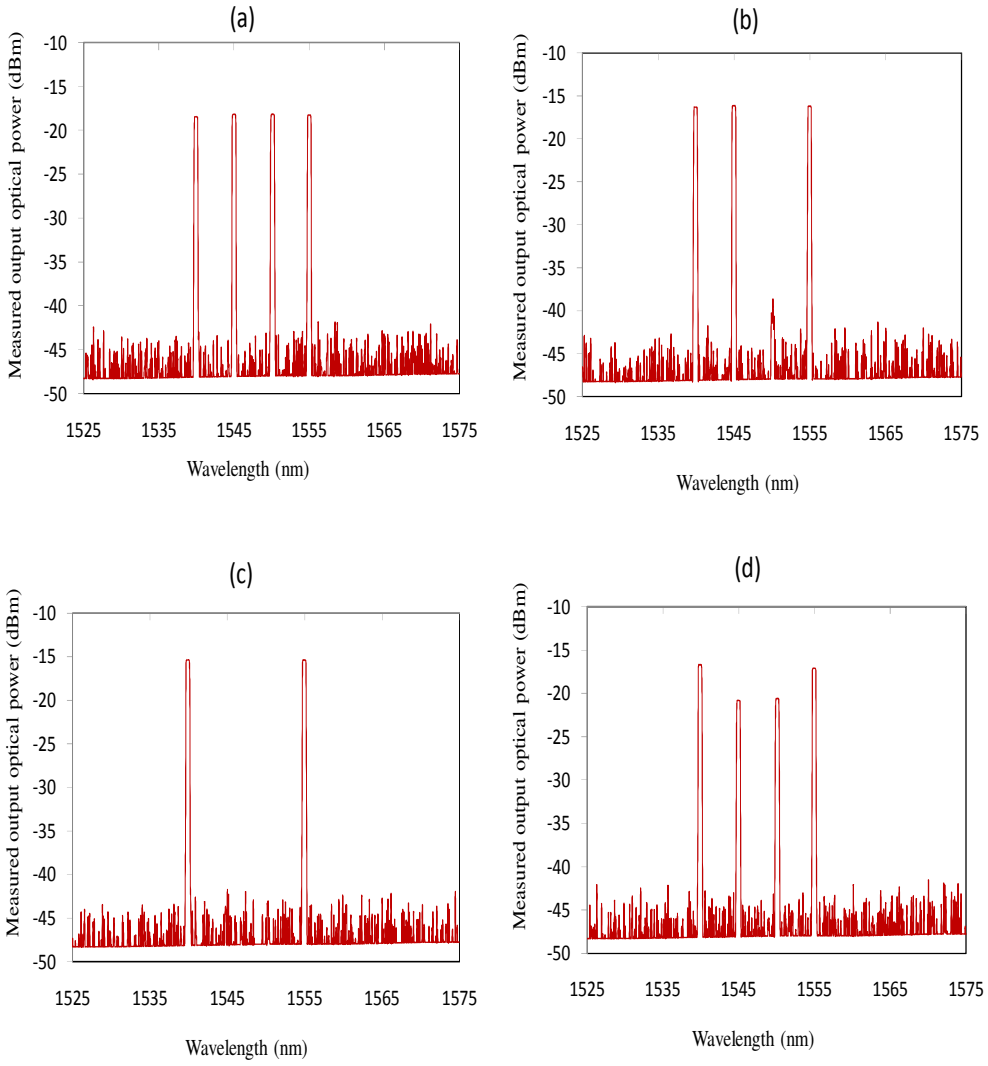

Fig. 4.25. Input signals launched into Ports 1, 2, 3, and 4, and output combined optical signal at Port 5 for phase holograms corresponding to splitting ratios of (a) 1.0:1.0:1.0:1.0, (b) 1.0:1.0:0.01:1.0, (c) 1.0:0.0:0.0:1.0 and (d) 1.0:0.5:0.5:1.0.

Fig. 4.25 demonstrates the ability of the reconfigurable optical combiner structure to realize arbitrary optical combining ratios through the use of optimized multicasting phase holograms. The measured output power combining ratios are in excellent agreement with the user defined ratios. Note that the crosstalk for dynamic splitting/combining is around -30 dB. The total insertion loss for the adaptive optical power

combiner, an additional 6 dB loss was measured (or a factor of 4) which is due to the inherent signal multicasting (1:4 splitting ratio).

4.7 THE TOTAL INSERTION LOSS

The total insertion loss of the optical power splitter was about 5 dB, to which the Opto-VLSI processor contributed around 3dB due to its low fill factor. The beam steering loss was 0.5 dB and the fibre collimator array in conjunction with the lens contributed the remaining 1.5 dB of insertion loss. However, the total insertion loss can be reduced through:

(i) An improved Opto-VLSI chip design, where the dead-space between pixels is reduced.
(ii) The use of broadband AR coatings for the various optical components.

The total insertion loss was relatively large for the adaptive optical power splitter. However, this adaptive optical power splitter structure has the potential to realize a large number of output ports with negligible insertion loss penalty. The latter feature makes the proposed splitter attractive for many emerging optical network applications, in comparison to other adaptive optical power splitters that have a limited number of output ports.

4.8 SUMMARY

The concepts of adaptive optical power splitter employing an Opto-VLSI processor and a 4-f imaging systems have been demonstrated through three demonstrations, namely:

1) A 1×2 adaptive optical power splitter based on an Opto-VLSI processor, a fibre collimator array and 4-f imaging systems (single lens).
2) A 1×4 adaptive optical power splitter based on an Opto-VLSI processor, a fibre array and 4-f imaging systems (single lens).

3) A 1×N lossless adaptive optical power splitter structure integrating Opto-VLSI processor, optical amplifiers, a fibre array and an array of 4-f imaging systems (lens array).

The concept of using the adaptive optical power splitter as an adaptive optical combiner has also been demonstrated. Experimental results have demonstrated that an input optical signal can arbitrarily be split into *N* signals and coupled into optical fibre ports by uploading optimized multicasting phase holograms onto the Opto-VLSI processor. The experimental results have also demonstrated that *N* input optical signals can dynamically be combined with arbitrary weights into a single optical fibre port. Excellent agreement between theoretical and experimental results has been demonstrated. The total insertion loss of the optical power splitter was about 5 dB. Results have also shown that the optical amplifiers can compensate for the insertion and splitting losses, thus enabling lossless splitter operation. A crosstalk level around -25 dB and a wavelength spectral range exceeding 40 nm have experimentally been measured. It is important to note that by increasing the width of the active area of the Opto-VLSI processor to 19 mm, the number of output fibre ports can be as high as 32, making the adaptive optical power splitter an attractive product for access optical networks and optical signal processing.

CHAPTER 5

BROADBAND ADAPTIVE RF POWER SPLITTER/COMBINER

5.1 INTRODUCTION

RF power splitters are key elements for applications based on RF signal processing, such as beamforming networks and smart antenna systems [94-98]. A multi-port reconfigurable broadband power splitter with variable splitting ratios allows such systems to operate with a high degree of flexibility, thus achieving multiple functions that are not possible with conventional fixed-ratio RF power splitters [99]. Conventional RF power splitters are mainly designed to operate within specific frequency ranges [100]. Various processes and technologies, such as, CMOS, BiCMOS, MESFET, and printed circuit board (PCB), have been used to develop RF power splitters [101-103].

The key specifications of a power splitter include the output port count, low loss, low cost, wide bandwidth, and compact size [99]. Broadband RF power splitters based on CMOS technology have recently been reported [104, 105], however, these RF splitters have limited flexibility in terms of realizing arbitrary splitting ratios while maintaining their broadband operation. A promising approach to splitting a broadband RF signal adaptively into different output ports is to use photonics technologies, in particular, Opto-VLSI processing.

This chapter presents the experimental results of the proposed broadband adaptive RF power splitter/combiner based on Opto-VLSI processor. The first part (Section 5.2) introduces the proposed broadband adaptive RF splitter. The second part (Sections 5.3 and 5.4) demonstrates the principle of the proposed broadband adaptive RF power splitter by realizing:

(i) A 1×4 Opto-VLSI-based adaptive RF power splitter.
(ii) A multiport broadband adaptive RF power splitter based on Opto-VLSI processing.

The chapter concludes with proof-of-concept demonstration of the proposed Opto-VLSI-based adaptive RF power combiner (Section 5.5).

5.2 PROPOSED BROADBAND ADAPTIVE RF POWER SPLITTER

Fig. 5.1 illustrates the principle of splitting an RF signal by modulating a continuous laser signal by the RF signal and splitting the RF-modulated optical signal in the optical domain using an Opto-VLSI processor driven by abeam multicasting phase hologram, then using a broadband photodetector array to generate the split RF signals.

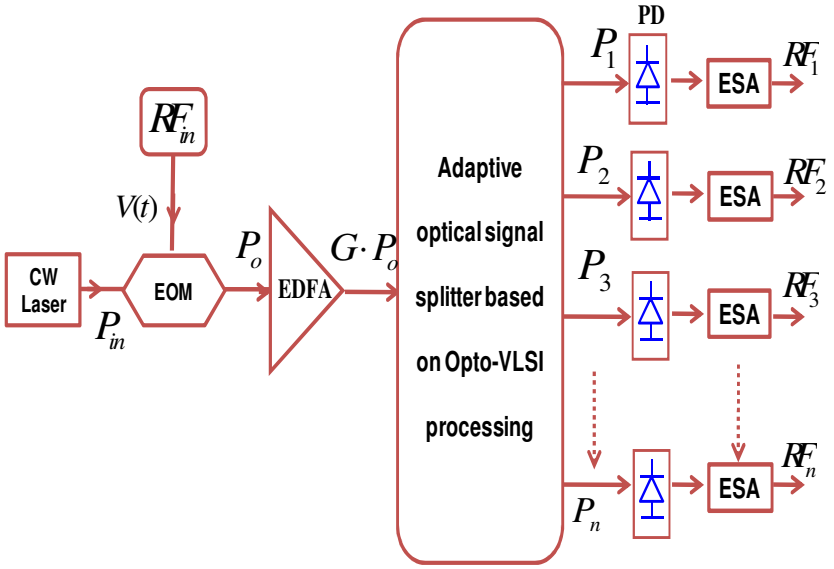

Fig. 5.1. Illustrate the concept of splitting an RF power signal in the optical domain.

As shown in Figure 2, the intensity of a continuous wave (CW) laser signal was externally modulated by an RF signal using a JDS Uniphase electro-optic modulator (EOM). The output optical power of the Mach-Zehnder electro-optic modulator (EOM) is given by [97]

$$P_o = \frac{P_{in}}{2}\left\{1+\cos\left[\pi\frac{(V_b+V(t))}{V_\pi}\right]\right\} \tag{5.1}$$

where

P_{in} is the optical power launched into the EOM.

$V(t)$ is the RF modulating voltage.

V_π is the EOM switching voltage.

For $V_m << V_\pi/2$ and $V_b = -V_\pi/2$, a small-signal sinusoidal modulating RF signal $V(t) = V_m \cos(\Omega t)$ of frequency Ω produces an output RF-modulated optical power given by [106]

$$P_{RF,o}(t) = \frac{P_{in}}{2}\sin\left[\pi\frac{V_m\cos(\Omega t)}{V_\pi}\right] \approx \frac{\pi P_{in} V_m}{2V_\pi}\cos(\Omega t) \tag{5.2}$$

The RF-modulated optical signal was amplified by an erbium-doped fibre amplifier (EDFA) and launched, as an input signal, into the fibre input port of the adaptive optical power splitter. By driving the Opto-VLSI processor with an optimized multicasting phase hologram, the RF-modulated optical beam can be split into n different RF-modulated optical beams with a user-defined splitting ratio. The RF-modulated optical power of the n^{th} split beams is given by

$$P_{RF,n}(t) = \alpha_n \cdot \beta \cdot G \cdot P_{RF,o}(t) \tag{5.3}$$

where α_n is the optical splitting ratios, G is the EDFA gain, and β accounts for the insertion losses due to the Opto-VLSI processor, the optical components, and fibre coupling. Note that these optical losses as well as the zeroth order optical power loss are typically compensated by the EDFA.

A photodetector (PD) array was used to detect the split RF-modulated optical signals emerging from the fibre output Ports. The RF photocurrents, $I_n(t)$, detected by the photodetector array are given by [106]

$$I_{RF,n}(t) = \Re P_{RF,n}(t) \tag{5.4}$$

where $\Re$ is the responsivity of the photodetector element.

With the use of a transimpedance amplifier (of impedance Z) after each photodetector element, the output RF signal is given by

$$V_{RF,n}(t) = Z \cdot I_{RF,n}(t) \tag{5.5}$$

The RF power splitting ratio for the nth RF port is defined as

$$\eta_n = \left| \frac{V_{RF,n,\max}}{V_m} \right|^2 \tag{5.6}$$

where $V_{n,RF,\max}$ is the amplitude of the output RF signal. Using Eqs (1)-(7), yields

$$\eta_n = \left| \frac{\pi \cdot Z \cdot \Re \cdot \beta \cdot G \cdot P_{in}}{V_\pi} \right|^2 \alpha_n^2 = A\alpha_n^2 \tag{5.7}$$

where $A = \left| \frac{\pi \cdot Z \cdot \Re \cdot \beta \cdot G \cdot P_{in}}{V_\pi} \right|^2$ (5.8)

Eq. (5.7) shows that the RF power splitting ratio is proportional to the square of the optical power splitting ratio.

5.3 DEMONSTRATION OFTHE ADAPTIVE RF POWER SPLITTER

5.3.1 System descriptions

Fig. 5.2 illustrates, through the setup that was used in the experiments, the proposed broadband adaptive RF splitter structure. The intensity of a 1550 nm continuous wave (CW) laser signal was externally modulated by an RF signal using a JDS Uniphase electro-optic modulator (EOM).

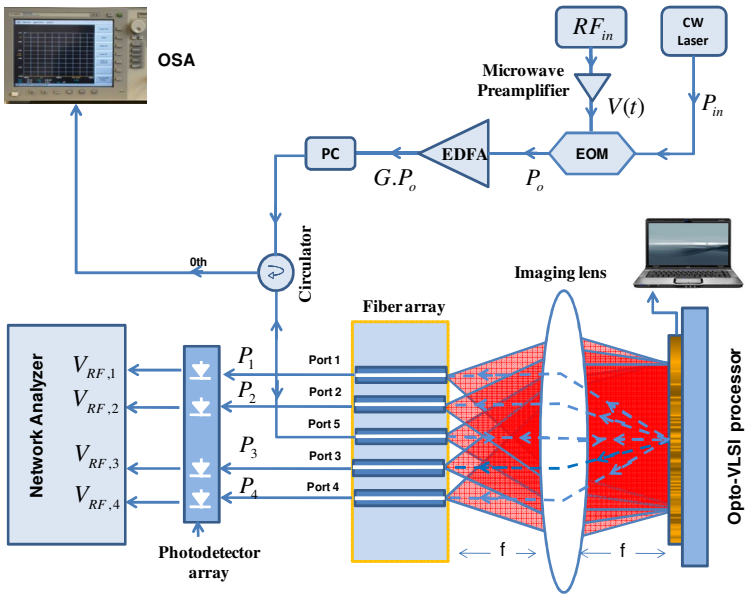

Fig. 5.2. Illustrate the experimental setup of the proposed broadband adaptive RF splitter structure, which is based on the use of an Opto-VLSI processor in conjunction with a 4-f imaging system.

The RF-modulated optical signal was amplified by an erbium-doped fibre amplifier (EDFA) and launched, as an input signal, into Port 5 of an optical fibre array of 250μmfibre-to-fibre spacing. This input RF-modulated optical signal was collimated through a lens of focal length f=25mm, to an optical beam diameter of 5.48 mm, illuminating around 3046 pixels of the Opto-VLSI processor, thus leading to a high diffraction efficiency and high optical splitting resolution.

By driving the Opto-VLSI processor with an optimized multicasting phase hologram, the optical beam illuminating the Opto-VLSI processor was split into four different optical beams (in addition to the 0^{th} order beam) which propagated along the optimized directions so that they were coupled back into the fibre array output ports through the 4-f imaging system. The split modulated optical signal coupled into the output ports

propagated along the angles $\theta_{2,3} = \pm 0.58$ and $\theta_{1,4} = \pm 1.16$ with respect to the 0^{th} order beam direction.

A photodetector (PD) array was used to detect the split optical signals emerging from Ports 1-4, and an oscilloscope and a network analyser were used to measure the corresponding RF output signals and frequency responses, respectively.

5.3.2 Experimental results and discussion

Several user-defined RF signal splitting scenarios were attempted in the experiments to demonstrate the capability of the proposed broadband adaptive RF power splitter. Figure 3 shows the measured output RF power levels ($V_{RF,1}$, $V_{RF,2}$, $V_{RF,3}$, and $V_{RF,4}$) coupled into the output RF Ports 1-4, respectively, for different splitting ratios. The input RF signal had amplitude of 220 mV peak-to-peak and a frequency of 2.3 GHz.

Fig. 5.3(a) demonstrates a scenario where the input RF power is split equally into the output ports by uploading phase hologram corresponding to splitting profile 0.057:0.051:0.050:0.062, resulting in approximately similar RF output signals for all the output RF ports. Fig. 5.3(b) shows the measured output RF voltages for a phase hologram corresponding to a splitting profile of 0.010:0.028:0.189:0.057. Fig. 5.3(c) shows the measured output RF voltages when the signal levels for Ports 1 and Port 2 were dropped to 50% and zero of their maximum values, respectively, corresponding to a splitting profile of 0.028:0.000:0.140:0.119.It is noted from Fig. 5.3 that for all scenarios the fluctuation in output RF voltage is less than 1 dB.

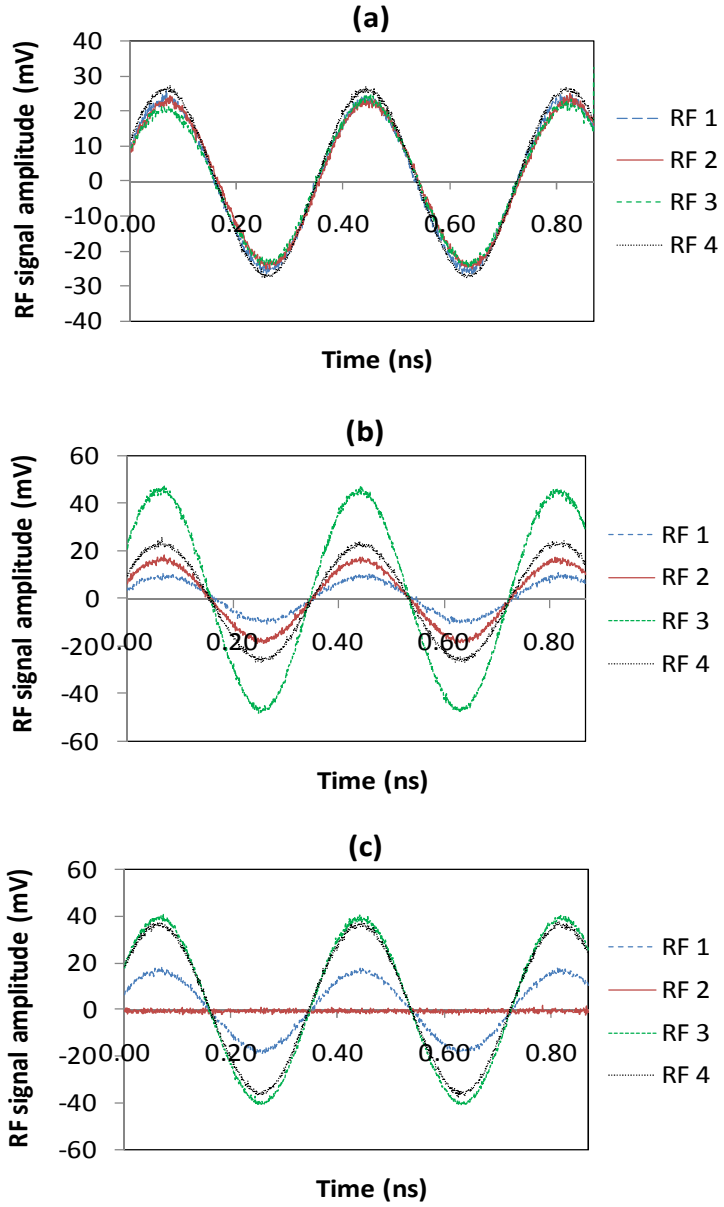

Fig. 5.3. Measured output RF power levels $V_{RF,1}$, $V_{RF,2}$, $V_{RF,3}$, and $V_{RF,4}$ coupled into the output RF Ports1-4, respectively, for an input RF signal of 220 mV peak-to-peak amplitude and frequency of 2.3 GHz split by uploading multicasting holograms onto the Opto-VLSI processor, which correspond to different splitting ratios: (a) 0.057:0.051:0.050:0.062, (b) 0.010:0.028:0.189:0.057 and (c) 0.028:0.000:0.140:0.119.

Table 5.1 shows additional scenarios where different splitting ratios corresponding to different multicasting phase holograms were optimized and uploaded onto the Opto-VLSI processor. It is important to notice from Table 5.1 that the measured optical power of the 0^{th} order optical signal was suppressed by more than 14 dB for all splitting holograms attempted in the experiments, therefore, the intensity of the zeroth order op-

tical signal was always insignificant compared to the intensities of the split output optical signals. However, small variations in the measured output signals were experienced, which are attributed to errors caused by the pixel resolution and optical beam misalignment. The broadband capability of the adaptive RF power splitter was also investigated experimentally in the next section.

Table 5.1 Different RF power splitting profiles generated through optimised multicasting phased holograms uploaded onto the Opto-VLSI processor, and the corresponding peak-to-peak voltages of the measured output RF signals at Ports 1-4. Also shown is the measured optical power of the zeroth order beam which was monitored by an optical spectrum analyser.

Applied Hologram (H)	$V_{RF,1}$ (p-p) **(mV)**	$V_{RF,2}$ (p-p) **(mV)**	$V_{RF,3}$ (p-p) **(mV)**	$V_{RF,4}$ (p-p) **(mV)**	**0^{th} order (dBm)**
No hologram	0	0	0	0	+4.0
H_1=0.057:0.051:0.050:0.062	52.4	49.9	49.3	54.8	-13.0
H_2=0.010:0.028:0.189:0.057	21.7	36.9	95.6	52.4	-12.8
H_3=0.028:0.000:0.140:0.119	37.0	4.3	82.3	75.8	-10.0
H_4=0.228:0.000:0.001:0.211	105.0	4.3	5.9	101.0	-14.0
H_5=0.056:0.002:0.077:0.188	52.0	9.0	61.0	95.3	-12.4
H_6=0.020:0.027:0.120:0.093	30.7	36.4	76.2	67.2	-11.0
H_7=0.096:0.029:0.033:0.089	68.0	37.7	40.2	65.8	-12.5

5.4 DEMONSTRATIONOF THE MULTIPORT BROADBAND ADAPTIVE RF POWER SPLITTER

5.4.1 Experimental set-up

Fig. 5.4 shows the experimental setup that was used to demonstrate the proof-of-concept of the proposed RF power splitter. The proposed structure consists of an Opto-VLSI processor, a 2-element lens array with adjustable lens spacing, and optical fibre array. All components were aligned to form two 4-f imaging systems. The Opto-VLSI processor used in the experiments has 1×4096 pixels, a pixel size of 1.0 μm×6.0 mm, a pixel pitch of 1.8μm (i.e., 0.8 μm of dead space between pixels), and an active area of 7.4 mm×6.0 mm. The lens array had two elements of focal length (*f*) 9 mm and diameter 3mm, and was placed between and at an equal distance, *f*, from both the fibre array and the Opto-VLSI processor. The intensity of a 1550 nm continuous wave (CW) laser signal was externally modulated by an RF signal using a JDS Uniphase electro-optic modulator (EOM). The RF-modulated optical signal was amplified by an erbium-doped fibre amplifier (EDFA) and launched, as an input signal, into Port 9 of an optical fibre array of 127μmfibre-to-fibre spacing.

By driving the Opto-VLSI with an optimized multicasting phase hologram, The RF-modulated optical power was split into five output ports 'Port 1, Port 2, Port 3, Port 4, and Port 10' (in addition to the 0^{th} order beam) which propagated along the optimized directions so that they were coupled back into the fibre array output ports through the 4-f imaging system. The output signal of Port 10 was amplified via an EDFA and then launched as second input into Port 11 to be split into Four output ports 'Port 5, Port 6, Port 7, and Port 8'. For both input RF-modulated optical beams (at Ports 9 and 11), the split RF-modulated optical beams propagated along ±0.81°, ±1.62°, and ±2.43° with respect to the direction of the 0^{th} order beam. After emerging from the optical fibres, both input RF-modulated optical signals were collimated through the corresponding lens, at a diameter of 1.962 mm. Each collimated beam illuminated around independently-addressed 1090 pixels of the Opto-VLSI processor, leading to high diffraction efficiency and high optical splitting angle.The active window of the Opto-VLSI processor was divided into two pixel blocks, separated by 934 un-addressed pixels. A photodetector (PD) array was used to detect the split optical signals emerging from Ports 1-8, and an oscilloscope and a network analyser were used to measure the corresponding RF output signals and frequency responses, respectively.

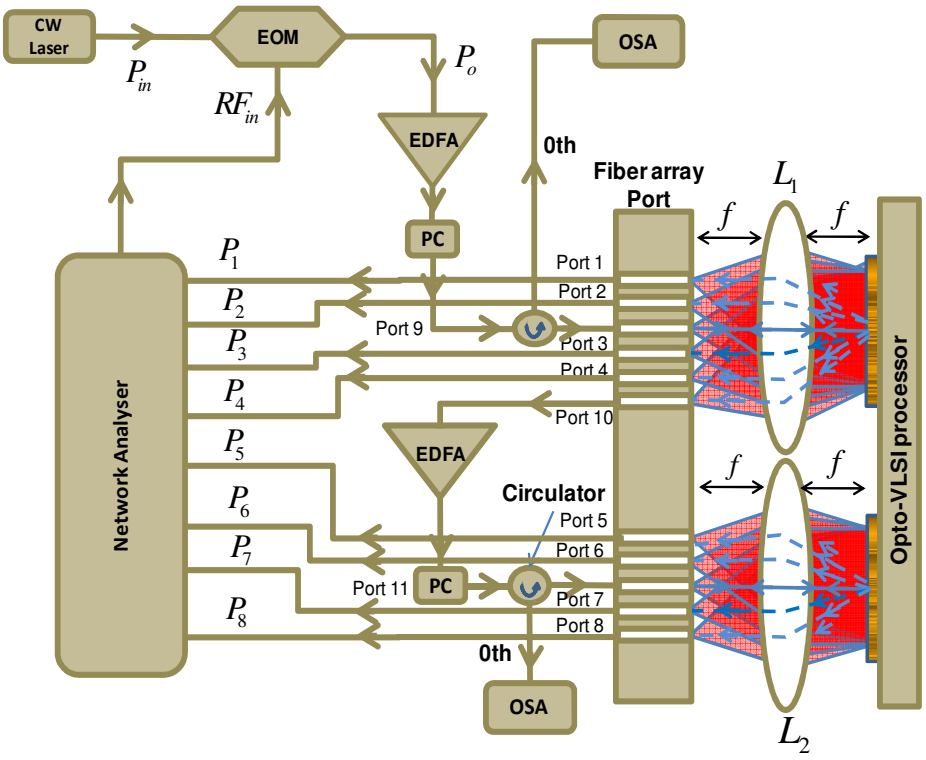

Fig. 5.4 Experimental setup of the proposed broadband adaptive RF splitter structure, which is based on the use of an Opto-VLSI processor in conjunction with an array of 4-f imaging systems.

5.4.2 Experimental results and discussion

As illustrated in Fig. 5.4, the RF frequency response of the adaptive splitter was measured by using a broadband vector network analyser that supplied and swiped the frequency of the input RF signal driving the EOM.

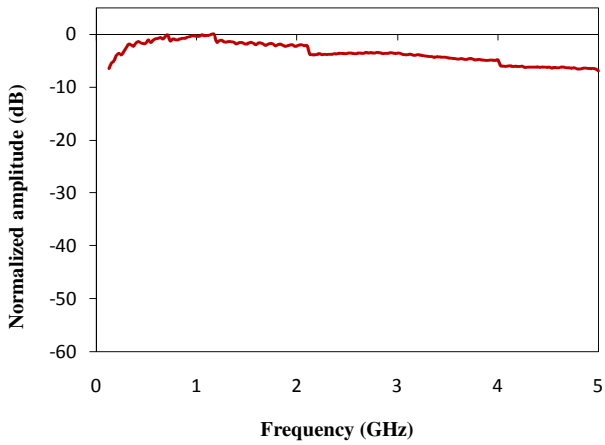

Fig. 5.5. The measured RF frequency response of the electro-optic modulator (EOM).

Fig. 5.5 shows the measured RF frequency response of the EOM. It is important to note that the roll-off of the frequency responses at high frequencies are attributed to the limited bandwidth (4 GHz) of the EOM used in the experiments. The output power at fibre Port 10 was maintained constant, then amplified via an EDFA and launched into Port 11 for subsequence split into Ports 7-8.

Fig. 5.6 shows the frequency responses of the splitter for different splitting scenarios, over a frequency range from 130 kHz to 5 GHz. For each desired splitting profile, optimized multicasting phase holograms were generated (using simulated annealing algorithms) and applied onto the corresponding pixels blocks. The ratios of output power level at fibre Port 10 was maintained constant in all splitting scenarios. The optical power at Port 10 was amplified via an EDFA, and then coupled into Port 11 for subsequent splitting into the output fibre Ports 5-8.

Fig. 5.6(a) demonstrates a scenario where the input RF power is split equally into the output Ports 1-8 by uploading computer-generated phase holograms corresponding to an RF splitting profile 1.00:1.00:1.00:1.00:1.00:1.00:1.00:1.00, resulting in a uniform RF responses for all the output Ports 1-8. Fig. 5.6(b) shows the measured output Port 1-8 RF responses when the power levels at Ports 1, 2, and 6 were reduced by 18 dB, 13 dB, and 7 dB, respectively, by uploading computer-generated phase holograms onto the Opto-VLSI processor, which correspond to an RF splitting profile of 0.01:0.04:1.0:1.00:1.00:0.23:1.00:1.00. Fig. 5.6(c) shows the measured RF responses when the power levels at Port 3 and Port 6 were suppressed by 30 dB and 20 dB, respectively, while those at Ports 1, 4, and 8 were reduced by 7 dB, corresponding to a splitting profile of 0.20:1.00:0.00:0.20:1.00:0.01:1.00:0.20. The experimental results shown in Fig. 5.6 demonstrate the ability of the proposed broadband adaptive RF splitter structure, shown in Fig. 5.4, to realize arbitrary RF splitting ratios through the use of optimized multicasting phase holograms uploaded onto the Opto-VLSI processor.

Note that the measured maximum output power fluctuation for the output ports was less than 2.0 dB. Also, the measured crosstalk level was less than -30 dB. Note also that, by using the erbium-doped fibre amplifier (EDFA), the insertion losses of the proposed RF splitter was compensated. Finally, it is noticed that the measured output RF power splitting ratios are in excellent agreement with the user-defined ratios used in the computer algorithm that was especially developed to generate the optimized multicasting phase holograms.

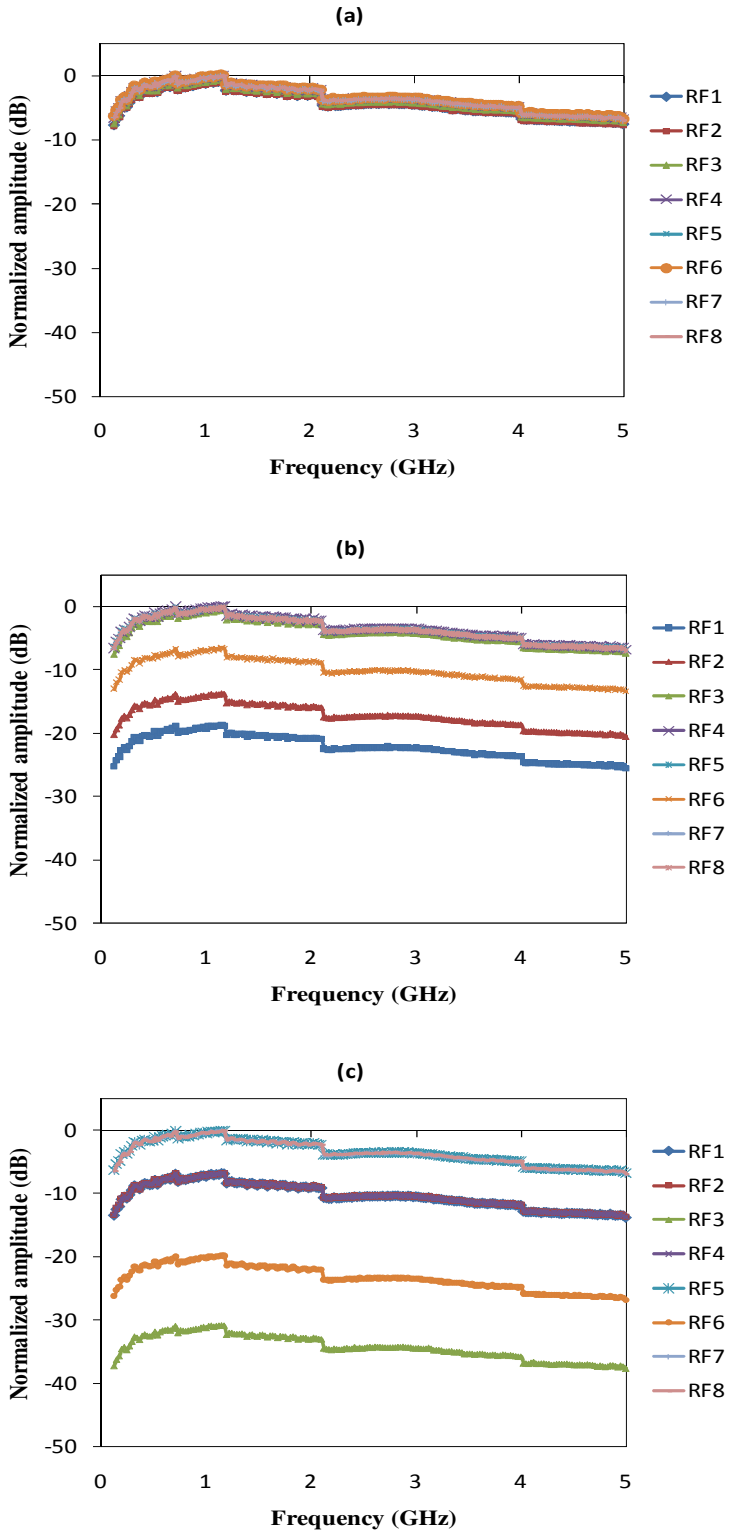

Fig. 5.6. Measured normalized RF spectrum coupled into the output RF Ports1-8, for an input RF frequency range from 130 kHz to 5GHz. Splitting was achieved by uploading multicasting holograms onto the Opto-VLSI processor, corresponding to different normalized RF power splitting ratios: (a) 1.00:1.00:1.00:1.00:1.00:1.00:1.00:1.00, (b) 0.01:0.04:1.0:1.00:1.00:0.23:1.00:1.00, and (c) 0.20:1.00:0.00:0.20:1.00:0.01:1.00:0.20.

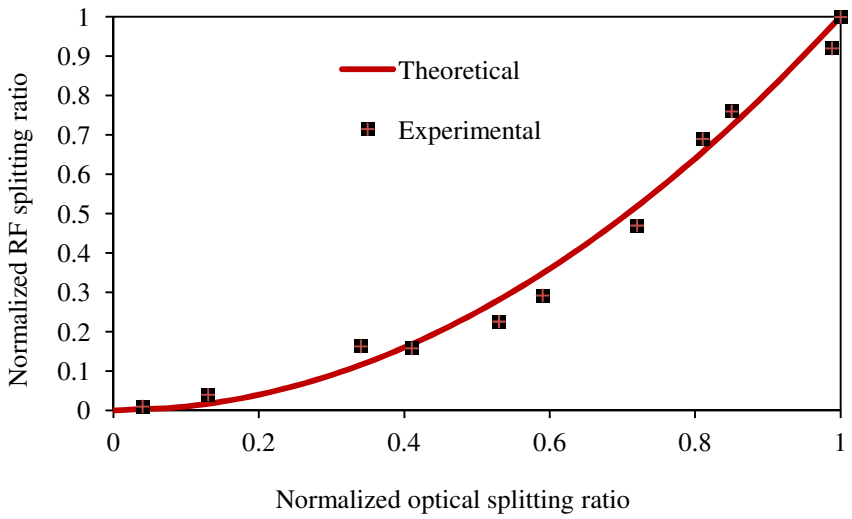

Fig. 5.7. Measured and theoretical RF splitting ratio versus optical splitting ratio for Port 3.

Fig. 5.7 shows the measured normalized RF splitting ratio, α_3, versus the normalized optical splitting ratio, η_3. Port 3 was selected to demonstrate the quadratic relationship between α_3 and η_3 expressed in Eq. (5.7). It is clear that the experimental results are in excellent agreement with the simulation results generated by the theoretical relationship of the RF and optical power splitting ratios governed by Eq. (5.7). Note that the constant A in Eq. (5.7) can be set to a unity value by controlling the EDFA gain.

The results displayed in Fig. 5.5-Fig. 5.7 demonstrate the principle of the proposed multiport broadband adaptive RF power splitter.

5.5 DEMONSTRATION OF ADAPTIVE RF POWER COMBINER BASED OPTO-VLSI PROCESSOR

5.5.1 System description

Fig. 5.8 illustrates, through the setup that was used in the experiments, the proposed Opto-VLSI based adaptive RF signals combiner structure. The intensity of two continuous waves (CW) laser signals, 1548 nm, and 1550 nm were externally modulated by an RF_1(780MHz) and RF_2 (1.3 GHz) analogue signals, respectively, using two electro-optic modulator (EOM). The EOM and the Opto-VLSI processor are polarization sensitive, thus two polarization controllers (PC) were used.

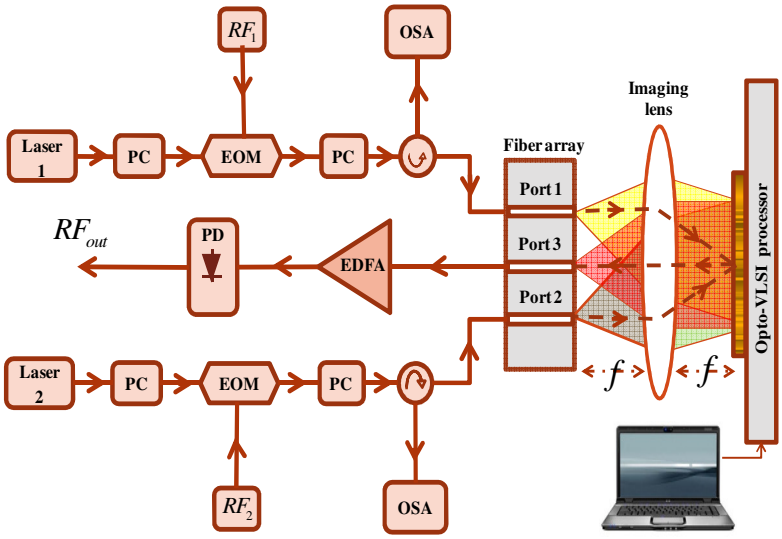

Fig. 5.8. Experimental setup used to demonstrate the capability of the proposed Opto-VLSI based adaptive RF signal combiner to adaptively combine two input RF signals into single output port with user-defined combing ratio.

The two RF-modulated optical signals, RF_1 and RF_2, were launched into the input fibre Port 1 and Port 2, respectively. This input RF-modulated optical signal were collimated through a lens of focal length f=25mm, to an optical beam diameter of 5.48 mm, illuminating around 3,046 pixels of the Opto-VLSI processor.

By driving the Opto-VLSI processor with an optimized multicasting phase hologram, the optical were combined and coupled into a single output fibre Port 3 through the 4-f imaging system. The output RF-modulated optical signal was amplified by an

erbium-doped fibre amplifier (EDFA) for insertion loss compensation. A photodetector (PD) was used to detect the output RF-modulated optical signals.

5.5.2 Experimental results and discussion

The principle of the adaptive optical combiner was demonstrated by launching two RF input signals into Ports 1and 2 and measuring the output signal from Port 3. Fig. 5.9 shows the measured input signals launched into the input fibre port 1 and 2.

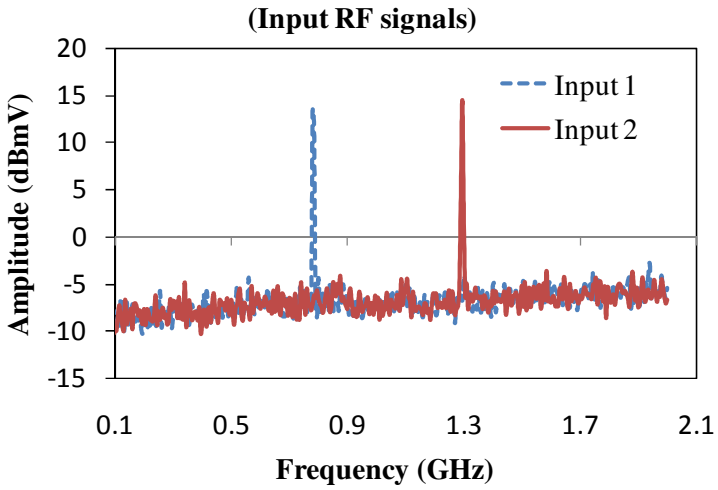

Fig. 5.9. The measured RF signals launched into the input Port 1 and 2.

Fig. 5.10 (a) shows the measure output combined optical signal using an optimized multicasting phase hologram uploaded onto the Opo-VLSI processor, which correspond to combining profile of 1.0:1.0,demonstrating that the two input RF signals can be combined with a uniform power level at output Port 3. Note that the small signal at 1.6GHz marked as noise generated by the signal generator. Fig. 5.10(b-e) shows the measure output combined optical signal where $RF_1$was attenuated by 4.5dB, 5.5dB, 14.5dB, and 24dB using an optimized multicasting phase hologram uploaded onto the Opo-VLSI processor corresponding to combining profile of 0.45:1.0, 0.28:1.0, 0.03:1.0, and 0.004:1.0, respectively. In Fig. 5.10(f), the power level of the signal $RF_1$was suppressed to zero by uploading an optimized phase hologram onto the Opto-VLSI processor which corresponding to combining profile of 0.0:1.0. Fig. 5.10(a-f) demonstrates the ability of the Opto-VLSI processor to combine the input RF signals with an arbitrarily weight profile and couple them into the output fibre Port 3.

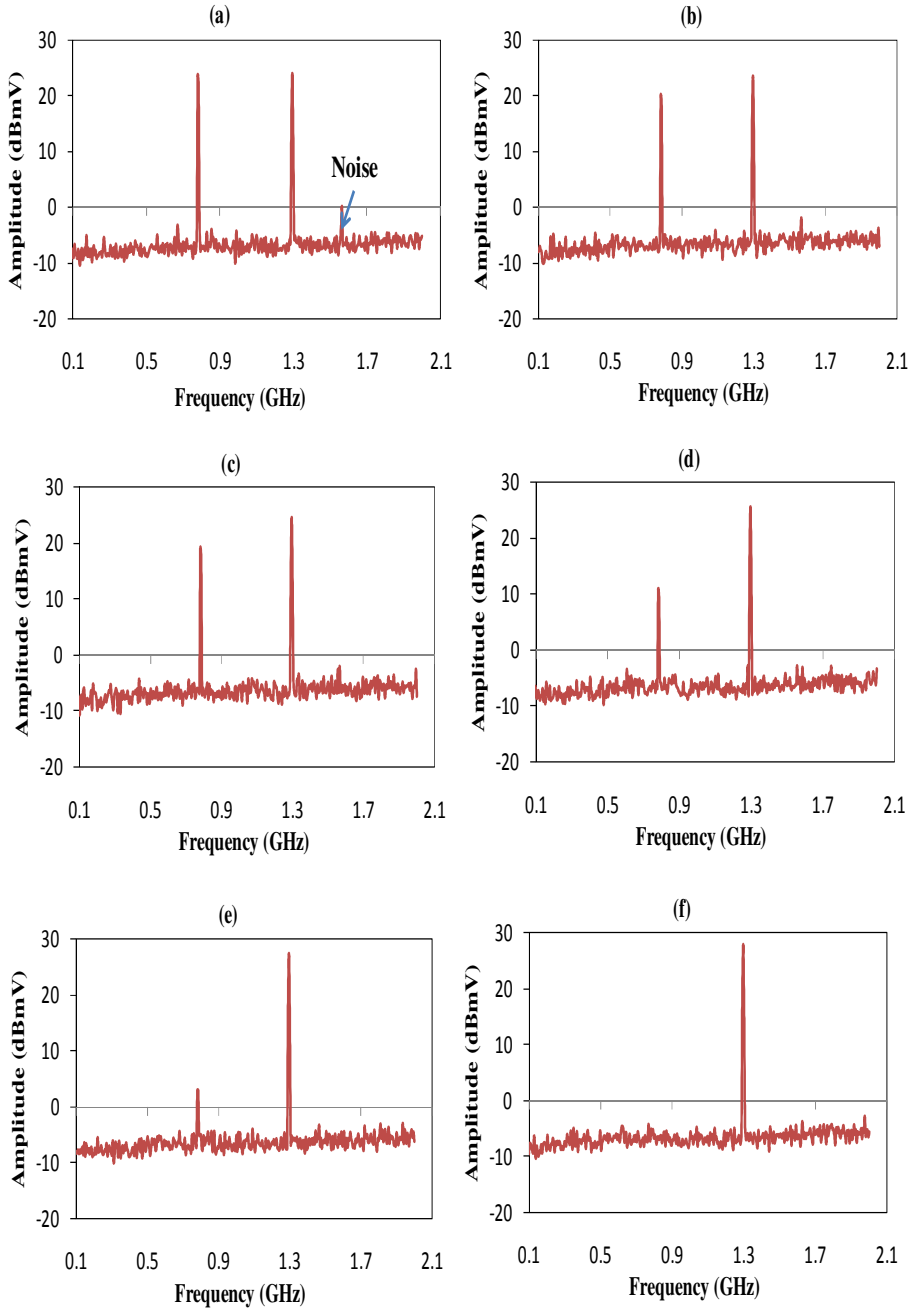

Fig. 5.10. The measured output combined RF signal at Port 3 for phase holograms corresponding to combing profiles of (a) 1.0:1.0, (b) 0.45:1.0, (c) 0.28:1.0, (d) 0.03:1.0, 0.004:1.0,and 0.0:1.0.

5.6 SUMMARY

A novel broadband adaptive RF power splitter/combiner structure based on Opto-VLSI processor is proposed and experimentally demonstrated. By uploading optimized multi-casting phase holograms onto the software-driven Opto-VLSI processor, an input RF signal is dynamically split into different output ports with user-defined splitting ratios. Also, multiple input RF signals can dynamically be combined with arbitrary user-defined weights. As a proof-of-concept demonstration, two input RF signals have been dynamically combined with different combing weights profiles.

CHAPTER 6

PHOTONIC MICROWAVE APPLICATIONS

6.1 INTRODUCTION

The processing of radio frequency (RF) and microwave signals in the optical domain is an attractive approach to overcome the bottlenecks of bandwidth, power loss, and electromagnetic interference (EMI) encountered in conventional electronic signal processing systems [19, 20, 107].A wide range of emerging RF signal processing applications require specifically high resolution, ultra-wide bandwidth, wide-range tunability, and fast reconfigurability. While these requirements are difficult to achieve using conventional all-electronic processing, they are feasible with photonics-based signal processing [108, 109]. Photonics-based RF signal processing can potentially provide advantages including [110]:

(i) high resolution broadband delay lines (transversal filters) through the use of Fibre Bragg Gratings (FBGs) or dispersion optical fibres
(ii) adaptive filtering of RF signals
(iii) fast sampling of RF signals
(iv) suppression of optical carriers and sidebands
(v) optical beam steering and splitting
(vi) optical coding for secure communications

Due to their small size, low weight and low power attenuation, optical fibres are excellent candidates for realising delay lines for the implementation of transversal RF filters. This chapter presents experimental results that demonstrate the concept of a new Photonic microwave filter employing an Opto-VLSI-based adaptive optical signal combiner. A single Opto-VLSI processor can be reconfigured in real time, allowing a large number of RF-modulated optical signals to be dynamically attenuated, thus making adaptive photonic RF signal processing practical [111].The demonstrated photonic microwave filter can be reconfigured via software, thereby synthesizing the weights of the filter taps by uploading multicasting phase hologram onto the Opto-VLSI processor.

6.2 TRANSVERSAL OPTICAL RF FILTER

Fig. 6.1 illustrates a traditional transversal filter realized by modulating an optical carrier by an RF signal and then splitting the resulting RF-modulated optical signal by a passive optical power splitter, thus generating a large number of taps. The use of optical fibre delay lines enables the generation of constant differential delays, while the variable attenuator array controls the weights of the delayed signals. However, these transversal filter structures have some limitations, mainly related to tunablitity and reconfigurablitiy.

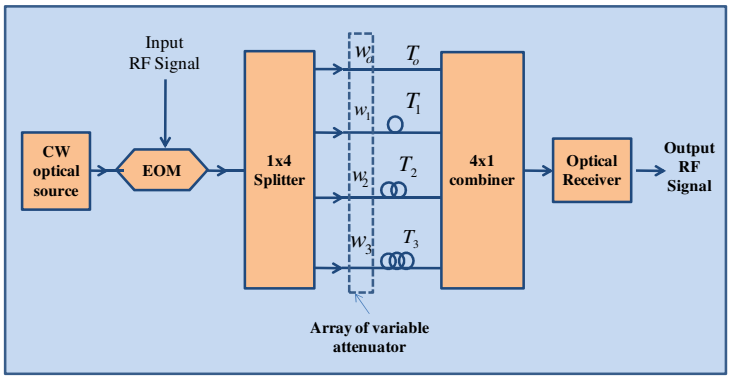

Fig. 6.1. Transversal filter structure employs a passive optical splitter/combiner, and an array of variable attenuator.

Fig. 6.2(a) shows another transversal filter structure employing an array of tunable lasers in conjunction with linear chirped fibre grating [112, 113]. As illustrated in Fig. 6.2(a), the output lasers signals are combined into a single port using optical combiner, and then modulated by an RF signal via an electro-optic-modulator (EOM). The chirped fibre grating provides linear group delay versus wavelength and allows very low time delay increments between samples to be generated, i.e., high sampling rate and very high free spectral range (FSR). However, the main disadvantage of this transversal filter structure is the relatively high cost especially when the number of tunable laser sources increases. To reduce the cost, another structure based on using only single tunable laser source in conjunction with fibre Bragg grating array has been proposed [114]. This structure uses a passive optical splitter to split the laser signal into multiport signals and optical attenuators for weight control, as illustrated in Fig. 6.2(b). However, this structure has an intrinsic limitation resulting from the interference between the detected signals thus causing fluctuation in the RF response [114].

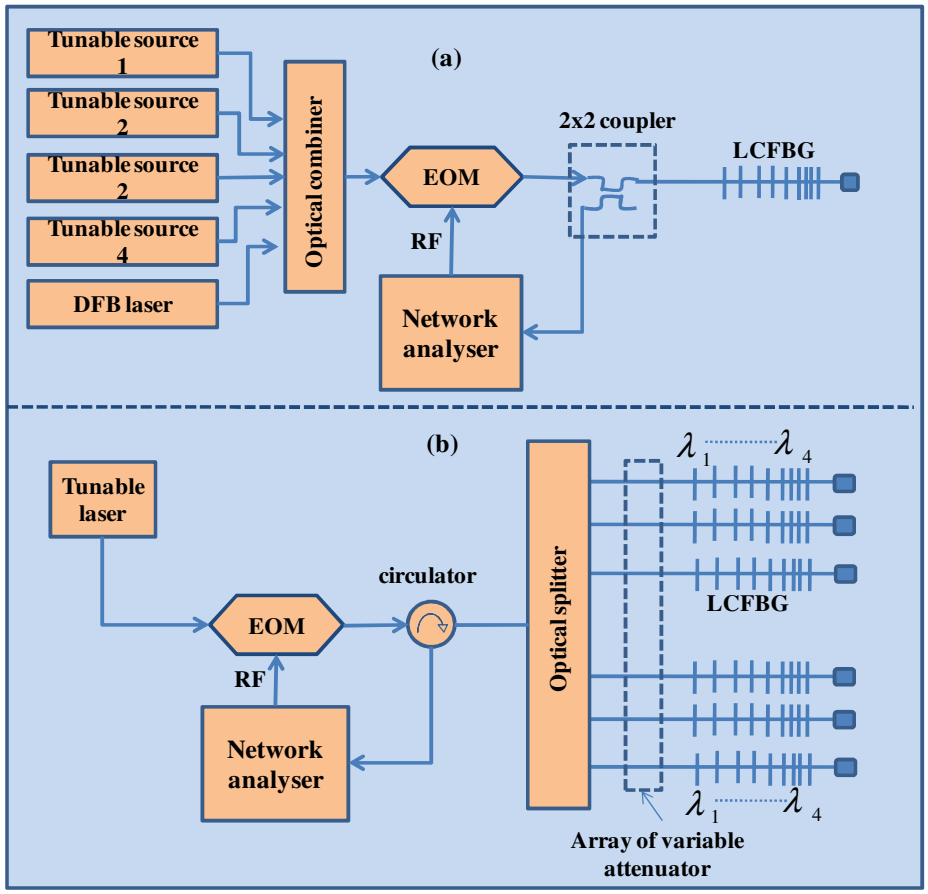

Fig. 6.2. Transversal filter structure based on the use of (a) an array of tunable lasers in combination with linear chirped fibre Bragg grating (LCFBG)and optical combiner/coupler (b)single tunable laser source in combination with LCFBG, optical splitter, and an array of variable attenuator.

The use of Fabry-Perot filter as slicing technique over a broadband optical source is used to obtain a sampled optical spectrum thus eliminating the need for an expensive laser array [115]. The poor flexibility of Fabry-Perot Filter is the main disadvantages of this filter structure. Fig. 6.3 illustrates a reported transversal filter structure based on spectral slicing using arrayed waveguide gratings (AWG) [116]. An array of variable attenuator is used to provide different filter-taps weights before the taps combined via a passive optical combiner (AWG can also be used as a combiner). The use of optical combiners in conjunction with variable optical attenuators is one of the potential approaches used to synthesise a transversal RF filter response with variable weights [113, 117]. However, for a high order transversal filter the implementation and control a large number of variable optical attenuators become impractical. The ability to dynamically

recombine the delayed RF-modulated optical signals with arbitrary weights has the potential to realise an adaptive transversal RF filter, whose resolution depends on the tap counts and the minimum attainable delay [19, 20]. Fig. 6.4 illustrates the use of adaptive optical combiner to replace the large number of the variable attenuator and the second AWG 2 in Fig. 6.3.

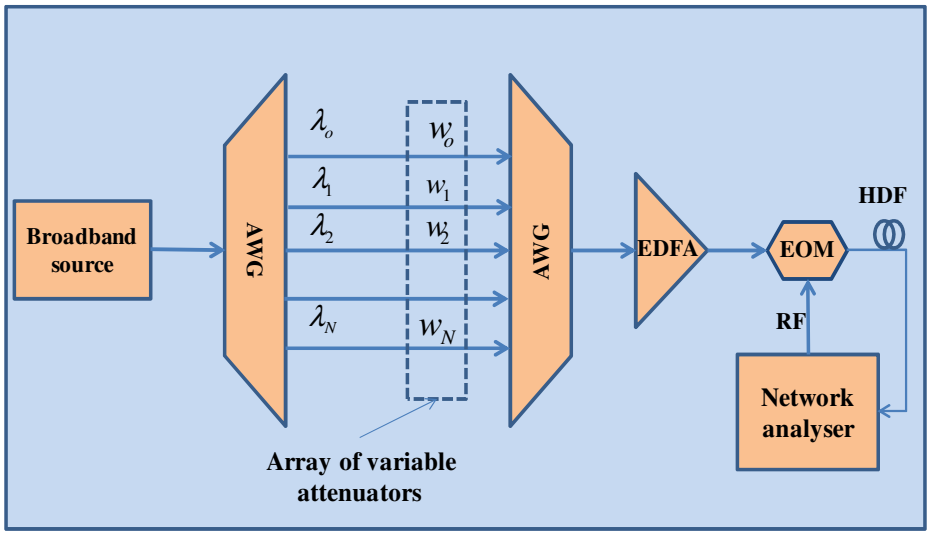

Fig. 6.3. Transversal filter structure employs an arrayed waveguide gratings (AWG 1) in combination with an arrayed variable optical attenuators and passive optical combiner (AWG 2).

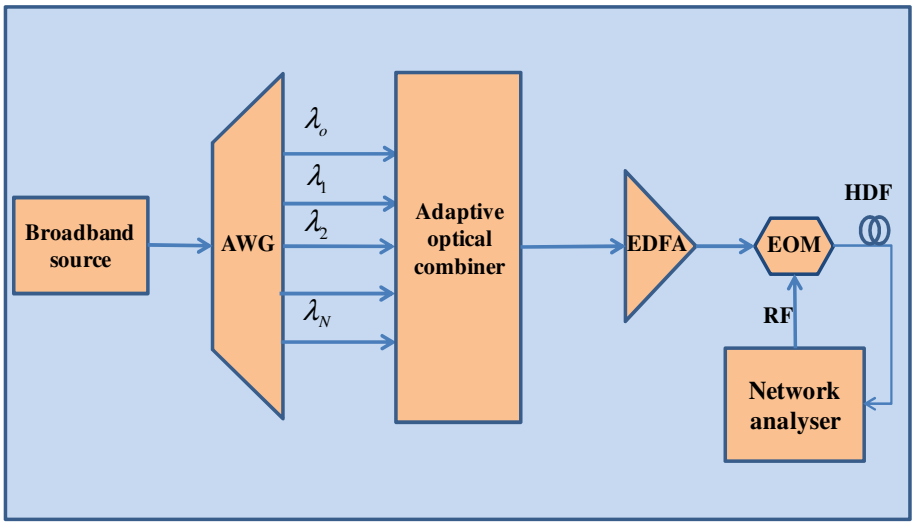

Fig. 6.4. Schematic diagram of transversal filter structure employs an arrayed waveguide gratings (AWG) in combination with an adaptive optical signals combiner instead of using an array of variable attenuators and passive optical combiner.

6.3 PROPOSED PHOTONIC MICROWAVE FILTER

The proposed photonic microwave filter is illustrated, through an experimental setup, in Fig. 6.5. A broadband laser source was sliced into 16 channels using arrayed waveguide grating (AWG). Four channels of similar output power and a wavelength separation of $\Delta\lambda$, were launched into the Opto-VLSI-based adaptive optical signals combiner (described in Chapter 4 in Section 4.8). The output combined optical signal was amplified by an erbium-doped fibre amplifier (EDFA). The amplified optical signal was externally modulated by an RF signal through an electro-optic modulator (EOM).

The wavelength division multiplexed (WDM) modulated light was launched into a high dispersion fibre (HDF), which has a dispersion coefficient of 382.5 ps/nm and insertion loss of 4.6 dB. Each WDM channel experienced an RF delay that depends on its centre wavelength. After photodetection, the generated output RF signal is the sum of delayed versions of the input RF signal, whose weights depend on the combination profile set by the Opto-VLSI processor. Therefore, the structure shown in Fig. 6.4 represents a photonic microwave filter, whose response can be tuned by the Opto-VLSI processor. A network analyser was used to generate the input RF signal and read out the filter response expressed as [40]:

$$H(f) = \sum_{r}^{M} w_r \exp\left(-j2\pi r f \tau\right) \tag{6.1}$$

where f is the RF frequency, M is the number of the detected RF-modulated wavebands, w_r is the rth tap weight, which is proportional to the optical power of the rth waveband, and τ is the time delay between adjacent wavebands introduced by the HDF. The time delay τ can also be expressed in terms of the dispersion of the HDF as

$$\tau = \alpha \cdot \Delta\lambda \tag{6.2}$$

where α denotes the dispersion coefficient of the HDF, and $\Delta\lambda$ is the adjacent waveband separation.

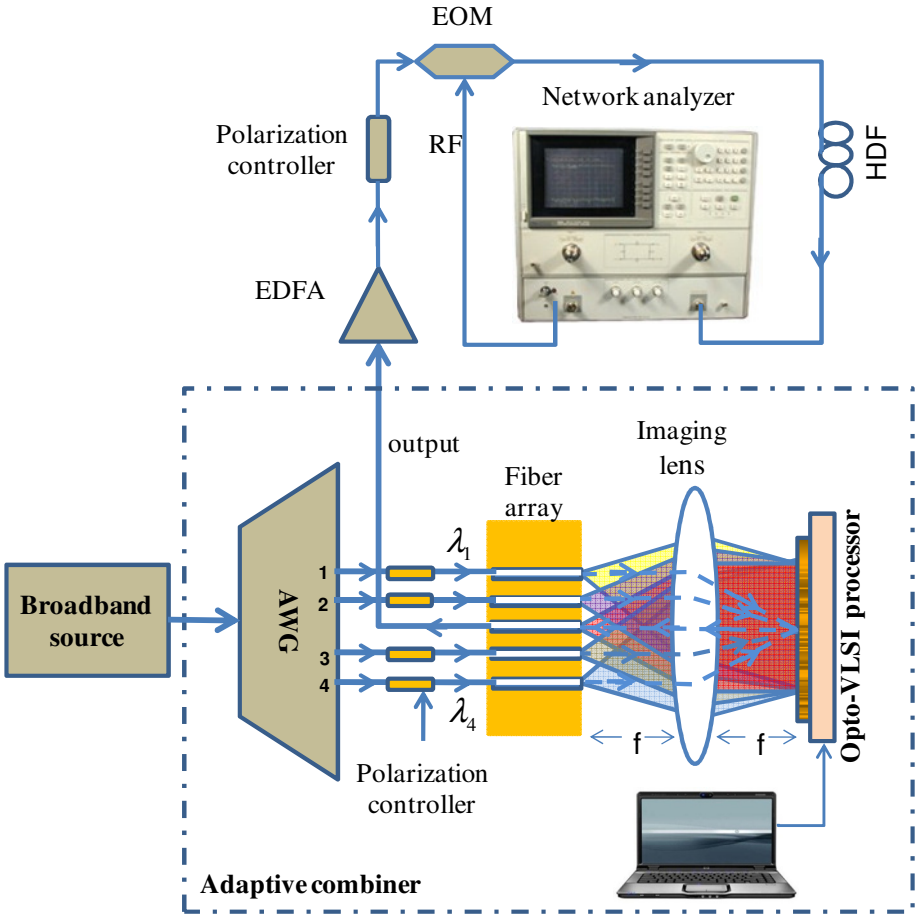

Fig. 6.5. Experimental setups of the proposed photonic microwave filter employing an Opto-VLSI-based adaptive optical combiner. Opto-VLSI-based adaptive optical combiner is described in Section 4.8.

6.4 EXPERIMENTAL RESULTS AND DISCUSSION

Several weight profiles were generated using an optimized multicasting phase hologram uploaded onto the Opto-VLSI processor to demonstrate the principle of the proposed photonic microwave filter experimentally.

Fig. 6.6(a), (c), and (e) show the weight profiles of the four WDM channels, spaced at $\Delta\lambda$ =1nm centre-to-centre, corresponding to combining profiles of {1, 1, 1, 1}, {0.6, 1.0, 1.0, 0.6}, and {0.5, 1.0, 0.8, 0.5}, respectively. Fig. 6.6(b), (d) and (f) show the corresponding measured and simulated RF responses. Excellent agreement between the measured and simulated RF responses is seen at low frequencies. The discrepancies at high frequencies are attributed to the limited bandwidth (4 GHz) of the EOM used in the experiments.

Fig. 6.7(a), (c), and (e) show the weight profiles corresponding to combining profile equal to {1, 1, 1, 1}, {0.6, 1.0, 1.0, 0.6}, and {0.5, 1.0, 0.8, 0.5}, respectively, when the WDM channel spacing was increased to $\Delta\lambda$ =2nm centre-to-centre. Fig. 6.7(b), (d) and (f) show the corresponding measured and simulated RF responses. Note that, by changing the WDM weights while keeping a constant WDM channel spacing, the center frequency of the filter is kept unchanged, while the filter's rejection is changed. By increasing the WDM channel spacing, a narrower pass band is synthesized.

The theoretical Main Lobe to Sidelobe Suppression Ratio (MSSR) for uniform tap filter is around 13 dB which is in excellent agreement with the experimental results. The MSSR value was increased up to 20dB when the weight profile was changed from {1, 1, 1, 1} to {0.6, 1.0, 1.0, 0.6} as evident from Fig. 6.6(d) and Fig. 6.7(d). The ability of the Opto-VLSI processor to control the MSSR value and the pass band of the microwave filter through the synthesis of optimized combination weight profile demonstrates the principle of the proposed photonic microwave filter.

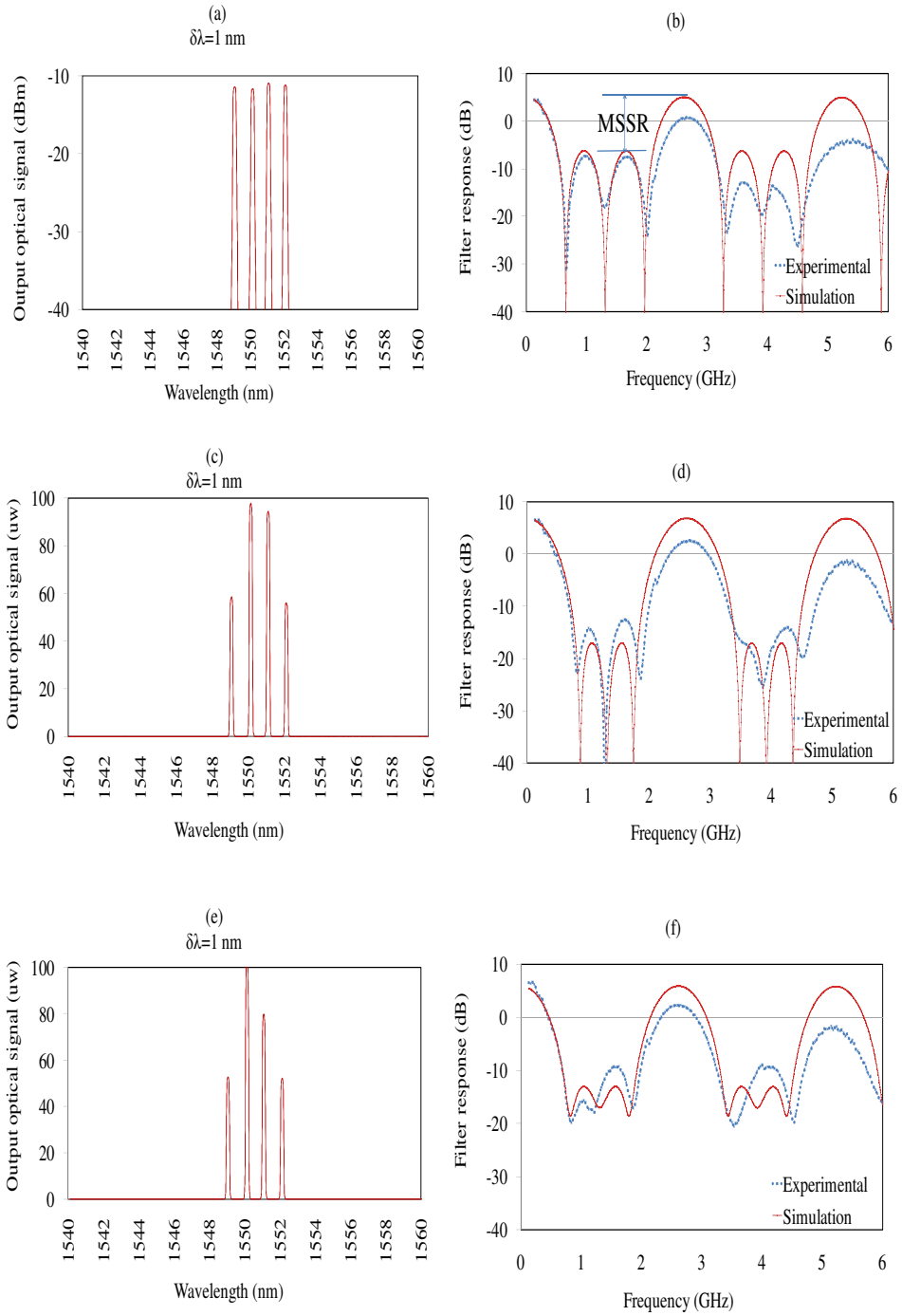

Fig. 6.6. (a), (c) and (e) Weight profiles of the four WDM RF-modulated channels and (b), (d) and (f) corresponding RF filter responses. Weight profile in (a) is {1, 1, 1, 1}, in (c) is {0.6, 1.0, 1.0, 0.6}, and in (e) {0.5, 1.0, 0.8, 0.5}. WDM channel spacing is 1nm centre-to- centre.

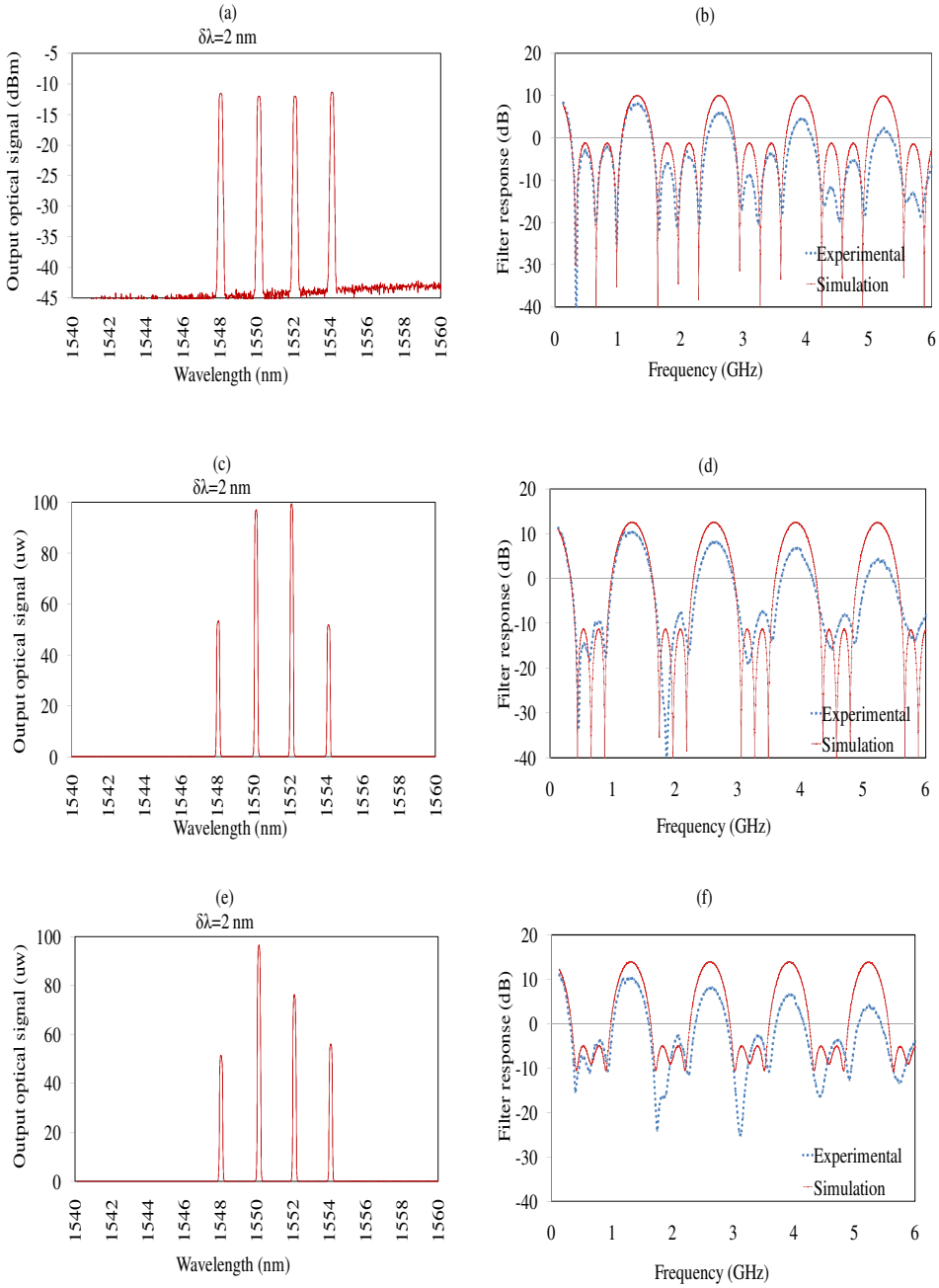

Fig. 6.7. (a), (c) and (e) Weight profiles of the four WDM RF-modulated channels and (b), (d) and (f) corresponding RF filter responses. Weight profile in (a) is {1, 1, 1, 1}, in (c) is {0.6, 1.0, 1.0, 0.6}, and in (e) {0.5, 1.0, 0.8, 0.5}. WDM channel spacing is 2nm centre-to- centre.

6.5 SUMMARY

A novel structure of photonic microwave filter that employ an Opto-VLSI based adaptive optical combiner has been proposed and experimentally demonstrated. Different weight profiles have been generated, demonstrating the ability of the Opto-VLSI based adaptive optical combiner to dynamically combine multiple input optical signals with user-defined weight profiles, thus realising a tunable microwave filter.

CHAPTER 7

CONCLUSIONS AND RECOMMENDATIONS

7.1 INTRODUCTION

The research activities that have been undertaken in this thesis focused on the development of an Opto-VLSI-based adaptive optical power splitter/combiner for next generation dynamic optical communication networks. The proposed and experimentally demonstrated adaptive optical power splitters have been based on the use of Opto-VLSI technology in conjunction with a 4-f imaging system.

Motivation for this research study has been the limitation of passive optical power splitters, as mentioned earlier in this thesis, and the demand for adaptive optical power splitters for many applications, including passive optical networks (PON) and photonic RF signal processing.

7.2 SUMMARY OF THE THESIS

This thesis has proposed and demonstrated the principle of novel Opto-VLSI-based adaptive optical splitters/combiners for next generation dynamic optical telecommunication networks. It has been demonstrated that, through optimized phase holograms driving the Opto-VLSI processor, these splitter structures adaptively split the optical power of an input signal into a larger number of output signals and couple them into output fibre ports.

Particularly, three adaptive optical power splitter structures have been experimentally demonstrated, namely:

(i) A 1×2 adaptive optical power splitter based on an Opto-VLSI processor, a fibre collimator array and 4-f imaging systems (single lens).

(ii) A 1×4 adaptive optical power splitter based on an Opto-VLSI processor, a fibre array and 4-f imaging systems (single lens).

(iii) A 1×N lossless adaptive optical power splitter structure integrating an Opto-VLSI processor, optical amplifiers, a fibre array, and an array of 4-f imaging systems (lens array).

All developed adaptive optical splitters have adequate inter-port crosstalk, compressed hardware and simple user interface. The concept of an adaptive optical signal combiner, which enables multiple optical signals to be combined with user-defined weight profiles into a single fibre port, has also been demonstrated.

A computer algorithm has especially been developed to drive the Opto-VLSI processor and generate the desired phase holograms that split an input signal arbitrarily and accurately to multiple output optical fibre ports, and also combine multiple input signals with arbitrary weights into a single output optical fibre port. Several novel adaptive RF power splitter structures have been proposed and demonstrated, with the key design feature of these structures being the use of Opto-VLSI processing in conjunction with a photodetector array and a 4-f imaging systems.

Experimental results have demonstrated that an input optical signal can arbitrarily be split into *N* signals and coupled into optical fibre ports by uploading optimized multicasting phase holograms onto the Opto-VLSI processor. They have also demonstrated that *N* input optical signals can be dynamically combined with arbitrary weights into a single optical fibre port. Excellent agreement between theoretical and experimental results has been observed. In addition, results have shown that optical amplifiers can compensate for the insertion and splitting losses, thus enabling lossless splitter operation. A crosstalk level around -25 dB and a wavelength spectral range exceeding 40 nm have been realized.

In addition, a novel broadband adaptive RF power splitter/combiner based on Opto-VLSI processor has been proposed and experimentally demonstrated. By uploading optimized multicasting phase holograms onto the software-driven Opto-VLSI processor, the input RF signal is dynamically split and directed to different output ports, with user-defined splitting ratios. Also, multiple input RF signals can be dynamically combined with arbitrary user-defined weights. As a proof-of-concept demonstration, two input RF signals have experimentally been combined with different user-defined weight profiles.

Furthermore, a photonic microwave filter employing an Opto-VLSI-based adaptive optical combiner has been proposed and demonstrated. The experimental results

have demonstrated that this Opto-VLSI-based adaptive optical combiner can dynamically direct multiple input optical signals to a single output, with user-defined weight profiles, thus realising a tunable microwave filter.

Overall, the demonstrated Opto-VLSI-based adaptive optical power splitter should potentially allow as many as 32 output ports to be supported while achieving high splitting resolution and dynamic range. This will greatly enhance the efficiency of optical communication networks.

7.3 RECOMMENDATIONS FOR FURTHER STUDY

In future, as a continuation of this research study, possible research investigations can be carried out to improve Opto-VLSI based adaptive optical power splitter are as follows:

- The proposed and developed adaptive optical power splitter/combiner of this study uses small Opto-VLSI window (1×4096 pixels) compared to the recent available in the market. A wider Opto-VLSI processor's window (1×12,288 pixels) will lead to an adaptive splitter of at least 32 output ports, which is highly recommended as a commercial product.

- The proposed adaptive optical power splitter was based on 1-D opto-VLSI processor. A 2-D Opto-VLSI processor could add more advantages to the proposed device not only in doubling the number of the output ports but also in realising:

    1) N×N Opto-VLSI based adaptive optical power splitter.

    2) Wavelength selective Opto-VLSI based adaptive optical splitters.

- Implementing the developed adaptive optical splitter/combiner in the field of beamforming networks and smart antenna systems.

- Demonstration of a tunable optical dispersion compensator employing the developed adaptive optical splitter/combiner.

BIBLIOGRAPHY

[1] M. D. Vaughn, D. Kozischek, D. Meis, A. Boskovic, and R. E. Wagner, "Value of reach-and-split ratio increase in FTTH access networks," *Lightwave Technology, Journal of,* vol. 22, pp. 2617-2622, 2004.

[2] R. P. Davey, D. Grossman, M. Rasztovits-Wiech, D. B. Payne, D. Nesset, A. E. Kelly*, et al.*, "Long-Reach Passive Optical Networks," *J. Lightwave Technol.,* vol. 27, pp. 273-291, 02/01 2009.

[3] J. O. Farmer and K. Bourg, "Practical deployment of passive optical networks," *Ieee Communications Magazine,* vol. 46, pp. 136-145, Jul 2008.

[4] K. Okamoto, "Photonic Lightwave Circuits," in *Photonics in Switching, 2007*, 2007, pp. 153-154.

[5] S. Jawhar, B. Cousin, and Z. Bitar, "Power fairness for multicast traffic in optical networks with adaptive light splitters," in *Broadband Networks and Fast Internet (RELABIRA), 2012 Symposium on*, 2012, pp. 29-34.

[6] Y. Z. Wen Liu, Chen Long, Luo Yong, and Keyu Wu. (2005, March 1) Variable optical power splitters create new apps. *LIGHTWAVE.*

[7] J. V. P. Lafata, "Perspective Application of Passive Optical Network with Optimized Bus Topology," *Journal of Applied Research and Technology,* vol. 10, pp. 340-346, 2012.

[8] W. Tsong-Ho and M. E. Burrowes, "Feasibility study of a high-speed SONET self-healing ring architecture in future interoffice fiber networks," in *Military Communications Conference, 1990. MILCOM '90, Conference Record, A New Era. 1990 IEEE*, 1990, pp. 916-921 vol.3.

[9] C.-H. Yeh and S. Chi, "Self-protection against fiber fault for ring-based power-splitting passive optical networks," *Optical Engineering,* vol. 47, Feb 2008.

[10] M. A. Esmail and H. Fathallah, "Fiber Fault Management and Protection Solution for Ring-and-Spur WDM/TDM Long-Reach PON," in *Global Telecommunications Conference (GLOBECOM 2011), 2011 IEEE*, 2011, pp. 1-5.

[11] Q. H. Chen, W. G. Wu, Z. Q. Wang, G. Z. Yan, and Y. L. Hao, "Design and Performance of MEMS Multifunction Optical Device Using a Combined In-Plane and Out-of-Plane Motion of Dual-Slope Mirror," *Lightwave Technology, Journal of,* vol. 28, pp. 3589-3598, 2010.

[12] M. G. Krishanthmohan Ratnam, and Kee Chaing Chua, "Optical Protection With Pre-Configured Backup Paths and Limited Backup Resource Sharing," presented at the ICN 2011 : The Tenth International Conference on Networks, St. Maarten,The Netherlands Antilles, 2011.

[13] W. T. P'ng, M. K. Abdullah, S. Khatun, S. B. Ahmad-Anas, and S. Shaari, "A novel protection scheme for Ethernet PON FTTH access network," 2008, pp. 700918-700918-8.

[14] D. Griffith and L. SuKyoung, "A 1+1 protection architecture for optical burst switched networks," *Selected Areas in Communications, IEEE Journal on,* vol. 21, pp. 1384-1398, 2003.

[15] W. Liu and K. Y. Wu, "An intelligent EDFA design for metro application," in *Apoc 2003: Asia-Pacific Optical and Wireless Communications; Materials, Active Devices, and Optical Amplifiers, Pts 1 and 2*. vol. 5280, C. J. ChangHasnain, D. Huang, Y. Nakano, and X. M. Ren, Eds., ed, 2004, pp. 167-171.

[16] B. Juswardy, X. Feng, and K. E. Alameh, "Opto-VLSI-based RF beamformer for Space Division Multiple Access network," in *High-Capacity Optical Networks and Enabling Technologies (HONET), 2010*, 2010, pp. 222-226.

[17] M. Liu and X. q. Shi, "Optical implementation for adaptive beamforming of array antenna," 2010, pp. 785112-785112-7.

[18] E. H. W. Chan, W. Zhang, and R. A. Minasian, "Photonic RF Phase Shifter Based on Optical Carrier and RF Modulation Sidebands Amplitude and Phase Control," *J. Lightwave Technol.,* vol. 30, pp. 3672-3678, 12/01 2012.

[19] J. Capmany, B. Ortega, D. Pastor, and S. Sales, "Discrete-time optical Processing of microwave signals," *Lightwave Technology, Journal of,* vol. 23, pp. 702-723, 2005.

[20] J. Capmany, B. Ortega, and D. Pastor, "A tutorial on microwave photonic filters," *Lightwave Technology, Journal of,* vol. 24, pp. 201-229, 2006.

[21] M. V. Drummond, R. N. Nogueira, P. P. Monteiro, M. A. Violas, C. Sterner, and P. Y. Fonjallaz, "Tunable Optical Dispersion Compensator Based on Power Splitting Between Two Dispersive Media," *Lightwave Technology, Journal of,* vol. 28, pp. 1164-1175, 2010.

[22] R. G. Lamont, D. C. Johnson, and K. O. Hill, "Power Transfer In Fused Biconical-Taper Single-Mode Fiber Couplers - Dependence On External Refractive-Index," *Applied Optics,* vol. 24, pp. 327-332, 1985 1985.

[23] K. Jedrzejewski, "Biconical fused taper-a universal fibre devices technology," *Opto-Electronics Review,* vol. 8, pp. 153-159, 2000.

[24] H. S. Daniel and D. R. Moore, "Single-mode MxN star couplers fabricated using fused biconical taper techniques," 1991, pp. 53-59.

[25] H. Takahashi, "Recent Progress on Planar Lightwave Circuit Technology for Optical Communication," 2009, p. ThD1.

[26] Y. Hibino, F. Hanawa, H. Nakagome, M. Ishii, and N. Takato, "High reliability optical splitters composed of silica-based planar lightwave circuits," *Lightwave Technology, Journal of,* vol. 13, pp. 1728-1735, 1995.

[27] K. Li, U. Krishnamoorthy, J. P. Heritage, and O. Solgaard, "Coherent micromirror arrays," *Opt. Lett.,* vol. 27, pp. 366-368, 03/01 2002.

[28] O. Solgaard, S. Lee, Y. Kyoungsik, U. Krishnamoorthy, K. Li, and J. P. Heritage, "Microoptical phased arrays for spatial and spectral switching," *Communications Magazine, IEEE,* vol. 41, pp. 96-102, 2003.

[29] S. Yamashita, M. Mita, H. Fujita, R. Hirade, T. Yamamoto, M. Kawai*, et al.*, "Spatial Light Phase Modulator With Bidirectional Tilt Piston Micromirror ArrayPart I: Principle and Design," *Microelectromechanical Systems, Journal of,* vol. 20, pp. 270-278, 2011.

[30] S. C. Gustafson, G. R. Little, V. M. Bright, J. H. Comtois, and E. A. Watson, "Micromirror arrays for coherent beam steering and phase control," 1996, pp. 65-74.

[31] S.-W. Chung and Y.-K. Kim, "Design and fabrication of 10×10 micro-spatial light modulator array for phase and amplitude modulation," *Sensors and Actuators A: Physical,* vol. 78, pp. 63-70, 1// 1999.

[32] J. Extermann, S. M. Weber, D. Kiselev, L. Bonacina, S. Lani, F. Jutzi*, et al.*, "Spectral phase, amplitude, and spatial modulation from ultraviolet to infrared with a reflective MEMS pulse shaper," *Opt. Express,* vol. 19, pp. 7580-7586, 04/11 2011.

[33] D. M. Marom, D. T. Neilson, D. S. Greywall, P. Chien-Shing, N. R. Basavanhally, V. A. Aksyuk*, et al.*, "Wavelength-selective 1×K switches using free-space optics and MEMS micromirrors: theory, design, and

implementation," *Lightwave Technology, Journal of,* vol. 23, pp. 1620-1630, 2005.

[34] C. Marxer, B. de Jong, and N. de Rooif, "Comparison of MEMS variable optical attenuator designs," in *Optical MEMs, 2002. Conference Digest. 2002 IEEE/LEOS International Conference on*, 2002, pp. 189-190.

[35] K. Isamoto, K. Kato, A. Morosawa, C. Changho, H. Fujita, and H. Toshiyoshi, "A 5-V operated MEMS variable optical attenuator by SOI bulk micromachining," *Selected Topics in Quantum Electronics, IEEE Journal of,* vol. 10, pp. 570-578, 2004.

[36] X. Chen, B.-b. Yan, F.-j. Song, Y.-q. Wang, F. Xiao, and K. Alameh, "Diffraction of digital micromirror device gratings and its effect on properties of tunable fiber lasers," *Appl. Opt.,* vol. 51, pp. 7214-7220, 10/20 2012.

[37] C. Qinghua, W. Wengang, Y. Guizhen, W. Ziqian, and H. Yilong, "Novel Multifunctional Device for Optical Power Splitting, Switching, and Attenuating," *Photonics Technology Letters, IEEE,* vol. 20, pp. 632-634, 2008.

[38] N. Collings, T. Davey, J. Christmas, D. Chu, and W. A. Crossland, "The Applications and Technology of Phase-Only Liquid Crystal on Silicon Devices," *Display Technology, Journal of,* vol. 7, pp. 112-119, 2011.

[39] M. N. Ernstoff, A. M. Leupp, M. J. Little, and H. T. Peterson, "Liquid crystal pictorial display," in *Electron Devices Meeting, 1973 International*, 1973, pp. 548-551.

[40] F. Xiao, B. Juswardy, and K. Alameh, "Tunable Photonic Microwave Filters Based on Opto-VLSI Processors," *Ieee Photonics Technology Letters,* vol. 21, pp. 751-753, May-Jun 2009.

[41] F. Xiao and K. Alameh, "Adaptive multi/demultiplexers for optical signals with arbitrary wavelength spacing," *Opt. Express,* vol. 18, pp. 12277-12282, 06/07 2010.

[42] F. Xiao, B. Juswardy, K. Alameh, and Y. T. Lee, "Novel broadband reconfigurable optical add-drop multiplexer employing custom fiber arrays and Opto-VLSI processors," *Opt. Express,* vol. 16, pp. 11703-11708, 08/04 2008.

[43] M. Shen, F. Xiao, S. Ahderom, and K. Alameh, "An Opto-VLSI-based reconfigurable optical adddrop multiplexer employing an off-axis 4-f imaging system," *Opt. Express,* vol. 17, pp. 14015-14022, 08/03 2009.

[44] L. Peng, X. Sang, B. Yan, X. Chen, Y. Wang, Y. Zhang, *et al.*, "Tunable dual-wavelength fiber laser based on an opto-VLSI processor and four-wave mixing in a photonic crystal fiber," *Optics & Laser Technology,* vol. 44, pp. 935-938, 6// 2012.

[45] X. Feng, K. Alameh, and Y.-T. Lee, "Tunable Multiwavelength Fiber Ring Lasers Based on an Opto-VLSI Processor," *Photonics Technology Letters, IEEE,* vol. 23, pp. 182-184, 2011.

[46] M. Shen, F. Xiao, and K. Alameh, "A novel reconfigurable optical interconnect architecture using an Opto-VLSI processor and a 4-f imaging system," *Opt. Express,* vol. 17, pp. 22680-22688, 12/07 2009.

[47] M. Aljada, S. Hwang, and K. Alameh, "Design of 10Gbps optical encoder/decoderstructure for FE-OCDMA system using SOAand opto-VLSI processors," *Opt. Express,* vol. 16, pp. 679-685, 01/21 2008.

[48] D. Simeonidou, R. Nejabati, G. Zervas, D. Klonidis, A. Tzanakaki, and M. J. O'Mahony, "Dynamic Optical-Network Architectures and Technologies for Existing and Emerging Grid Services," *J. Lightwave Technol.,* vol. 23, p. 3347, 10/01 2005.

[49] A. Kodi and A. Louri, "Reconfigurable and adaptive photonic networks for high-performance computing systems," *Appl. Opt.,* vol. 48, pp. E13-E23, 08/01 2009.

[50] Y. Sakamaki, T. Saida, T. Hashimoto, and H. Takahashi, "Low-Loss Y-Branch Waveguides Designed by Wavefront Matching Method," *J. Lightwave Technol.,* vol. 27, pp. 1128-1134, 05/01 2009.

[51] K. B. Chung and J. S. Yoon, "Properties of a 1 x 4 optical power splitter made of photonic crystal waveguides," *Optical and Quantum Electronics,* vol. 35, pp. 959-966, Aug 2003.

[52] I. Park, H.-S. Lee, H.-J. Kim, K.-M. Moon, S.-G. Lee, B.-H. O, *et al.*, "Photonic crystal power-splitter based on directional coupling," *Opt. Express,* vol. 12, pp. 3599-3604, 07/26 2004.

[53] B. Chen, L. Huang, Y. Li, C. Liu, and G. Liu, "Flexible optical waveguide beam splitters based on directional coupling," *J. Opt. Soc. Am. B,* vol. 28, pp. 2680-2684, 11/01 2011.

[54] Y. Zhang, L. Liu, X. Wu, and L. Xu, "Splitting-on-demand optical power splitters using multimode interference (MMI) waveguide with programmed modulations," *Optics Communications,* vol. 281, pp. 426-432, 2/1/ 2008.

[55] A. Cleary, S. Garcia-Blanco, A. Glidle, J. S. Aitchison, P. Laybourn, and J. M. Cooper, "An integrated fluorescence array as a platform for lab-on-a-chip technology using multimode interference splitters," *Ieee Sensors Journal,* vol. 5, pp. 1315-1320, Dec 2005.

[56] M. Djavid, A. Ghaffari, F. Monifi, and M. S. Abrishamian, "Photonic crystal power dividers using L-shaped bend based on ring resonators," *J. Opt. Soc. Am. B,* vol. 25, pp. 1231-1235, 08/01 2008.

[57] A. Ghaffari, F. Monifi, M. Djavid, and M. S. Abrishamian, "Photonic crystal bends and power splitters based on ring resonators," *Optics Communications,* vol. 281, pp. 5929-5934, 12/1/ 2008.

[58] A. Ghaffari, M. Djavid, and M. S. Abrishamian, "Power splitters with different output power levels based on directional coupling," *Appl. Opt.,* vol. 48, pp. 1606-1609, 03/10 2009.

[59] P. A. Besse, E. Gini, M. Bachmann, and H. Melchior, "New 2×2 and 1×3 multimode interference couplers with free selection of power splitting ratios," *Lightwave Technology, Journal of,* vol. 14, pp. 2286-2293, 1996.

[60] Q. Lai, M. Bachmann, W. Hunziker, P. A. Besse, and H. Melchior, "Arbitrary ratio power splitters using angled silica on silicon multimode interference couplers," *Electronics Letters,* vol. 32, pp. 1576-1577, 1996.

[61] D. S. Levy, Y. M. Li, R. Scarmozzino, and R. M. Osgood, "A multimode interference-based variable power splitter in GaAs-AlGaAs," *Photonics Technology Letters, IEEE,* vol. 9, pp. 1373-1375, 1997.

[62] J. Chen, Z. Li, S. Yue, and Q. Gong, "Ultracompact surface-plasmon-polariton splitter based on modulations of quasicylindrical waves to the total field," *Journal of Applied Physics,* vol. 109, Apr 1 2011.

[63] C. Zhou and P. Kohli, "Ultracompact beam splitters based on plasmonic nanoslits," *Journal of Applied Physics,* vol. 109, May 1 2011.

[64] F. Ratovelomanana, N. Vodjdani, A. Enard, G. Glastre, D. Rondi, and R. Blondeau, "Active lossless monolithic one-by-four splitters/combiners using

optical gates on InP," *Photonics Technology Letters, IEEE,* vol. 7, pp. 511-513, 1995.

[65] S. L. Xiao, Q. J. Zeng, and J. X. Wang, "Tunable optical splitter technology," in *Active and Passive Optical Components for Wdm Communications Ii*. vol. 4870, A. K. Dutta, A. A. S. Awwal, N. K. Dutta, and K. Okamoto, Eds., ed, 2002, pp. 532-539.

[66] H. Wen-Hao, L. Ko-Chun, L. Jiun-Yun, W. Yir-Shyuan, W. Wang, x, *et al.*, "Polarization splitter with variable TE-TM mode converter using Zn and Ni codiffused LiNbO₃ waveguides," *Selected Topics in Quantum Electronics, IEEE Journal of,* vol. 11, pp. 271-277, 2005.

[67] Z. Liming and M. Zhu, "Variable optical power splitter based on channel waveguide," in *Communications and Photonics Conference and Exhibition (ACP), 2009 Asia*, 2009, pp. 1-2.

[68] Y. Kobayashi and S. Kakio, "Acoustooptic Bragg diffraction using leaky surface acoustic wave in Ti-diffused rotated Y-Cut LiNbO3 waveguide," in *OptoeElectronics and Communications Conference (OECC), 2011 16th*, 2011, pp. 693-694.

[69] Y. Zeng, W. Liu, C. Long, Y. Luo, and Q. Xiao, "A 1 ×2 variable optical power splitter development," *Lightwave Technology, Journal of,* vol. 24, pp. 1566-1570, 2006.

[70] X. Zhao, "Dynamic power optical splitter," USA Patent US 7068939 B2, Jun 27, 2006.

[71] R. M. Matic, "Reconfigurable Optical beam Splitter and Method," USA Patent, 1997.

[72] Z. Wang, R. Zheng, K. E. Alameh, R. Robertson, U. Mueller, and L. Bloom, "Opto-VLSI-based dynamic optical splitter," *Electronics Letters,* vol. 40, pp. 1445-1446, Oct 28 2004.

[73] P. F. McManamon, P. J. Bos, M. J. Escuti, J. Heikenfeld, S. Serati, X. Huikai, *et al.*, "A Review of Phased Array Steering for Narrow-Band Electrooptical Systems," *Proceedings of the IEEE,* vol. 97, pp. 1078-1096, 2009.

[74] F. Xiao, K. Alameh, and T. Lee, "Opto-VLSI-based tunable single-mode fiber laser," *Optics Express,* vol. 17, pp. 18676-18680, 2009/10/12 2009.

[75] I. G. Manolis, T. D. Wilkinson, M. M. Redmond, and W. A. Crossland, "Reconfigurable multilevel phase holograms for optical switches," *Photonics Technology Letters, IEEE,* vol. 14, pp. 801-803, 2002.

[76] S. Serati and J. Stockley, "Advanced liquid crystal on silicon optical phased arrays," in *Aerospace Conference Proceedings, 2002. IEEE*, 2002, pp. 3-1395-3-1402 vol.3.

[77] K. M. Johnson, D. J. McKnight, and I. Underwood, "Smart spatial light modulators using liquid crystals on silicon," *Quantum Electronics, IEEE Journal of,* vol. 29, pp. 699-714, 1993.

[78] X. Wang, D. Wilson, R. Muller, P. Maker, and D. Psaltis, "Liquid-Crystal Blazed-Grating Beam Deflector," *Applied Optics,* vol. 39, pp. 6545-6555, 2000/12/10 2000.

[79] X. Wang, B. Wang, P. J. Bos, J. E. Anderson, and P. F. McManamon, "2-D liquid crystal optical phased array," in *Aerospace Conference, 2004. Proceedings. 2004 IEEE*, 2004, pp. 905-913 Vol.2.

[80] X. H. Wang, B. Wang, J. Pouch, F. Miranda, M. Fisch, J. E. Anderson*, et al.*, "Liquid crystal on silicon (LCOS) wavefront corrector and beam steerer," in *Advanced Wavefront Control: Methods, Devices, and Applications*. vol. 5162, J. D. Gonglewski, M. A. Vorontsov, and M. T. Gruneisen, Eds., ed, 2003, pp. 139-146.

[81] C. K. Poh and K. Alameh, *Improving the steering efficiency of 1x4096 Opto-VLSI processor using direct power measurement method*, 2006.

[82] S. J. Walker and J. Jahns, "Array generation with multilevel phase gratings," *Journal of the Optical Society of America A,* vol. 7, pp. 1509-1513, 1990/08/01 1990.

[83] F. Wyrowski, "Upper bound of the diffraction efficiency of diffractive phase elements," *Optics Letters,* vol. 16, pp. 1915-1917, 1991/12/15 1991.

[84] S. T. Ahderom, M. Raisi, K. Alameh, and K. Eshraghian, "Testing and analysis of computer generated holograms for microphotonic devices," in *Field-Programmable Technology, 2004. Proceedings. 2004 IEEE International Conference on*, 2004, pp. 47-52.

[85] S. H. Tao and X. Yuan, "Practical Implementation of the Phase-Quantization Technique in an Iterative Fourier-Transform Algorithm," *Applied Optics,* vol. 43, pp. 2089-2092, 2004/04/01 2004.

[86] G.-z. Yang, B.-z. Dong, B.-y. Gu, J.-y. Zhuang, and O. K. Ersoy, "Gerchberg-Saxton and Yang-Gu algorithms for phase retrieval in a nonunitary transform system: a comparison," *Applied Optics,* vol. 33, pp. 209-218, 1994/01/10 1994.

[87] J. Rosen and J. Shamir, "Application of the projection-onto-constraint-sets algorithm for optical pattern recognition," *Optics Letters,* vol. 16, pp. 752-754, 1991/05/15 1991.

[88] R. Liu, B.-Y. Gu, B.-Z. Dong, and G.-Z. Yang, "Design of diffractive phase elements that realize axial-intensity modulation based on the conjugate-gradient method," *Journal of the Optical Society of America A,* vol. 15, pp. 689-694, 1998/03/01 1998.

[89] M. P. Dames, R. J. Dowling, P. McKee, and D. Wood, "Efficient optical elements to generate intensity weighted spot arrays: design and fabrication," *Applied Optics,* vol. 30, pp. 2685-2691, 1991/07/01 1991.

[90] S. Mingya, K. Alameh, and Y.-T. Lee, "Opto-VLSI-based integrated reconfigurable optical add-drop multiplexer with enhanced performance," in *High-Capacity Optical Networks and Enabling Technologies (HONET), 2009 6th International Symposium on*, 2009, pp. 62-66.

[91] D. P. Kelly, J. T. Sheridan, and W. T. Rhodes, "Fundamental diffraction limitations in a paraxial 4-f imaging system with coherent and incoherent illumination," *Journal of the Optical Society of America A,* vol. 24, pp. 1911-1919, 2007/07/01 2007.

[92] T. Kurihara and Y. Takaki, "Improving viewing region of 4f optical system for holographic displays," *Optics Express,* vol. 19, pp. 17621-17631, 2011/08/29 2011.

[93] B. E. A. Saleh and M. C. Teich, *Fundamentals of Photonics*: Wiley, 2013.

[94] R. A. Minasian and K. E. Alameh, "High Capacity Optical Beam Forming for Phased Arrays with Fiber Gratings and Frequency Conversion for Beat Noise Control," *Applied Optics,* vol. 38, pp. 4665-4670, 1999/07/20 1999.

[95] R. A. Minasian, K. E. Alameh, and N. Fourikis, "Wavelength-Multiplexed Photonic Beam-Former Architecture For Microwave Phased-Arrays," *Microwave and Optical Technology Letters,* vol. 10, pp. 84-88, Oct 5 1995.

[96] Y. Xiaoke, T. X. H. Huang, and R. A. Minasian, "Photonic Beamforming Based on Programmable Phase Shifters With Amplitude and Phase Control," *Photonics Technology Letters, IEEE,* vol. 23, pp. 1286-1288, 2011.

[97] K. E. Alemeh, R. A. Minasian, and N. Fourikis, "High capacity optical interconnects for phased array beamformers," *Lightwave Technology, Journal of,* vol. 13, pp. 1116-1120, 1995.

[98] R. A. Minasian and K. E. Alameh, "Optical-fiber grating-based beamforming network for microwave phased arrays," *Microwave Theory and Techniques, IEEE Transactions on,* vol. 45, pp. 1513-1518, 1997.

[99] M. J. a. M. J. Uddin, "Power splitter architecture and applications," *Progress in Electromagnetics Research C,* vol. 18, pp. 231-244, 2011.

[100] M. J. Uddin, M. I. Ibrahimy, M. B. I. Reaz, and Ieee, *Development of power control module in RFID reader circuit: A mentor graphic simulation approach*, 2008.

[101] J. C. Chiu, J. M. Lin, and Y. H. Wang, "A novel planar three-way power divider," *IEEE Microwave and Wireless Components Letters,* vol. 16, pp. 449-451, Aug 2006.

[102] A. H. Baree and I. D. Robertson, "Monolithic MESFET distributed baluns based on the distributed amplifier gate-line termination technique," *Ieee Transactions on Microwave Theory and Techniques,* vol. 45, pp. 188-195, Feb 1997.

[103] L. H. Lu, Y. T. Liao, and C. R. Wu, "A miniaturized Wilkinson power divider with CMOS active inductors," *IEEE Microwave and Wireless Components Letters,* vol. 15, pp. 775-777, Nov 2005.

[104] S. G. Mao and Y. Z. Chueh, "Broadband composite right/left-handed coplanar waveguide power splitters with arbitrary phase responses and balun and antenna applications," *Ieee Transactions on Antennas and Propagation,* vol. 54, pp. 243-250, Jan 2006.

[105] S. Y. Lee and C. C. Lai, "A 1-v wideband low-power CMOS active differential power splitter for wireless communication," *IEEE Transactions on Microwave Theory and Techniques,* vol. 55, pp. 1593-1600, Aug 2007.

[106] R. H. a. M. O'Sullivan, *Fiber Optic Measurement Techniques*: Elsevier Academic Press, 2009.

[107] J. Capmany, J. Mora, I. Gasulla, J. Sancho, J. Lloret, and S. Sales, "Microwave Photonic Signal Processing," *Lightwave Technology, Journal of,* vol. 31, pp. 571-586, 2013.

[108] R. A. Minasian, K. E. Alameh, and E. H. W. Chan, "Photonics-based interference mitigation filters," *Microwave Theory and Techniques, IEEE Transactions on,* vol. 49, pp. 1894-1899, 2001.

[109] Y. Jianping, "Photonic generation of microwave arbitrary waveforms," in *OptoeElectronics and Communications Conference (OECC), 2011 16th*, 2011, pp. 356-357.

[110] X. Feng, B. Juswardy, and K. Alameh, "Tunable Photonic Microwave Filters Based on Opto-VLSI Processors," *Photonics Technology Letters, IEEE,* vol. 21, pp. 751-753, 2009.

[111] T. Mengual, B. Vidal, and J. Marti, "Continuously tunable photonic microwave filter based on a spatial light modulator," *Optics Communications,* vol. 281, pp. 2746-2749, May 2008.

[112] J. Capmany, D. Pastor, and B. Ortega, "New and flexible fiber-optic delay-line filters using chirped Bragg gratings and laser arrays," *Microwave Theory and Techniques, IEEE Transactions on,* vol. 47, pp. 1321-1326, 1999.

[113] D. Pastor and J. Capmany, "Fibre optic tunable transversal filter using laser array and linearly chirped fibre grating," *Electronics Letters,* vol. 34, pp. 1684-1685, 1998.

[114] G. Yu, W. Zhang, and J. A. R. Williams, "High-performance microwave transversal filter using fiber Bragg grating arrays," *Photonics Technology Letters, IEEE,* vol. 12, pp. 1183-1185, 2000.

[115] J. Capmany, D. Pastor, and B. Ortega, "Fibre optic microwave and millimetre-wave filter with high density sampling and very high sidelobe suppression using subnanometre optical spectrum slicing," *Electronics Letters,* vol. 35, pp. 494-496, 1999.

[116] D. Pastor, B. Ortega, J. Capmany, S. Sales, A. Martinez, and P. Muñoz, "Optical microwave filter based on spectral slicing by use of arrayed waveguide gratings," *Opt. Lett.,* vol. 28, pp. 1802-1804, 10/01 2003.

[117] J. Capmany, D. Pastor, and B. Ortega, "Efficient sidelobe suppression by source power apodisation in fibre optic microwave filters composed of linearly chirped fibre grating by laser array," *Electronics Letters,* vol. 35, pp. 640-642, Apr 1999.